The long-term measurement of total evaporation over *Acacia mearnsii* using large aperture scintillometry

Alistair D Clulow
B.Sc. Hons. (Hydrology)
University of Natal

Submitted in partial fulfillment of the requirements for the degree of

MASTER OF SCIENCE
Agrometeorology Discipline
School of Environmental Sciences
Faculty of Science and Agriculture
University of KwaZulu-Natal
Pietermaritzburg
South Africa

December 2007

Declaration

I hereby declare that the research work reported in this thesis is the result of my own original investigations except where acknowledged.

Signed_____

Alistair D Clulow

Signed_____

Supervisor: Michael J Savage

Professor of Agrometeorology

Acknowledgements

I wish to record my sincere gratitude to:

Prof. C. S. Everson for his mentoring, support and always making himself available to assist me. Thank you Buck Rogers!

Lucas Ngidi and Joshua Xaba for their help and enthusiasm with field work

Prof. M. J. Savage for his valuable scientific input and speedy responses

Dr. C. Jarmain for her assistance with scientific matters

My colleagues Marilyn Govender, Mark Gush, and Peter Dye for arranging their work schedules around my studies

Mondi Forests for allowing access to the Canema-Mistley estate for scientific research and assistance with labour

The Water Research Commission for funding

My family Suzanne and Noah for their support and encouragement

Abstract

A large aperture scintillometer (LAS) was operated continuously over a distance of 575 m from 19 August 2006 to 29 September 2007 in the South African KwaZulu-Natal midlands mistbelt area over Wattle (*Acacia mearnsii*). The LAS measurements of the structure parameter of the refractive index of air (C_n^2), were used to calculate the sensible heat flux. The shortened energy balance equation was used to estimate the latent energy flux as a residual from which the total evaporation (*ET*) was calculated. The LAS estimates of sensible heat flux during the short transition period (1 hour) between stable and unstable conditions were on occasion erroneous and required verification. Advection was also found to affect sensible heat flux estimates. Long-term operation of the LAS was however found to be possible even at remote sites, producing reliable and continuous results.

The LAS estimates of sensible heat are sensitive to zero-plane displacement height and wind speed data impact and these should be derived as accurately as possible. Tree heights were measured at monthly intervals and a zero-plane displacement and effective height were calculated every two weeks. The sensible heat flux was thus processed in two week blocks of data corresponding to progressive effective heights.

The tree growth rate was consistent over time and was not affected by seasonality, indicating that reduced air temperatures, rainfall and solar irradiance in winter are not limiting growth. The average growth rate was 0.37 m per month or 4.5 m per year.

The LAS *ET* was compared to the American Society of Civil Engineers - Environmental and Water Resources Institute (ASCE-EWRI) short grass reference evaporation (ET_{sz}) for a seven-month period and was found to compare favourably ($R^2 = 0.78$) with outliers caused by advection and rainfall events. Calculations of grass reference evaporation at hourly and daily intervals provide different results. The daily estimates are lower than the

hourly estimates by 17 % on average. Where hourly data is summed to calculate a daily ET_{sz}, night-time values should be included.

The LAS *ET* measurements were validated against the Priestley and Taylor (1972) method of estimating ET and found to be in good agreement (R^2=0.94). The Priestley and Taylor daily total latent energy flux, from 22 August 2006 to 29 September 2007, was 9 % higher than the LAS results on average.

The Bowen ratio for the entire period is less than 1, indicating that the latent energy flux dominates at the site. The *ET* over the period of measurement (13 months) is 1250 mm and the rainfall is 750 mm. This confirms previous results at the site using the Bowen ratio energy balance method showing that the *ET* exceeds the rainfall by 45 % and justifies further research into soil water, ground water and root interactions in the deep soil profile.

Table of Contents

List of Tables

List of Figures

List of Abbreviations and Symbols

Roman Symbols

b	empirical constant (0.48)	
c	wave speed in a given medium	m s^{-1}
c_p	the specific heat capacity of air	J kg^{-1} K^{-1}
c_s	specific heat capacity of soil	J kg^{-1} K^{-1}
c_{ds}	specific heat capacity of dry soil	J kg^{-1} K^{-1}
c_w	specific heat capacity of water	J kg^{-1} K^{-1}
C_d	denominator constant	s m^{-1}
C_n	numerator constant	K mm s^{-3} Mg^{-1}
C_n^2	structure parameter of refractive index	$m^{-2/3}$
C_T^2	structure parameter of air temperature	K^2 $m^{-2/3}$
d	depth of soil heat flux plates below soil surface	m
d	zero plane displacement height	m
D	LAS aperture diameter	m
e_a	water vapour pressure	kPa
e_s	saturated water vapour pressure	kPa
e_z	mean ambient water vapour pressure at height z	kPa
	above the ground	kPa
Ea	water vapour transport flux	mm
ET	total evaporation	mm
ET_{LAS}	LAS-based total evaporation	mm
ET_{os}	ASCE-EWRI tall crop (0.5 m) reference	
	evaporation	mm
$ET_{P\text{-}T}$	Priestley and Taylor-based total evaporation	mm
ET_{sz}	ASCE-EWRI short grass (0.12 m) reference	
	evaporation	mm
f_T	universal stability function	
F_h	sensible heat flux	W m^{-2}
$F_{h(free)}$	sensible heat flux from the free convection method	W m^{-2}
F_{plate}	soil heat flux 80 mm below the soil surface	W m^{-2}

F_s	soil heat flux	W m^{-2}
F_{stored}	stored soil heat flux	W m^{-2}
g	gravitational acceleration	m s^{-2}
h	vegetation height	m
I_s	solar irradiation	W m^{-2}
k	von Karman's constant	
K_c	crop factor	unitless
K_h	turbulent exchange coefficient	m^2 s^{-1}
L	LAS path length	m
L_d	infrared irradiance upwards	W m^{-2}
L_{Ob}	Obukhov length	m
L_u	infrared irradiance downwards	W m^{-2}
L_vF_w	latent energy flux	W m^{-2}
$L_vF_{w(LAS)}$	LAS-based latent energy flux	W m^{-2}
$L_vF_{w(P\text{-}T)}$	Priestley and Taylor-based latent energy flux	W m^{-2}
$\frac{n}{N}$	fraction of possible sunshine during the daytime	
P	atmospheric pressure	kPa
r	reflection coefficient	unitless
r_a	aerodynamic resistance for water vapour	s m^{-1}
r_s	bulk canopy surface resistance	s m^{-1}
R_n	net irradiance	W m^{-2}
S	flux of soil heat storage	W m^{-2}
T	absolute air temperature	K
T	air temperature	ºC
T_o	surface temperature	ºC
T_z	air temperature at height z above the ground	ºC
T_*	temperature scale of turbulence	K
u_*	friction velocity	m s^{-1}
u_z	wind speed at height z	m s^{-1}
U_2	wind speed at a height of 2 m	m s^{-1}
W_f	wind function	m s^{-1}
z	height above surface	m
z_o	roughness length	m

Z_{eff_Avg}	average effective height	m
Z_{eff_Fc}	effective height of free convection	m
$Z_{effWgtAvg}$	weighted averaged effective height	m
Z_{LAS}	effective height of the LAS beam above the surface	m

Greek symbols

β	Bowen ratio	
δT	finite difference in actual air temperature	ºC
δz	height increment	m
Δ	slope of saturated vapour pressure vs air temperature relationship	kPa ºC^{-1}
$\Delta\theta$	finite difference in potential temperature	ºC
Δt	output time interval	s
ΔT_s	change in soil temperature	K
γ	psychrometric constant	kPa ºC^{-1}
θ_v	soil volumetric water content	m^3 m^{-3}
λ	wavelength	m
λE	evaporative latent energy flux	MJ m^{-2}
ρ_a	density of air	kg m^{-3}
ρ_s	bulk density of soil	kg m^{-3}
ρ_w	density of water	kg m^{-3}
$\sigma^2_{\ln I}$	variance of the logarithm of LAS beam	
υ	frequency	Hz
ψ_m	Businger-Dyer correction for stability	

Abbreviations

ASCE	American Society of Civil engineers
ASCE-EWRI	American Society of Civil Engineers – Environmental and Water Resources Institute
AWS	Automatic weather station
BLS	Boundary layer scintillometer
CFL	Constant flux layer

FAO-56	Food and Agriculture Organisation, paper no. 56
GPS	Global positioning system
IBL	Inner boundary layer
LAS	Large aperture scintillometer
LED	Light emitting diode
MOST	Monin-Obukhov similarity theory
PBL	Planetary boundary layer
RS	Roughness sublayer
SL	Surface layer
SLS	Surface layer scintillometer
VPD	Vapour pressure deficit

1. Introduction

The expanding human population has resulted in the need for increased food and timber production giving rise to increased competition for water between industries, municipalities and farmers. In addition, the scarcity of water is exacerbated by problems associated with water pollution and contamination, soil erosion, the invasion of alien vegetation and groundwater depletion. The implementation of a sustainable water resources management plan is required to meet these increasing demands on water resources. Evaporation is a significant component in the hydrological cycle and it is therefore critical that it can be understood and quantified (Savage *et al*., 2004).

In an attempt to control water use, the 1998 Republic of South Africa National Water Act refers to the volumetric determination of water for purposes of water allocation. In order to audit water use in the natural environment it is important to consider how evaporation will be estimated as part of the hydrological cycle especially from heterogeneous areas with exotic vegetation types that may have a high water use.

The Two Streams catchment experiments have been used over the last seven years to study the impact of trees on hydrological processes (Everson *et al.*, 2007). The experiments provide a good opportunity for studies to extend our understanding of other processes such as low flows and deeper soil water dynamics. The Two Streams catchment is one of the few remaining small catchment research areas in South Africa. Streamflow gauging was started in 1999 in a mature stand of wattle trees (*Acacia mearnsii)*. Following a short calibration period, all the trees in the "B" riparian zone were cleared in July 2000. The trees in the remainder of the catchment were removed in 2004/05 and the catchment has recently (August 2006) been replanted with wattle. With seven years of intense hydrological monitoring, this catchment presents an ideal opportunity to study the impact of the newly planted crop on the water balance of the catchment and direct research towards previously unanswered questions.

Burger (1999), for example, estimated total evaporation (*ET*) using the Bowen ratio energy balance method and showed that annual total evaporation exceeded annual rainfall when measured over *A. mearnsii* at Two Streams during the exponential growth phase. This suggests that either the instruments used are providing incorrect results, or that tree roots are tapping into groundwater and depleting soil water reserves from within the deep soil profile. Internationally, Baldocchi and Xu (2006) investigated the Mediterranean Oak (*Quercus douglasii*) for similar reasons. The trees were able to survive extended periods without water and total evaporation was also found to exceed rainfall.

Scintillometry has been used in a number of studies internationally to estimate total evaporation (Meijninger *et al*., 2006; Ezzahar *et al*., 2006) and exhibits a number of advantages over other methods such as Bowen ration and eddy covariance (Savage *et al*., 2004). The use of scintillometry has recently experience a renewed enthusiasm (de Bruin, 2002) and this document expands on the theory of scintillometry and reports on the estimates of *ET* over *A. mearnsii* at the Two Streams site. Although the theory of scintillometry does not account for advection, some studies have shown estimates from scintillometry affected by advection to be consistent and accurate (Hoedjes *et al*., 2002). The extended data set allows for an initial assessment of the impact of advection at Two Streams.

A nearby weather station is used to calculate a short grass reference evaporation (ET_o) according to the American Society of Civil Engineers-Environmental and Water Resources Institute method (ET_{sz}) based on the original Penman-Montieth combination equation. The Penman-Montieth method is internationally recognised and popular for a number of reasons including the relatively low data requirements and the relationship established between the reference and the total evaporation known as the crop factor. This allows agronomists and hydrologists to estimate total evaporation from standard weather station data which is commonly collected on a country-wide scale. The scintillometer results of total evaporation are compared to the short

short grass reference for a period of seven months and a crop factor for *A.mearnsii* is calculated.

A comprehensive data set is recorded from when the trees were planted for a period of 13 months. This includes weather data as well as plant growth data. Tree height data was required for the processing of the scintillometer data because the beam height above the canopy is critical in the calculation of sensible heat flux. To capture this adequately, data was processed every two weeks with updated tree heights.

In summary the objectives of this work are to:

- investigate the use of a large aperture scintillometer over commercial forestry;
- establish the reliability of the long-term use of large aperture scintillometry at remote sites;
- confirm the results of Burger (1999) showing total evaporation over *A.mearnsii* to exceed rainfall at the Two Streams site during the exponential growth phase;
- investigate the new American Society of Civil Engineers-Environmental and Water Resources Institute method of calculating a short grass reference evaporation;
- estimate a crop factor from scintillometer and weather station data for *A.mearnsii*;
- investigate the impact of advection on scintillometer data.

2. Energy Balance Method of Determining Total Evaporation

2.1. Energy and Evaporation

At the earth's surface, using a shortened energy balance, four different types of energy flux are identified, namely, net irradiance (R_n), sensible heat flux (F_h), latent energy flux (L_vF_w) and soil heat flux (F_s). By the principle of the conservation of energy at the earth's surface, the different components of the system are linked to each other through the energy balance equation. If all components except L_vF_w are measured, the energy balance equation may be used to determine L_vF_w as a residual term and from that the total evaporation (ET). There are other energy components such as advection and canopy storage but for simplicity, these are considered negligible in many studies (Savage *et al.*, 1997). The data in this study does however show the impact of advection and this is discussed further in Chapter 5.

In the environment, the energy in the system is constantly changing and for this reason, energy is measured as a flux. An energy flux in a given direction is the amount per unit time passing through a unit area normal to that direction. The SI units of energy flux are J s^{-1} m^{-2} or W m^{-2}.

The energy balance conventions for the shortened energy balance are written as:

$$R_n = F_h + L_vF_w + F_s \text{ or} \qquad 2.1$$

$$R_n + F_h + L_vF_w + F_s = 0 \qquad 2.2$$

The two conventions are essentially based on the sign given to the direction of the flux. Both can be used but the sign of the fluxes needs to be understood in each case. In the first formula all radiative fluxes directed towards the surface are positive, while other (non radiative) fluxes directed away from the surface are positive. This equation emphasises the importance of R_n and how the sum of the other fluxes is equal to R_n. In the second convention all fluxes directed towards the surface are positive and away from the surface are negative and

the sum of the fluxes is zero. This convention emphasises the conservation of energy at the earth's surface. The typical daytime flux situation is represented graphically in Fig. 2.1 according to the first convention.

The approximate magnitude of the fluxes on a typical day with clear skies is indicated by the length of the lines. The fluxes are however highly dependant on cloud and surface cover.

2.2. Net Irradiance

Ayra (2001) and Campbell and Norman (1998) provide thorough descriptions of radiation physics and definitions. Essentially, radiation is the transfer of energy by rapid oscillation of electromagnetic fields, even in a vacuum. Radiation is characterised by its wave length (λ) and frequency (υ) in:

$$\lambda = \frac{c}{\upsilon} \qquad 2.3$$

where c is the wave speed in a given medium.

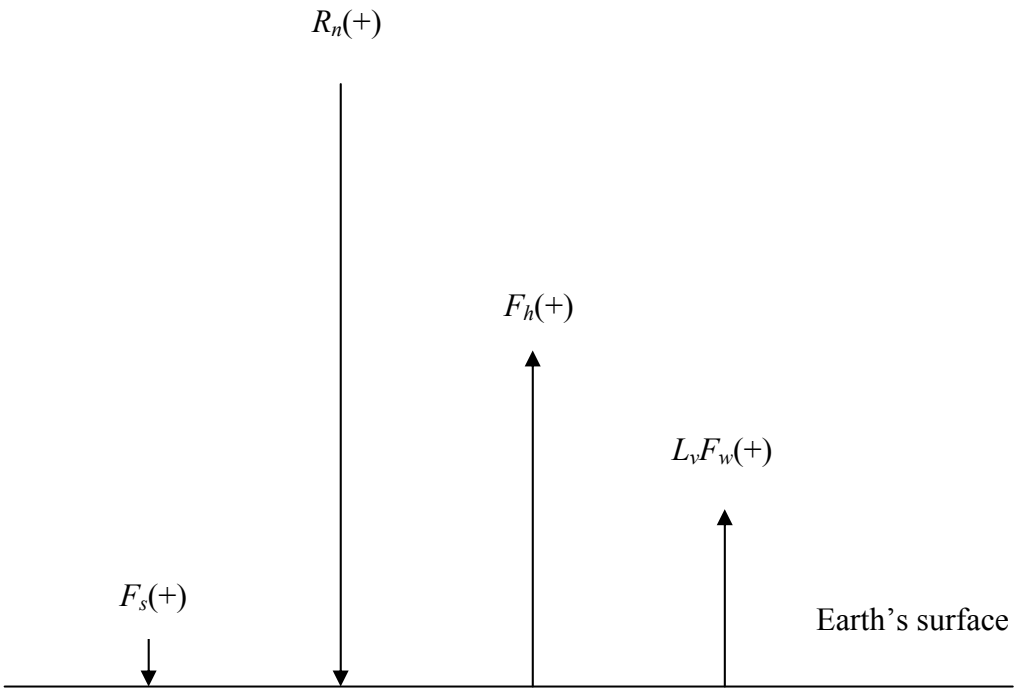

Fig. 2.1. The four most important energy fluxes at the earth's surface for the daytime.

All waves travel at the same speed (c) in a vacuum. When they travel in a medium their speed varies with frequency. Visible light occupies a very narrow range of the possible wavelengths and has a range from 400 to 700 nm. Shortwave radiation is confined to the wavelength range of 150 to 4000 nm and infrared radiation to the range of 3000 to 100 000 nm providing very little overlap between the two spectra (Ayra, 2001). The materials in the atmosphere and the earth's surface absorb some of the solar irradiance and will themselves emit radiation. These materials are at a much lower temperature than the sun and thus emit radiation with a much longer wavelength.

The shortwave solar irradiance at the outer limits of the atmosphere is approximately 1368 W m^{-2}, and is known as the solar constant (Ayra, 2001). At the surface of the earth the shortwave radiation sources are direct solar radiation, reflected shortwave radiation and diffuse shortwave radiation. Shortwave radiation may be reflected a number of times by the earth's surface and clouds. This reflection is dependant on the reflection coefficient of the reflecting surface. The surface reflection coefficient describes the ratio of the global shortwave reflected radiation and the corresponding incident radiation. A number of authors (Brutsaert, 1982; Rosenberg *et al.*, 1983; Allen *et al.*, 1998) provide typical values of different surface reflection coefficients. Diffuse radiation is radiation that has been scattered by molecules and particles in the atmosphere and is the shortwave radiation found in shaded areas.

Infrared radiation has two components namely, upwards from the surface (L_u) and downwards from the atmosphere (L_d). The upward infrared radiation emitted by the earth's surface is the dominant form of radiation at night. The amount of infrared radiation is dependant on the emissivity and temperature of the radiating surface. Clouds and different gases form some of the sources of infrared radiation in the atmosphere. Greenhouse gases in particular, absorb and emit infrared radiation (Ayra, 2001).

Net irradiance is the difference between the total upward and downward irradiance and is the source of energy at the earth's surface and can be expressed as:

$$R_n = I_s(1 - r) + L_d - L_u \qquad 2.4$$

where I_s is the incoming shortwave irradiance (W m^{-2}), and r is the reflection coefficient of the underlying surface.

R_n is important to evaporation studies because it is the source of energy that drives the processes of evaporation and is a major component in the energy balance equation.

Generally, throughout the world, direct and diffuse incoming shortwave irradiance is measured more commonly compared to net irradiance (Rosenberg *et al.*, 1983). For this reason numerous attempts have been made to relate and derive net irradiance from solar irradiance measurements (Ortega-Farias *et al*., 2000; Aldos *et al*., 2003) and Rosenberg *et al.* (1983) describe one of these methods known as the empirical Linacre equation developed in 1968:

$$R_n = (1 - r)\, I_s - 1.11\left(0.2 + 0.8\frac{n}{N}\right)(100 - T) \qquad 2.5$$

where $\frac{n}{N}$ is the fraction of sunshine duration during the daytime and T is the air temperature (ºC). The measurement of net irradiance is discussed further in Chapter 5.

2.3. Soil Heat Flux

The component of energy flux that heats or cools the ground surface is known as the soil heat flux. Rosenberg *et al.* (1983) provides a comprehensive explanation of the laws of heat conduction and the thermal properties of soil. Brutsaert (1982) describes the different methods that have been used over the

years to determine F_s including the temperature gradient method (Kamball *et al*., 1976), soil calorimetry (de Vries *at al*., 1986) and empirical relationships (Cellier *et al*., 1996). The use of heat flux plates is however well established and is recommended by Mayocchi and Bristow (1995) and Savage et al., (2004). Although it is generally the smallest component of the energy balance, it should not be ignored in the case of sub-daily energy balance measurements and may be significant where the soil surface is exposed (Brutsaert, 1982).

Despite a good understanding of the effects of porosity, soil water content, organic matter and texture on soil heat flux, Mayocchi and Bristow (1995) state that there is still some confusion on just how F_s should be estimated. They provide a clear framework for field measurements and emphasise the importance of including heat storage in the soil.

Ideally, the F_s should be determined at the soil surface. Due to practical limitations and the impact of installing heat flux plates near the surface, the plates are usually buried at depths greater than 10 mm below the surface (Mayocchi and Bristow, 1995). Campbell (2003) recommends a depth of 80 mm. A correction is applied to the measured flux at a depth of 80 mm to account for the heat storage that occurs in the layer between the heat flux plate and the surface:

$$F_s = F_{plate} + F_{stored} \qquad 2.6$$

where:

$$F_{stored} = \frac{\rho_s \, \Delta T_s \, c_s \, d}{\Delta t} \qquad 2.7$$

where F_s is the soil heat flux at the surface (W m^{-2}), F_{plate} is the heat flux at a depth of 80 mm (W m^{-2}), F_{stored} is the flux of heat storage in the soil above the plate (W m^{-2}), ρ_s is the bulk density of soil (kg m^{-3}), ΔT_s is the temporal change in temperature over the output interval (K), c_s is the specific heat

capacity of soil (J kg^{-1} K^{-1}), d is the depth of the heat flux plates in the soil (m) and Δt is the output time interval (s).

The specific heat capacity of the soil is calculated by adding the specific heat of dry soil to that of soil water on a mass basis:

$$\rho_s \, c_s = \rho_s \, c_{ds} + \rho_w \, \theta_v \, c_w \qquad 2.8$$

where c_{ds} is the specific heat capacity of dry mineral soil (840 J kg^{-1} K^{-1}), ρ_w is the density of water (kg m^{-3}), θ_v is the volumetric water content (m^3 m^{-3}) and c_w is the specific heat capacity of water (4190 J kg^{-1} K^{-1}).

Typically the soil temperature is averaged across two depths, namely, 20 and 60 mm in order to calculate ΔT_s.

2.4. Sensible Heat Flux

Nicholls and Smith (1982) define F_h and comment on terminology used and misleading inferences that have drawn regarding the definition of F_h due to the complex nature of the flux. Sensible heat flux is defined as the absorption or transference of heat energy flux due to a change in temperature between the surface and the overlying air. This process excludes any influence of phase changes such as the vapourisation of water. In this case, the phase change of water without significant change in temperature is allocated to latent energy flux.

Energy from the surface is transferred by conduction (molecules of air that are in direct contact with the surface) and convection (energy transferred between the surface and the air). Convection in this context is the mass motion of air resulting in transportation and mixing of air particles (Rosenberg *et al.*, 1983). The flow of heat energy due to temperature differences between the earth's surface and the air without involving a phase change of water is called the sensible heat flux. Generally, during the day when the earth's surface is heated, energy is disposed of to the cooler air in the form of sensible heat. At

night the earth's surface becomes cooler than the atmosphere and energy is transferred in the opposite direction.

Except for the very thin layer of air immediately in contact with the surface where energy transfer takes place by conduction, the transfer of F_h is governed by turbulence. Rosenberg *et al.* (1983) define the vertical flux of sensible heat flux as:

$$F_h = \rho_a \, c_p \, K_h \frac{\partial \theta}{\partial z} \qquad 2.9$$

where ρ_a is the air density (kg m^{-3}), c_p is the specific heat capacity of air at constant pressure (J kg^{-1} K^{-1}), K_h is the turbulent exchange coefficient (m^2 s^{-1}) and $\frac{\partial \theta}{\partial z}$ is the vertical gradient in potential temperature (K m^{-1}).

Rosenberg *et al.* (1983) further state that in the lowest 2 to 3 m of atmosphere, $\frac{\partial \theta}{\partial z}$ can be approximated by $\frac{\partial T}{\partial z}$, to give the vertical gradient of actual air temperature.

Rosenberg *et al.* (1983) continue to explain atmospheric stability and how it is usually expressed by the Richardson number and Obukhov parameter. They explain analogous equations for momentum, sensible heat and vapour fluxes and how the sensible and latent energy fluxes can be calculated independently and directly using eddy covariance where high frequency measurements of vertical wind speed, air temperature and water vapour content for example are recorded. This method relies on the covariance between the vertical wind speed and absolute humidity fluctuations for an estimation of latent energy flux. Eddy covariance is considered an absolute technique for latent energy flux estimation since net irradiance and soil heat flux are not required and the energy balance equation is not used (Savage *et al.*, 1997). In this document, scintillometry is applied to estimate sensible heat flux and is explained further in Chapter 5.

2.5. Latent Energy Flux

In order for evaporation to take place, energy is required in the form of latent energy. The latent energy of evaporation for water is 2.454 MJ kg^{-1}. This means that 2.454 MJ of energy is required for the evaporation of 1 kg of water without a significant change in temperature of the water (Ayra, 2001). From this, if the latent energy flux is known, the amount of water evaporated can be calculated.

By rearranging Eq. 2.1, the shortened energy balance equation provides an estimation of the L_vF_w as a residual amount:

$$L_vF_w = R_n - F_h - F_s \qquad 2.10$$

The disadvantage associated with the residual method is that if one of the measured components of the energy balance is incorrect or for example advection is present, the error is carried through to the residual amount.

2.6. Energy Balance Closure

The major components of the surface energy balance are net irradiance, sensible heat flux, soil heat flux and latent energy flux which together form the shortened energy balance equation (Eq 2.1). If these four components are measured accurately and independently then Eq. (2.1) is satisfied. Numerically, closure can be calculated as,

$$R_n - F_s - F_h - L_vF_w = c \qquad 2.11$$

where c is the energy balance closure (W m^{-2}) and closure is satisfied if c = 0 W m^{-2}.

Where the four components of Eq. (2.11) have been measured independently the energy balance closure is used as an indication of the accuracy of the

independent measurements and it is assumed that the smaller the closure, the more accurate the measurement. However, energy balance closure could be achieved if two components of Eq. 2.11 are incorrect but the errors cancel each other out and closure is equal to zero (Savage *et al*., 2004). This may give the impression that the components have been measured accurately which is not actually the case.

In studies, using a range of methods such as eddy covariance, where closure was not achieved, the vast majority found higher energy input by radiation fluxes than losses by soil heat flux and turbulent fluxes (Oncley *et al*., 2007). In these cases the measured flux should either be adjusted, the error accepted (Twine et al., 2000), or an independent measurement method adopted. Lack of closure should be considered a serious problem as it indicates errors in measurement.

In a number of studies reasons are given for the lack of energy balance closure (Stannard et al., 1994; Twine *et al*., 2000; Wilson *et al*., 2002; Foken *et al*., 2006a; Foken *et al*., 2006b; Cava *et al*. 2007) and include: (1) sampling errors associated with different temporal and spatial scales for the terms in Eq. (2.11), (2) a systematic bias in instrumentation, (3) neglected energy sinks, (4) the loss of low and/or high frequency contributions to the turbulent flux, (4) neglected advection of scalars, (6) measurement errors related to sensor separation, alignment problems and interference from tower of instrument mounting structures, and (7) errors in the measurement of R_n and/or F_s.

Two micrometeorological methods that provide direct measurements of surface scalar fluxes are the Bowen ratio energy balance method (BREB) and the eddy covariance (EC) method used in conjunction with an infrared gas analyser. It is advisable when using methods that estimate the latent heat flux as a residual to run a direct measurement technique for a reasonable period of time in order to confirm results.

3. The American Society of Civil Engineers (ASCE) Automatic Weather Station (AWS) Reference Evaporation

3.1. Introduction

Many professionals including water resource managers, crop scientists and water engineers will know that the Penman equation is synonymous with evaporation estimation. A minority are however likely to understand the complex methodology and development of the original Penman equation of 1948 (Penman, 1948) through to the more recent American Society of Civil Engineers - Environmental and Water Resources Institute (ASCE-EWRI) method.

The development of the original equation appears to have been subject to an ongoing battle between simplification of the equation and accuracy of the results. Simplification has been driven mainly by inadequate data sets, low computing power and user capability. Accuracy is driven by an improved understanding of the environment, higher quality sensors, modelling requirements and a need to apply the methods in different climatic regions over many decades. For this reason many versions of the original equation have been proposed and some have many followers. Allen *et al.* (2000) lists the six main reference evaporation equations that have been developed over the years (Kimberly Penman, CIMIS Penman, FAO Penman, ASCE Penman-Monteith, FAO-56 Penman-Monteith and NRCS Penman-Monteith). For this reason it has been considered necessary to develop a standardised equation to bring commonality to the estimation of reference evaporation. Most recently, this has resulted in the ASCE-EWRI standardised reference evaporation equation (Allen *et al*., 2006) which will be discussed further in this chapter.

3.2. Terminology Relating to Evaporation

Evaporation is the process whereby liquid water is converted to water vapour and removed from the evaporating surface (Allen *et al.*, 1998). Latent energy is required to change the state of the water molecules from a liquid to a vapour. Solar irradiance, air temperature (convection) and surface temperature

(conduction) are the sources of this energy. Air movement and/or a water vapour pressure gradient are then required to remove the water vapour from the surface. The climatological parameters considered of extreme importance when assessing evaporation are solar irradiance, air temperature, air humidity and wind speed.

Transpiration is the process of vapourisation of liquid contained in plant leaves through small openings in the leaf called stomata. Transpiration rate is controlled by soil water availability, plant characteristics and the climatic parameters controlling evaporation (Allen *et al.*, 1998).

Total evaporation is a combination of evaporation and transpiration. In nature they frequently both occur simultaneously and it is difficult to separate the two components. Evaporation from the soil surface dominates in the early stages of development of a crop, while transpiration begins to dominate later when the canopy begins to shade the soil surface.

Reference evaporation (ET_o) is the total evaporation from a reference surface and is related to the transpiration of various crops by means of a crop factor where the crop is not short of water or nutrients and fully covers the soil surface. The concept of reference evaporation allows the study of the evaporative demand of the atmosphere independently of the crop type, crop growth, management practices and soil factors. This allows for the comparison of ET_o values from different locations or different seasons as long as they refer to the same reference surface. A further advantage of referring to ET_o is that the only factors affecting ET_o are climatic parameters and consequently it can be computed from weather data. An open water surface was suggested in the past as a reference surface. This is however very different to a typical land surface with plants and it was felt that relating ET_o to a specific crop would incorporate the biological and physical processes more realistically. Short grass that fully covers the surface and that is not short of water (nor nutrients) is an extremely well studied surface and has been accepted world wide as a reference surface (Allen *et al.*, 1998). More specifically, the grass reference has an assumed height of 0.12 m, a fixed canopy surface resistance of 50 s m^{-1}

during the daytime, 200 s m^{-1} during the night-time and a surface reflectivity of 0.23. For daily computations a surface resistance of 70 s m^{-1} is used. Tall crop reference evaporation (0.5 m high crop) is similar to grass reference evaporation except that a value of 30 s m^{-1} is used for the canopy surface resistance during the daytime and for daily computations a surface resistance of 45 s m^{-1} is applied. At night-time the canopy surface resistance for a tall crop is also 200 s m^{-1}.

3.3. The Penman Equation

The original Penman combination equation dates back to a publication by Penman (1948). It is called the 'combination equation' because it is physically based on two terms, namely, the energy balance and aerodynamic/bulk transfer formulas. Ayra (2001) explains how the two terms were combined by Penman. He also explains the assumptions Penman made and how he used the Bowen ratio to derive the original Penman equation, based on daily data:

$$\lambda E = \frac{\Delta \left(R_n - F_s\right) + \gamma \, \lambda \, E_a}{\Delta + \gamma} \qquad 3.1$$

where λE is the evaporative latent energy flux (MJ m^{-2}), Δ is the slope of the saturated vapour pressure *vs* air temperature relationship (kPa $ºC^{-1}$), R_n is the net irradiance (MJ m^{-2}) [Penman calculated R_n using the reflection coefficient and emissivity of the surface], F_s is the soil heat flux (MJ m^{-2}), γ is the psychrometric constant (kPa $ºC^{-1}$), λ is the latent energy of vapourisation (MJ kg^{-1}) and E_a is the water vapour transport flux (mm).

The term E_a can be interpreted as the drying power of air and Penman defined E_a empirically as:

$$E_a = W_f \left(e_s - e_z\right) \qquad 3.2$$

where W_f is the wind function expressed as a linear function of wind speed (m s^{-1}) at a reference height (2 m) above the ground, e_s is the saturated water vapour pressure (kPa) at mean air temperature and e_z is the mean ambient water vapour pressure (kPa) at a reference height (2 m) above the ground.

Ayra (2001) comments on the sound theoretical and physical background of the Penman equation, but adds that some consider it to be semi-empirical. Howell (2000) states that the theory of Penman was ahead of its time, but that a lack of computing power and complication over original English units resulted in most engineers using simpler equations such as the Blaney-Criddle (Blaney *et al*., 1950) and Thornthwaite (Thornthwaite, 1948) equations.

The impact of the Penman equation was that it was possible to calculate a potential evaporation (now called grass reference evaporation, ET_o) for a fresh green crop, of about the same colour as grass, completely shading the ground, of fairly uniform height, and never short of water (Howell, 2000) nor nutrients.

Ayra (2001) states that the observational procedure is simplified by the ingenious way in which the surface temperature has been eliminated from the final result through expressing the slope of the saturation water vapour pressure vs the air temperature relationship (Δ) in finite difference form:

$$\Delta \simeq \frac{e_s(T_o) - e_s(T_z)}{T_o - T_z} \qquad 3.3$$

where T_o is the surface temperature (ºC) and T_z is the air temperature at a specified height z above the ground surface (ºC).

Data requirements are hence fulfilled by most standard weather stations that provide estimates at a height of 2 m of net irradiance, wind speed, air temperature, relative humidity and soil heat flux at ground level.

3.4. The Penman-Monteith Equation

With time, improvements were made to the original Penman equation in the form of the Kimberly Penman equation and one of the further milestones in the development was the Penman-Monteith equation. It included new work around the resistance parameters. Penman initially calculated an open water evaporation and used fractions to convert that to soil or plant evaporation. The resistance parameter distinguishes between aerodynamic resistance and surface resistance factors. The surface resistance parameter, r_s, describes the resistance of water vapour flow through stomata openings, the total leaf area and soil surface. The aerodynamic resistance, r_a, describes the resistance from vegetation upward and involves friction from air flowing over vegetated surfaces. The Penman-Monteith form of the combination equation for daily computations is:

$$\lambda ET = \frac{\Delta\, r_a \left(R_n - F_s\right) + \rho_a c_p \left(e_s - e_a\right)}{\Delta\, r_a + \gamma\, \left(r_a + r_s\right)} \qquad 3.4$$

where r_a is the aerodynamic resistance for water vapour (s m^{-1}), e_a is the water vapour pressure (kPa) and r_s is the bulk canopy surface resistance (s m^{-1}).

The new parameters in the Penman-Monteith equation require calculation. The aerodynamic resistance (r_a) is derived from an equation using zero-plane displacement height, roughness lengths and wind speed measurements (Howell and Evett, 2004). The bulk surface resistance (r_s) describes the resistance of vapour flow through the transpiring crop and evaporating soil surface. An estimation of the r_s of a dense full cover crop is related to canopy leaf area and leaf stomatal resistance. Leaf stomatal resistance is crop dependant but also changes with crop maturity and is derived through plant physiological studies.

3.5. The FAO-56 Penman-Monteith Equation

In 1975 the Food and Agriculture Organisation (FAO) published guidelines to determine crop water requirements as FAO Irrigation and Drainage paper No. 24 (Doorenbos *et al.*, 1975). In 1990 a consultation of experts was organised by FAO together with the International Commission for Irrigation and Drainage and with the World Meteorological Organisation to review the FAO-24 guidelines. These guidelines were published in 1998 and have become known as the FAO-56 Penman-Monteith method (Allen *et al.*, 1998).

One of the most significant contributions of the panel was to define the reference crop as, 'a hypothetical crop with an assumed height of 0.12 m having a surface resistance of 70 m s^{-1} and a reflection coefficient of 0.23, closely resembling an extensive surface of green grass of uniform height, actively growing and adequately watered that fully covers the soil' (Allen *et al.*, 1998). By further assuming a constant for γ (the psychrometric constant), simplifying the air density (ρ_a), using a surface resistance (r_s) of 70 m s^{-1} and estimating aerodynamic resistance (r_a) from an inverse function of wind speed, the FAO-56 equation became:

$$\lambda ET = \frac{0.408\Delta\left(R_n - F_s\right) + \gamma \frac{900}{T+273} U_2 \left(e_s - e_a\right)}{\Delta + \gamma\left(1 + 0.34U_2\right)} \qquad 3.5$$

where T is the mean air temperature (ºC) at a height of 2 m, and U_2 is the mean wind speed (m s^{-1}) at a height of 2 m.

The equation uses standard weather station data including solar irradiance, air temperature, relative humidity and wind speed. All sensors should be mounted at a height of 2 m above an extensive surface of green grass, shading the ground and not short of water (Allen *et al.*, 1998) or nutrients.

The FAO-56 Penman-Monteith equation is a representation of the physical factors at a height of 2 m and physiological factors at the surface controlling

the evaporation process. By using the FAO-56 Penman-Monteith definition for ET_o, it is possible to calculate crop coefficients K_c by relating the measured total evaporation ET to the calculated ET_o:

$$K_c = \frac{ET}{ET_o} \qquad 3.6$$

Allen *et al.* (1998) describe how the equation can be re-arranged to calculate crop water use if ET_o is calculated from weather data and K_c is known. The crop coefficient is defined for different crops and in most cases a dual crop coefficient is used to represent two stages in the growth of a crop. Allen *et al.* (1998) provide details in Chapter 6 and 7 of the FAO-56 guidelines on the different crop coefficients suggested for different crops and the possible adjustments that can be made. A pan coefficient is also available where pan evaporation data exists.

The equation can be applied for monthly, ten-day, daily and even hourly time-steps depending on the availability of the data.

In the FAO-56 guidelines, comprehensive details are supplied regarding data requirements and criteria. Chapter 3 describes the meteorological data including the conversion of units and in many cases assistance to users in estimating certain variables when data is not available.

Howell and Evett (2004) state that the FAO-56 guidelines presented by Allen *et al.* (1998) were a significant milestone in developing a consistent methodology in the determination of R_n and F_s.

3.6. The ASCE-EWRI Penman-Monteith Equation

In May 1999, in the United States of America, the Irrigation Association requested the Evapotranspiration in Irrigation and Hydrology Committee – Environmental and Water Resources Institute (American Society of Civil Engineers) (ASCE-EWRI), to establish and define a benchmark reference

evaporation equation (Allen *et al.*, 2006). The primary challenges faced by the committee were to address: (1) the requirement of diversity of application of the equation, (2) standardisation of the reference, (3) different time steps, (4) meteorological data requirements, and (5) the estimation of R_n, F_s and water vapour pressure deficit. The basis for the equation and parameters came from the FAO-56 Penman-Monteith and in its new form the equation is:

$$ET_{sz} = \frac{0.408\Delta\left(R_n - F_s\right) + \gamma \frac{C_n}{T+273} U_2 \left(e_s - e_a\right)}{\Delta + \gamma\left(1 + C_d U_2\right)} \qquad 3.7$$

where ET_{sz} is the standardised reference crop evaporation for short (ET_{os}) or tall (ET_{rs}) surfaces (mm), C_n is the numerator constant that changes with reference type and the calculation time step (K mm s^3 Mg^{-1} d^{-1} or K mm s^3 Mg^{-1} h^{-1}) and C_d the denominator constant that changes with reference type and calculation time step (s m^{-1}).

ASCE-EWRI recommended two surfaces as references and that each have appropriate constants and standardised computational procedures. The two surfaces are a short crop (ET_{os}) with an approximate height of 0.12 m (similar to clipped, cool season grass) and for a tall crop (ET_{rs}) with an approximate height of 0.5 m (similar to full-cover alfalfa). These particular references were established as they are common surfaces and well documented in the literature.

Allen *et al.* (2006) document in their final report suggested values for C_n and C_d, which, are essentially simplifications of aerodynamic resistance and surface resistance. They state in the report that for the review process the equation was tested at 49 sites across the USA and was found to be reliable. They recommend its use for calculating a reference evaporation and in turn crop coefficients. The document is very comprehensive and provides guidelines on data integrity, missing data, time steps and crop coefficients.

These continued efforts and developments have contributed to the growing popularity of the ASCE-EWRI Penman-Monteith equation in becoming an industry standard. Authors such as Gavilan *et al.* (2006) use it as a benchmark against which to measure the performance of new methods, indicating the status and reliability that it has achieved.

Campbell Scientific (1999, Logan, Utah, USA) has incorporated the ASCE-EWRI version of the Penman-Monteith equation into their hard coded calculations available in a program builder called Shortcut. An Application Note is available on-line at: ftp://ftp.campbellsci.com/pub/outgoing/apnotes/evap.pdf which discusses how the different components of the equation are derived. This Application Note is however a reference to the Penman-Monteith method based on FAO-56 guidelines and has not been updated to meet the ASCE-EWRI protocols. For the CR10X and CR23X loggers, the instructions are generated in the program and the methodology can be followed. For the newer CRBasic loggers such as the CR200, CR1000 and CR3000, the methodology has been updated to use the ASCE-EWRI protocols. The instruction consists of two lines of code and the user is not able to see the calculations and methodology employed in calculating the ET_{sz}.

It should be noted that the two time-steps available (hourly and daily) to output ET_{sz} at, use different solutions. The result is that the hourly data summed for a day is unlikely to equal the daily result. An example of this is presented in Chapter 6.

Two options are available to the user depending on how solar irradiance is measured. The more accurate calculation is possible if net irradiance is measured. If only solar irradiance is measured then the net irradiance is estimated using the reflection coefficient of the earth's surface and the estimated infrared components.

4. A Review of Large Aperture Scintillometry

4.1. Introduction

A scintillometer is an instrument designed for optically measuring the path-averaged structure parameter of the refractive index of air (C_n^2) over horizontal path lengths. It consists of a transmitter or light source of known wavelength directed towards a receiver. A receiver measures intensity fluctuations in the beam from the transmitter. These fluctuations are called scintillations and are caused as a result of weak refractive scattering by turbulent eddies between the transmitter and the receiver. Changes in air temperature, water vapour pressure and to a lesser extent changes in atmospheric pressure, change the refractive index of air, causing scattering. The refractive scattering is produced by atmospheric perturbations caused by fluctuations in sensible heat and latent energy that refract the light beam. The structure parameter of the refractive index of air (C_n^2) is thus a measure of the turbulent strength of the atmosphere causing scintillations of the light beam from the transmitter. A simple illustration of scintillations is the twinkling of a star at night. The light source of a star is constant but appears to the viewer to flicker due to turbulence in the earth's atmosphere.

de Bruin (2002) writes a concise overview describing the renaissance of scintillometry. He comments on the emergence of scintillometry in the 1960s, and the impressive progress made in the 1970s on understanding the theory of turbulence in the atmosphere which is the foundation of scintillometry. He mentions some of the defining contributions including reviews by Andreas (1990) documenting some of the significant milestones in scintillometry. There was however reduced interest shown in the 1980s and 1990s but there has since been a renewed interest in the 21st century. He does not elaborate on the reasons for these cycles which took place but they are likely to be as a result of a number of factors. The advances and advantages of the scintillometer are discussed later in this document and provide some of the possible reasons for this revival.

There are a number of different types of scintillometers. The large aperture scintillometer (LAS) was developed in the 1970s (Wang *et al.*, 1978). It is not only used to measure C_n^2, but also wind speed across the path of the scintillometer (Ochs *et al.*, 1976), rain rates and drop size distributions (Hill, 1992) and inner scale turbulence (Hartogenesis *et al.*, 2002). The LAS is defined by the size of the aperture, which is 0.152 mm, and the optical wavelength of 880 nm. Savage *et al.* (2004) describe the theory of the Fresnel Zone explaining the difference between the Surface Layer Scintillometers (SLS), the LAS, and the Boundary Layer Scintillometer (BLS). The SLS has a small aperture and is sensitive to small eddies of about 12.9 mm which would occur closer to the ground surface. It has a pathlength of 80 to 250 m. The LAS is sensitive to eddies of about 68.6 mm and can operate between 2.5 and 4.5 km. The BLS is sensitive to eddies up to 93.8 mm and operates at path lengths in the 0.5 to 8 km range (Savage *et al.*, 2004; Kipp and Zonen, 2007; Odhiambo, 2007). This chapter will focus on the LAS method.

4.2. Principles of Scintillometry

The theory of scintillometry has developed through the decades but the concepts and ideas were worked on by scientists such as Tatarskii (1961) who performed work on 'Wave propagation in a turbulent medium' and Monin and Obukhov (1954) who investigated the 'Basic laws of turbulent mixing in the ground layer of the atmosphere'. It has developed as a complex subject requiring a good understanding of electromagnetic wave propagation, the structure of the atmosphere and meteorology to mention a few. An attempt is made here to give a review of the principles involved in the derivation of the sensible heat flux (F_h) using LAS data.

The receiver is connected to a logging device which is sensitive to the structure parameter of the refractive index of air, C_n^2. This is in turn linked to the structure function parameter for air temperature, C_T^2 which is then linked to a derivation of the sensible heat flux. The parameter C_n^2 can be seen as the 'turbulent strength' of the atmosphere which describes the ability of the

atmosphere to transport scalars such as sensible heat flux, latent energy flux and to a lesser extent dust and gases.

The theoretical description of the LAS was first given by Wang et al. (1978) in which they derived an expression relating the variance of the logarithm of the intensity fluctuations of the measured light intensity, $\sigma^2_{\ln I,}$ to the structure parameter of the refractive index of air, C_n^2 where:

$$C_n^2 = 1.12\,\sigma_{\ln I}^2\, D^{\frac{7}{3}}\, L^{-3} \qquad 4.1$$

where D is the aperture diameter (m), and L is the beam path length (m).

Air temperature, humidity and to a lesser extent atmospheric pressure fluctuations cause air density fluctuations which result in fluctuations in C_n^2. In this way C_n^2 is divided into the structure parameters of temperature (C_T^2), relative humidity ($C_Q{}^2$) and a covariant term C_{TQ}. As a simplification, Wesley (1976) showed that for a LAS, operating at a near-infrared wave length, C_n^2 is related to $C_T{}^2$ as follows:

$$C_T^2 = C_n^2 \left(\frac{T^2}{-0.78\times10^{-6} P} \right)^2 \left(1 + \frac{0.03}{\beta} \right)^{-2} \qquad 4.2$$

where C_T^2 is the structure parameter of temperature, T is the absolute air temperature (K), P is the atmospheric pressure (kPa), and β is the Bowen ratio. The Bowen ratio is commonly used in micrometeorology and is defined as:

$$\beta = \frac{F_h}{L_v F_w} \qquad 4.3$$

The final step in the determination of F_h is to establish the link with C_T^2. This link is derived from the Monin-Obukhov Similarity Theory (MOST) (Wyngaard *et al.*, 1971). Only the unstable solution will be considered for which the Obukhov length (L_{Ob}) is negative:

$$\frac{C_T^2(Z_{LAS}-d)^{2/3}}{T_*^2} = f_T(\frac{Z_{LAS}-d}{L_{Ob}}) \qquad 4.4$$

where Z_{LAS} is the effective height of the scintillometer beam above the surface taking the sensitivity distribution of the beam, topography and vegetation height into account(m), d is the zero plane displacement height (m), T_* is the temperature scale of turbulence (K) and f_T is the universal stability function.

Savage *et al.* (2004) quotes a definition of L_{Ob} by Obukhov (1946), its originator, as 'the characteristic height of the sublayer of dynamic turbulence'. They further state that the relevance of this is that L_{Ob} represents the thickness of the layer of dynamic influence near the surface in which shear or friction effects are always important. They also provide estimates of L_{Ob} based on windless days, convective days and night conditions. Meijninger *et al.* (2002) defines L_{Ob} mathematically as:

$$L_{Ob} = \frac{u_*^2 T}{gkT_*} \qquad 4.5$$

$$\text{where } T_* = \frac{-F_h}{\rho_a c_p u_*} \qquad 4.6$$

$$\text{and } u_* = \frac{ku}{\ln\left(\frac{z-d}{z_o}\right) - \psi_m\left(\frac{z-d}{L_{Ob}}\right)} \qquad 4.7$$

where u_* is the friction velocity (m s^{-1}), g is the gravitational acceleration (m s^{-2}), k is the von Karman constant, u is the horizontal wind speed (m s^{-1}), z is the height of the wind speed measurement (m), z_o is the roughness length (m) [≈

0.1 times the canopy height], and Ψ_m is the Businger-Dyer correction for stability.

Ayra (2001) describes how the similarity hypothesis was first proposed by Monin and Obukhov in 1954. They deduced that in a horizontally homogeneous surface layer, the mean flow and turbulent properties are dependant on four independent variables namely: the height above the surface (z), the friction velocity (u_*), the surface kinematic heat flux ($F_h/\rho_a c_p$), and the buoyancy variable (g/T_o) where T_o is the surface temperature.

The following assumptions are made in the similarity hypothesis (Ayra, 2001):

- flow is horizontally homogeneous and quasistationary,
- the turbulent fluxes of momentum and heat are independent of height,
- the molecular exchanges are insignificant in comparison with turbulent exchanges,
- the rotational effects can be ignored in the surface layer and
- the influence of surface roughness, boundary layer height and geostrophic winds is fully accounted for through u_*.

In summary, C_n^2 data together with air temperature, wind speed, surface roughness and displacement height, are used to calculate F_h by solving the equations above iteratively for a known function f_T. The instruction manual to the Kipp and Zonen LAS provides a comprehensive flowchart description of the steps followed in deriving F_h from LAS measurements.

When the LAS is installed relatively high (greater than 10 m) above the surface and the contribution of friction velocity is relatively small, the free convection method can be applied:

$$F_{h(free)} = \rho_a \, c_p \, b \left(Z_{LAS} - d\right)\left(\frac{g}{T}\right)^{\frac{1}{2}} \left(C_T^2\right)^{\frac{3}{4}} \qquad 4.8$$

where $F_{h(free)}$ is the sensible heat flux derived using the free convection method (W m^{-2}), and b is an empirical constant of approximately 0.48.

The Kipp and Zonen LAS manual lists the data required to compute sensible heat flux:

- mean of C_n^2 (measured as UCN2 on the logger-Appendix A),
- mean of signal strength (Udemod),
- variance of signal strength,
- path length,
- effective beam height,
- zero displacement height,
- atmospheric pressure,
- air temperature,
- horizontal wind speed,
- Bowen ratio,
- height of anemometer and
- surface roughness.

4.3. Structure of the Atmosphere and the Application of the Monin-Obukhov Similarity Theory (MOST)

An understanding of the structure of the atmosphere is critical as MOST is only applicable under certain conditions. Savage *et al.* (2004) describe the structure of the atmosphere and comment on the ambiguity of terminology in the literature regarding the various layers.

The planetary boundary layer (PBL) is the air surrounding the earth which is significantly affected by the earth's surface and within which exchanges of momentum, heat and mass occur. The Surface Layer (SL) is the lowest 10% of the PBL. In the SL, the variation of fluxes is considered negligible with respect to their value at the surface. This means that fluxes measured at a level in the SL can be considered representative of the exchange processes happening between the earth's surface and the atmosphere.

The SL is divided into the Roughness Sublayer (RS) and the Constant Flux Layer (CFL). The RS is the layer influenced by the features such as trees and buildings. In the CFL the fluxes are assumed to be horizontally and vertically constant due to turbulent mixing. This is the layer in which the theory of MOST can be applied and dictates the heights at which a scintillometer system should be installed. To avoid measurement within the RS an estimate can be derived for the size, form and distribution of the roughness elements.

The application of MOST, even in the CFL involves assumptions and has been a subject of much controversy. Foken (2006) describes the development of MOST over the last 50 years and states that although there are many assumptions and possible faults with the early work, modern instruments and error checking have improved accuracies. Despite this, Foken (2006) states that it is only applicable under ideal conditions and the theory only has an accuracy of 10 to 20%.

4.4. Heterogeneous Surfaces and the boundaries of the Monin-Obukhov Similarity Theory (MOST)

Theoretically, MOST only applies over level homogenous surfaces with no advection (Savage *et al.*, 2004). One of the distinctions and advantages of the LAS over point methods available to estimate the sensible heat flux is that the LAS measures an area-averaged flux and can be used over heterogeneous surfaces due to the theory of blending height. Meijninger *et al.* (2002) puts forward a useful explanation of blending height. Over heterogeneous areas with different surface roughnesses, separate inner boundary layers (IBLs) develop within the SL. Assuming the horizontal extent of the patches is relatively small, the top of each IBL becomes diffuse at its upper limit within the SL. At a certain level above the top of the IBLs, the signatures of the individual patches merge due to turbulent mixing. This height is referred to as the blending height. Above the blending height an area-averaged surface flux of sensible heat will be measured provided the LAS beam is still in the SL. Below the blending height, fluxes from individual patches will be measured. In this case turbulence is not in equilibrium and MOST may be violated. A number of studies have been undertaken over heterogeneous terrain using a

LAS (Beyrick *et al.*, 2002; Meijninger *et al.*, 2002; Meijninger *et al*., 2006). In a study by Ezzahar *et al.* (2006), a LAS was used over heterogeneous grids and compared to results from an eddy covariance system. The results of sensible heat flux were in good agreement suggesting that there is only a small violation of MOST and that a LAS can be used below the blending height. This is very important since placement of a scintillometer with its beam height above the blending height can be costly and restrictive.

Hoedjes *et al.* (2002) used a LAS under conditions of advection of dry air over irrigated areas. In this case, the energy flux used for evaporation exceeds net irradiance at times but it was found that MOST still applies under daytime unstable conditions where net irradiance is positive. MOST was only violated close to near-neutral conditions. This provides evidence that the LAS measurements based on the theory of MOST can provide estimates of sensible heat flux beyond the theoretical boundaries of MOST. This makes the LAS a suitable instrument of choice for the measurement of sensible heat flux in non-ideal situations and is a distinct advantage of the instrument.

4.5. Determination of Effective Height (Z_{LAS})

The ability of the LAS to determine fluxes at large scales is particularly attractive to modellers who need area average fluxes for input or verification purposes. Hydrological studies often need fluxes at catchment scales and remote sensing techniques need fluxes at satellite pixel scale. As discussed in the previous chapter, scintillometers are therefore often used over heterogeneous and non-flat terrain where non-ideal situations are encountered and are still able to provide good estimates of sensible heat flux despite non-ideal conditions.

Across a long pathlength the LAS may be installed over valleys or between mountains or buildings which may result in a slanted scintillometer beam. Where a scintillometer beam height varies or is slanted, the measurements represent not only a horizontal, but also a vertical average of C_T^2. The average height of the beam across the pathlength does not represent the height of the

vertically averaged C_T^2 because C_T^2 does not vary linearly with height. To complicate matters further, the sensitivity of the scintillometer is weighted towards the middle of the beam for an equally-sized transmitter and receiver according to a normalised weighting function *G(u)* discussed below.

These conditions of slanted beams over uneven topography give rise to difficulty in estimating the height of the scintillometer beam above the surface (Z_{LAS}). Hartogensis *et al.* (2003) stress the sensitivity of F_h to Z_{LAS} under unstable conditions. They show that for free convection conditions, a relative error in Z_{LAS} causes an equal relative error in F_h. For neutral conditions, a relative error in F_h due to Z_{LAS} is half the relative error in Z_{LAS}. The fact that F_h is so sensitive to Z_{LAS} shows the importance of determining Z_{LAS} as accurately as possible where the LAS beam is not at a constant height above the ground.

Hartogensis *et al.* (2003) was able to derive a lengthy equation for effective height, but was able to simplify it for certain conditions if the variation along the path is relatively small. The original equation can be simplified in three ways according to site and temporal conditions. The first considers either neutral or free convection conditions. For the effective height of the beam for free convection, Z_{eff_Fc} (m), for which $Z_{LAS}/L_{Ob} \rightarrow \infty$, is defined by:

$$Z_{eff\_Fc} = \left(\int_0^1 Z(u)^{-\frac{4}{3}} G(u)\, du \right)^{-\frac{3}{4}} \qquad 4.9$$

where *Z(u)* is the scintillometer beam height along the path (m), *G(u)* is the weighting function describing the contribution of $C_T^2(u)$ at each point along the normalised path, *u*, to the total LAS weighted C_T^2.

For the neutral case ($Z_{LAS}/L_{Ob} \rightarrow 0$):

$$Z_{eff\_Fc} = \left(\int_0^1 Z(u)^{-\frac{2}{3}}\ G(u)\, du \right)^{-\frac{3}{2}} \qquad 4.10$$

In the second approximation by Hartogensis *et al*. (2003), the influences of stability and height dependency of the original equation are assumed negligible and in the calculation of $Z_{eff\_WeightAvg}$, $Z(u)$ is weighted with weighting function $G(u)$:

$$Z_{eff\_WeightAvg} = \int_0^1 Z(u)\ G(u)\ du \qquad 4.11$$

In the third approximation by Hartogensis *et al*. (2003), the scintillometer weighting function, $G(u)$ is left out of consideration leaving:

$$Z_{eff\_Avg} = \int_0^1 Z(u)\ du \qquad 4.12$$

Meijninger (*pers. comm*., 2007) recommends that the effective height should be obtained from an average of the results from Eqs. 4.11 and 4.12.

4.6. Roughness Length and Zero Plane Displacement

A number of the equations involving MOST require estimates of the zero plane displacement (Eq. 4.4) and roughness length (Eq. 4.7). These parameters are usually found by fitting a logarithmic wind profile equation to measured wind profiles. Monteith and Unsworth (1990) state that it is widely accepted that the horizontal wind speed variation with vertical height under neutral stability obeys the semi-logarithmic law:

$$\frac{u_z}{u_*} = \frac{1}{k}\ln\left(\frac{z-d}{z_0}\right) \qquad 4.13$$

where u_z is the horizontal wind speed at height z (m s^{-1}).

Using Eq. 4.13, Rosenberg *et al.* (1983) describes how it is possible to solve for d and z_o with wind profile measurements. Measuring wind profiles is, however, inconvenient especially at a catchment scale where roughness length and zero plane displacement heights are variable. For this reason attempts have been made to relate them to easily measurable properties of the earth's surface. Early attempts were made to define them according to a fraction of the vegetation height. Typically it was found that $z_o = 0.13$ h and $d = 0.66\ h$, where h is the average height of the vegetation (Verhoef *et al.*, 1997). More recently Kipp and Zonen (2007) recommend values of 0.10 h and 0.67 h for surface roughness and zero plane displacement, respectively. It is, however, clear that the plant height is not the only contributing factor and that the structure and distribution of the vegetation such as in sparse canopies or row crops for example, will also contribute to roughness length and displacement height.

4.6.1. Roughness Length

The roughness length is an expression that describes the aerodynamic roughness of the earth's surface. It is dependant on the height of the roughness elements as well as the distribution. Guidelines can be found in Table 4.1 (Weiringa, 1998), but it is reported by Kipp and Zonen (2007) that over homogenous surfaces the rule of thumb, $z_0 = 0.10\ h$, is sufficiently accurate (Kipp and Zonen, 2007).

4.6.2. Zero Plane Displacement

Zero plane displacement indicates the mean level at which momentum is absorbed by the individual elements of the plant. It is thus the height at which the top of the roughness elements on the earth's surface, if packed closely together, begin to act like a displaced surface and the wind speed is zero.

The ratio of d/h depends on the spacing of the roughness elements and on the ratio of the accumulated area of each element to a unit area of the underlying surface (Rosenberg *et al.*, 1983). Estimation of d is complicated by the fact that plants adjust to the mechanical force of the wind. The roughness elements

bend with the wind and become more streamlined depending on the strength of the wind thus changing the zero plane displacement height.

A number of studies suggest various methods for determining zero plane displacement using wind profiles (Riou, 1984; Zoumakis, 1992; Takagi *et al.*, 2003) and Zhang *et al.* (1999) suggest a method using air temperature fluctuations. Savage *et al.* (2004) describe a method of determining *d* based on single level measurements of the standard deviation of the vertical wind speed and sensible heat flux density and Kanda *et al.* (2002) describe a method of determining *d* over an urban environment using two scintillometers simultaneously at two different heights. Practically, *d* is a parameter that can be difficult to derive and is one of the biggest potential problem areas (except for short vegetation or for cases where the measurement height greatly exceeds *d*) when applying MOST (Foken, 2006).

Table 4.1. The eight different terrain classifications and their typical roughness length (Wieringa, 1998).

Surface classification	**Roughness length z_o (m)**	**Landscape features where *h* is the vegetation height**
Sea	0.0002	Open water, snow with fetch above 3 km
Smooth	0.0050	Featureless land, ice
Open	0.0300	Flat terrain with grass or very low vegetation
Roughly open	0.1000	Cultivated area, low crops, separated by distance of 20 *h*
Rough	0.2500	Open landscape, scattered shelter belts, obstacles separated by 15 *h*
Very rough	0.5000	Landscape with bushes, young dense forest separated by 10 *h*
Closed	1.0000	Open spaces separated by *h* such as a mature forest or low-rise built up area
Chaotic	>2.0000	Irregular distribution of large elements such as a city centre or large forest with clearings

A number of studies suggest various methods for determining zero plane displacement using wind profiles (Riou, 1984; Zoumakis, 1992; Takagi *et al.*, 2003) and Zhang *et al.* (1999) suggest a method using air temperature fluctuations. Savage *et al.* (2004) describe a method of determining *d* based on single level measurements of the standard deviation of the vertical wind speed and sensible heat flux density and Kanda *et al.* (2002) describe a method of determining *d* over an urban environment using two scintillometers simultaneously at two different heights. Practically, *d* is a parameter that can be difficult to derive and is one of the biggest potential problem areas (except for short vegetation or for cases where the measurement height greatly exceeds *d*) when applying MOST (Foken, 2006).

4.7. Footprint Concept Applied to the LAS

Meijninger *et al.* (2002) describes the footprint concept as relevant when measurements are conducted below the blending height over heterogeneous terrain. A portion of the surface in an upwind direction will influence the measurements. The footprint model applies to scintillometry in the same way in which fetch applies to point measurements and Savage *et al.* (2004) describe the relationship between the upwind fetch, the canopy height and the greatest height that sensors should be mounted.

The footprint model is a useful tool to determine the source areas for the turbulent fluxes. It can be interpreted as the field of view of the instrument. There are a number of footprint models available and Meijninger *et al.* (2002) uses the model of Horst and Weil (1992) which depends on measurement height, surface roughness and atmospheric stability. The Lagrangian footprint model is commonly used and gives as output, the contribution of any upwind surface flux, to the measured flux at some point downwind at a certain height (Meijninger *et al.*, 2002). It is easy to conceptualise that, when advection occurs, the higher the scintillometer, the further away is the contributing surface area to the measurements.

4.8. Saturation

A scintillometer can only yield meaningful data under weak scintillating conditions (Savage *et al.*, 2004). In order to prevent saturation, C_n^2 must remain below a certain threshold. Saturation occurs when the scintillation intensity rises above the limit of the theory. When this occurs, the relationship between the scintillations and the structure parameter of the refractive index of air fails (Kohsiek *et al.*, 2005).

In order to avoid saturation, pathlength and measured height are the only variables that can be adjusted. More scintillations are observed as the pathlength increases. More scintillations are also observed nearer the earth's surface. The correct combination of pathlength and height need to be reached in order for the scintillations to be below the saturation criteria. Kipp and Zonen (2007) present the minimum installation height for the LAS as a function of path length. In addition, in dry air F_h is large resulting in higher C_n^2 values. This should be considered if an installation is starting to approach a condition where saturation may occur.

Kohsiek *et al.* (2005) investigate saturation of a LAS over a 10 km pathlength. They applied two methods of correction to saturated LAS data and compared to eddy covariance measurements. They found that the method according to the theory of Hill and Clifford (1981) gave satisfying results. Despite these findings, the correction of saturation does increase the potential for errors in the results and should be avoided.

4.9. Advantages and Disadvantages of Scintillometry

Advantages of scintillometry over other methods used to measure sensible heat flux include:

- scintillometer measurements are insensitive to flow distortions around the instrument,

- an area averaged estimate is made rather than a point measurement, enabling a comparison with meteorological models and remote sensing satellites,
- point based measurements based on MOST require horizontal homogeneity which is not always practical in a real world situation,
- the LAS provides an aerially averaged sensible heat flux over a heterogeneous surface using the concept of blending height and has been shown to give energy balance closure (Foken *et al.*, 2006b),
- there are no moving parts that can wear out mechanically,
- Bowen ratio and eddy covariance measurements are very sensitive to sensor height, whereas the LAS installation has fewer constraints regarding beam height, and
- scintillometry gives statistically more reliable data than other methods (Chehbouni *et al.*, 1998).

Disadvantages include:

- LAS measurements alone do not allow a differentiation to be made between stable and unstable atmospheric conditions and the direction of F_h. This can be achieved by using a sonic anemometer or two air temperature measurements at two different heights in the boundary layer,
- a number of assumptions are made in the derivation of Eq. 4.1, and
- the cost of the instrument and the mounting of the transmitter and receiver units as well as the maintenance are significant. A LAS can currently be purchased for approximately R400 000.

5. Materials and Methods

5.1. Description and location of the Two Streams area

The Two Streams catchment is situated 70 km from Pietermaritzburg, KwaZulu-Natal, South Africa near Seven Oaks on the Greytown road (29.21º East, 30.65º South). The Bioregion is 'midlands mistbelt grassland'. The area is generally hilly with rolling landscapes and a high percentage of arable land. It is dominated by forb-rich, tall sour *Themeda triandra* grasslands of which only a few patches remain due to invasion of native *Aristida junciform.* Soil forms are apedal and plinthic and are derived mainly from the Ecca Group with dolerite dykes and sills. Rainfall is primarily in summer with an annual rainfall ranging from 730 to 1280 mm. Rain is most commonly from summer thunderstorms or cold fronts. Mist can be heavy and frequent and can add significantly to precipitation. Moderate frosts, droughts, hail and berg winds are also common to the area (Mucina and Rutherford, 2006).

5.2. Site Descriptions

5.2.1. ASCE-EWRI Automatic Weather Station (AWS)

The site requirements for a weather station used to estimate the reference evaporation are clearly expressed in the literature (Allen *et al.*, 2006). A suitable site requires an area with at least 50 m of short grass in all directions and similar vegetation beyond that. The Two Streams catchment is intensively farmed with sugarcane and commercial forestry leaving a limited number of potential sites in the vicinity. A suitable area was found approximately 1 km from the main scintillometer site with a suitably extensive area of kikuyu grass (Figs 5.1 and 5.2). The area was fenced to protect the station against cattle and the grass was kept at reasonable length.

Fig. 5.1. The AWS site at Two Streams.

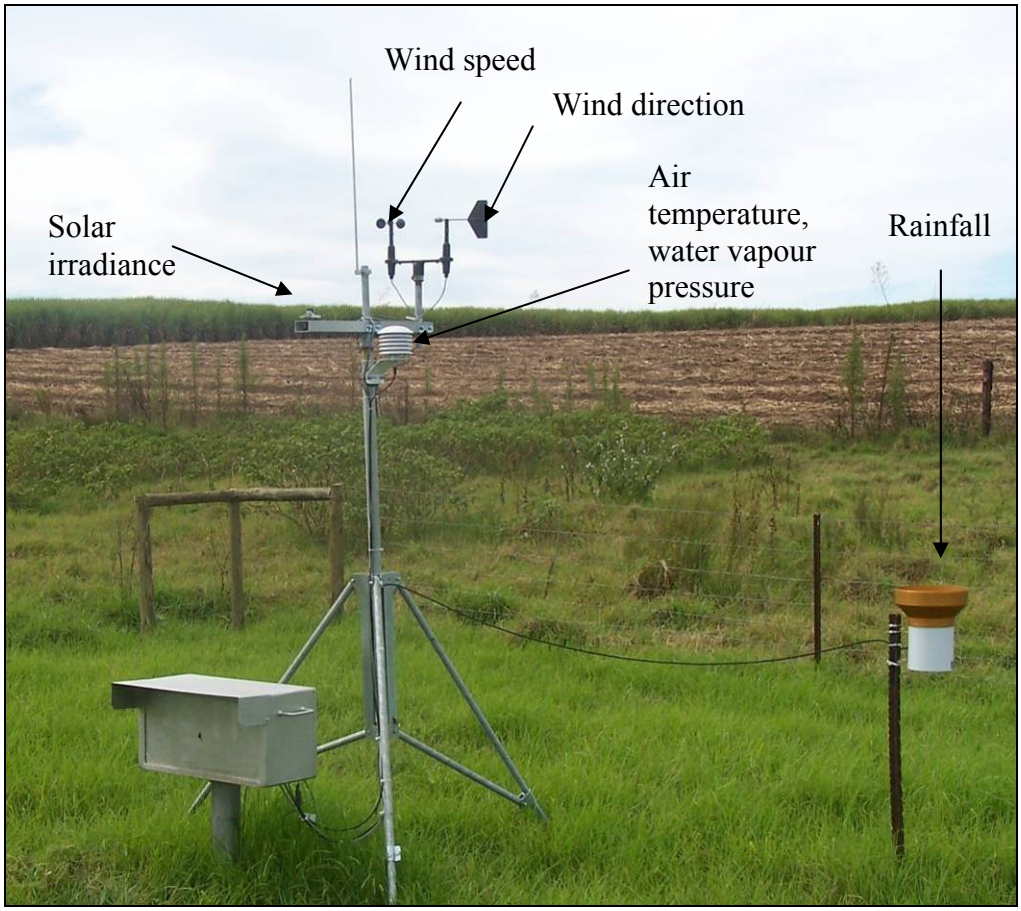

Fig. 5.2. The AWS sensors.

5.2.2. Scintillometer Transect

The LAS can operate at a minimum pathlength of 250 m and up to distances of 4500 m. At the Two Streams site, a suitable location was found with a pathlength of 575 m with an East-West orientation. The six hectare compartment was fallow and about to be planted to *A. mearnsii* which suited the purpose of the project. The fetch in the predominant wind directions, South-East and North-West, was 1 km and 0.5 km respectively. The surrounding areas are also planted to *A. mearnsii* but are at different stages in their development. The site is also close to existing installations including raingauges and gauging weirs.

The topography of the transect was suitable as the beam would be high enough above the surface to avoid saturation, although not high enough to use the free convective solution (Eq. 4.8). A trimble GPS was used to derive a topographical profile description of the site (Fig. 5.3).

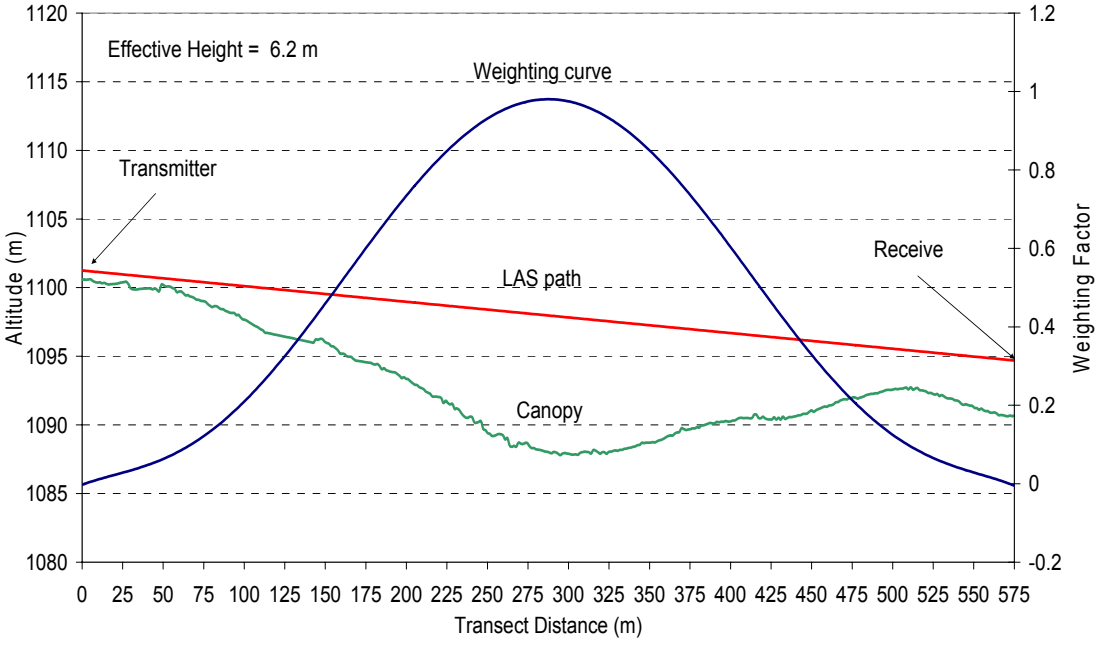

Fig. 5.3. Topographical profile of the canopy surface along the LAS transect; also showing the path of the scintillometer beam and the normalised weighting curve used in the calculation of effective height.

5.2.3. Energy Balance Weather Station

An additional weather station was required to complement the LAS data. In order to obtain representative measurements of the conditions along the transect, the station was sited at the centre of the transect. Initially, while the crop was very short the sensors were mounted on a standard weather station tripod at a height of 2 m. As the crop grew, it was necessary to raise the sensors and a scaffolding tower was constructed to gain height. It is critical that the wind speed measurements are clear of the tree canopy and as close to the height of the LAS beam as can practically be achieved.

5.3. Equipment and Data Recording

5.3.1. ASCE-EWRI AWS Measurement System

The primary purpose of the AWS was to provide an estimate of the grass reference evaporation. This was calculated from the sensors listed in Table 5.1 using the Campbell Scientific CRBasic programming language. The sensors were controlled and data was stored on a Campbell Scientific CR1000 data logger. A 10 s execution interval was used as sufficiently frequent without drawing excessive power from the battery. Climatic data was stored at 10 min, 20 min, hourly and daily intervals. The short grass reference evaporation was calculated hourly and daily. Table 5.2 shows how outputs were calculated based on the different output instructions.

In addition, dew point, water vapour pressure, saturated water vapour pressure and water vapour pressure deficit were also calculated on the logger using air temperature and relative humidity. These are useful for assessing condensation on the LAS.

Table 5.1. Summary of the sensors and measurements at the automatic weather station.

Measurement	**Sensor**	**Scan rate (s)**	**Height (m)**	**Output interval and units**
Wind speed and wind direction	RM Young wind sentry	10	2	10 min, 20 min, 60 min and daily (m s^{-1})
Relative humidity and air temperature	Vaisala HMP50	10	2	10 min, 20 min, 60 min and daily (%, ºC)
Solar irradiance	LI-200SZ	10	2	10 min , 20 min, 60 min (W m^{-2}) and daily (MJ m^{-2})
Rainfall (0.1 mm resolution)	Texas Instruments raingauge	10	1.2	10 min, 20 min, 60 min and daily (mm)

Table 5.2. Output instructions and output intervals of the automatic weather station data.

Measurement	**10 min, 20 min, hourly output and their units**	**Daily output and units**
Wind speed and direction	Vector average (m s^{-1}, º)	Vector average (m s^{-1}, º)
Air temperature	Average (ºC)	Maximum (ºC), Minimum (ºC)
Relative humidity	Sample (%)	Maximum (%), Minimum (%)
Solar irradiance	Average (W m^{-2})	Totalise (MJ m^{-2})
Rainfall	Totalise (mm)	Totalise (mm)
Battery voltage		Maximum (V), Minimum (V)

5.3.2. The LAS Measurement System

The LAS used at Two Streams was made by Kipp and Zonen and was designed to measure the structure constant of the refractive index of air together with a few basic meteorological observations. The light source of the transmitter operates at a near-infrared wavelength of 880 nm. At this wavelength, the observed scintillations are caused primarily by turbulent temperature fluctuations. In this way, the scintillations measured by the receiver can be related to the sensible heat flux. The carrier beam is 7 kHz and the aperture diameter is 0.152 m. For further information on the theory of scintillometry refer to Chapter 4. Some of the features of the Kipp and Zonen LAS are:

- heated receiver and transmitter windows reduce condensation problems,
- a simple Fresnel lens construction avoids beam obstruction by a transmitting or receiving LED,
- on-board calibration allows rapid and on-site verification of accuracy,
- lightning and surge protection are standard on the transmitter and receiver,
- the infrared light source is safe for eyes,
- 12 VDC power is required, and
- alignment is simplified with pan and tilt adjusters.

The LAS was initially mounted on a single level of scaffolding 3 m above the ground (Fig. 5.4). As the crop increased in height, the transmitter and receiver units were raised to an appropriate height (Fig. 5.5). Further stages of scaffolding were used to raise the LAS. The LAS was mounted inside a safe-box with an opening on one side for the beam. The safe box provides protection from the elements and is also a theft deterrent. The scaffolding was stabilised with steel cables on each corner to prevent any movement of the tower. This is critical, particularly to the transmitter as any movement has an exaggerated affect on the alignment of the beam over the length of the path.

Fig. 5.4. Transmitter at a height of approximately 3 m. The inset (top left) shows the transmitter mounted on a base that allowed easy pan and tilt adjustments.

Fig. 5.5. Receiver at a height of approximately 9 m. The inset (bottom left) shows the receiver signal strength indicated on a needle dial.

Power was supplied by four 100 A h batteries requiring charging at approximately 4 weekly intervals. Fig. 5.6 shows the battery voltage at the receiver over time. Small daily fluctuations occurred due to diurnal temperature fluctuations. A wind generator was used to augment the power although this was not beneficial at the site due to insufficient wind. When the wind blew sufficiently to generate power, the voltage was increased but not significantly enough to extend the time between battery charges.

The current drain of the transmitter increases with path length. For a transect of 575 m, the transmitter current drain was approximately 0.125 A. The receiver current drain was approximately 0.25 A without the internal LAS lens heater connected. The heater draws an additional 1 A and was, for this reason, not connected at the site. The high current drain of the heater units is unfortunate as heat on the lenses would have dried condensed water or rainwater more quickly reducing the loss of data in the early morning. At remote sites where 220 VAC electricity is not available the use of the heaters is not practical due to limited battery power.

A limitation of the LAS is that it does not provide the direction of the sensible heat flux. During the day when conditions are most often unstable, the flux is directed away from the surface as there is heating of the atmosphere. At night when conditions are most often stable, the flux is toward the surface and there is cooling of the atmosphere. For the purpose of this study the flux was assumed to be positive while the net irradiance was positive. This assumption was confirmed during a four week period by mounting two fine-wire thermocouples one above the other separated vertically by 2 m. The air temperature difference showed a positive flux during the day and a negative flux at night.

Alignment of the transmitter and receiver units requires precision and is an iterative process. Rifle telescopes were mounted on each unit to assist. A signal strength meter at the back of the receiver, gives an indication of alignment. The transmitter and receiver units are controlled by panning and tilting the units at both ends until the maximum signal strength is obtained.

Once the rifle telescopes are sighted on well-aligned scintillometers, they can be used very effectively to get the initial alignment at new sites.

The signal strength on the transmitter and path length potentiometer on the receiver was set to appropriate values and the user manual gave an indication of suitable ranges. The path length values on the dial are not in meters but in relative units.

A Campbell Scientific CR23X logger was used to store the data from the receiver LAS. The program for this station is included as Appendix A. The data, based on input measurements every second, were averaged every 10 min and stored in the logger memory.

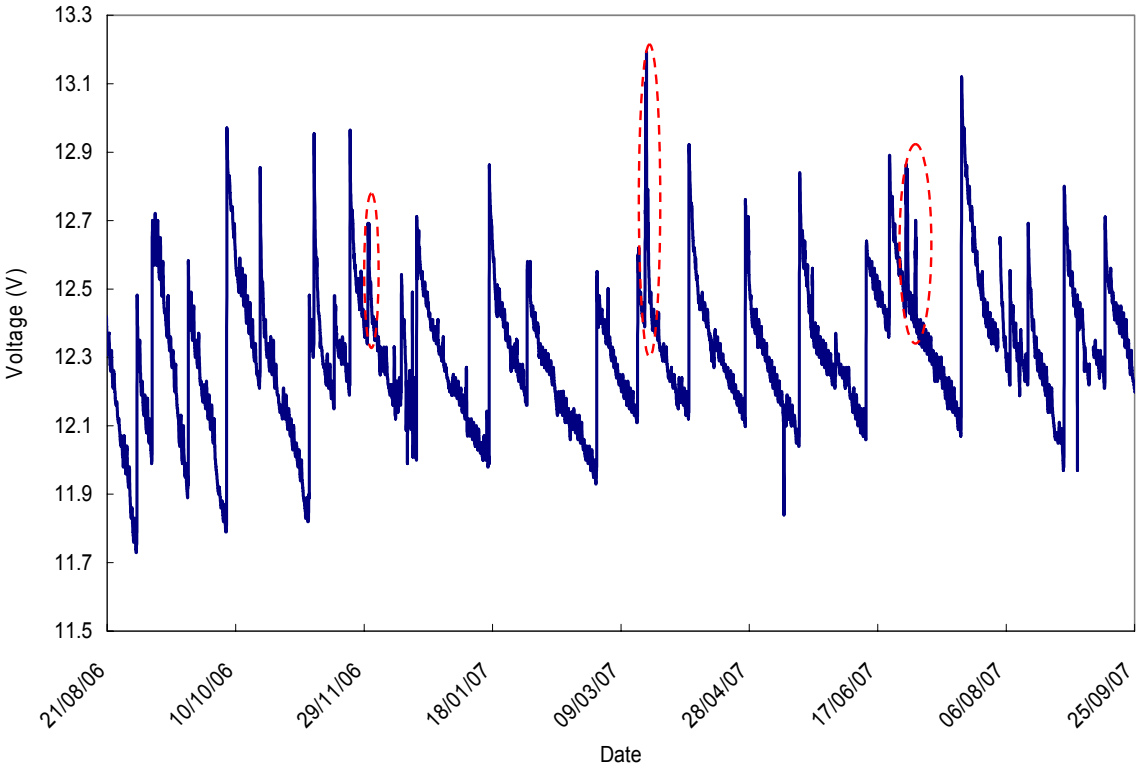

Fig. 5.6. Battery voltage at the LAS receiver site. The impact of the wind generator is indicated by vertical ellipses.

5.3.3. Energy Balance Weather Station

Net irradiance, soil heat flux and horizontal wind speed above the canopy are additional measurements required for the calculation of the latent energy flux using the Winlas software and the shortened energy balance (Eq. 2.1). In addition, wind direction, relative humidity and air temperature were also measured at the site for completeness. Table 5.3 shows the details of the measurements. Height of the sensors above the canopy varied as the trees grew and at various intervals, depending on tree growth rate, the sensors were raised as required.

Table 5.3 Sensors and measurements at the energy balance weather station (scan rate of 10 s and an output interval of 10 min and daily).

Measurement and units	**Sensor**	**Location**
Wind speed (m s^{-1}) and wind direction (º)	RM Young wind sentry	2 m above canopy
Relative humidity (%) and air temperature (ºC)	Vaisala CS500	2 m above canopy
Net irradiance (W m^{-2})	REBS Q*7.1 Net radiometer	2 m above canopy
Soil temperature (ºC)	Soil temperature averaging probes	20 and 60 mm below soil surface
Soil heat flux (W m^{-2})	REBS soil heat flux plates	80 mm below soil surface
Rainfall (0.1 mm resolution)	Texas Instruments raingauge	2 m above canopy

Fig. 5.7 shows the instrumentation of the energy balance weather station site. The instruments required little maintenance in general although it is important to monitor the condition of the Q*7.1 net radiometer domes (also called windshields) especially during months when rain and hail may occur. As the domes become older, they become milky in colour and brittle, indicating that

replacement is necessary. Replacement is most likely on a six month to one year interval. Silica gel in the net radiometer should be replaced when it becomes pink in colour and the o-rings that seal the domes should be in good condition.

In the logger program, net irradiance was modified for horizontal wind speed due to the effect of convective cooling. This was performed dynamically on the measured wind speed. The net radiometer should never be shaded and is normally directed towards north in the southern hemisphere. It must be levelled and checked as the level position can be upset by birds landing on the sensor. This measurement is critical to the energy balance equation as it is the largest component relative to the others and should be determined as accurately as possible.

In the early stages of measurement, the wind speed measurements were made at a height of 2 m. As the tree heights approached 2 m, the wind speed data showed a decline in average wind speed due to friction offered by the trees. Wind speed is critical in the calculation of the sensible heat from the LAS and a method of adjusting the wind speed was sought. The neutral log wind profile equation was used to estimate the wind speed at a higher level.

The soil flux measurements were installed at the base of the tower on the north side to avoid shading from the tower. A representative area was chosen and the sensors were installed as per Fig. 5.8. During installation, minimal disturbance to the surface is necessary to avoid creating a non-representative surface reflection coefficient.

The net irradiance was stored directly in the logger memory. Soil heat flux was calculated using the data from the soil heat flux plates, the soil temperature averaging probes and the Campbell Scientific CS616 volumetric soil-water reflectometer using Eqs 2.6 and 2.7.

Fig. 5.7. The energy balance weather station site.

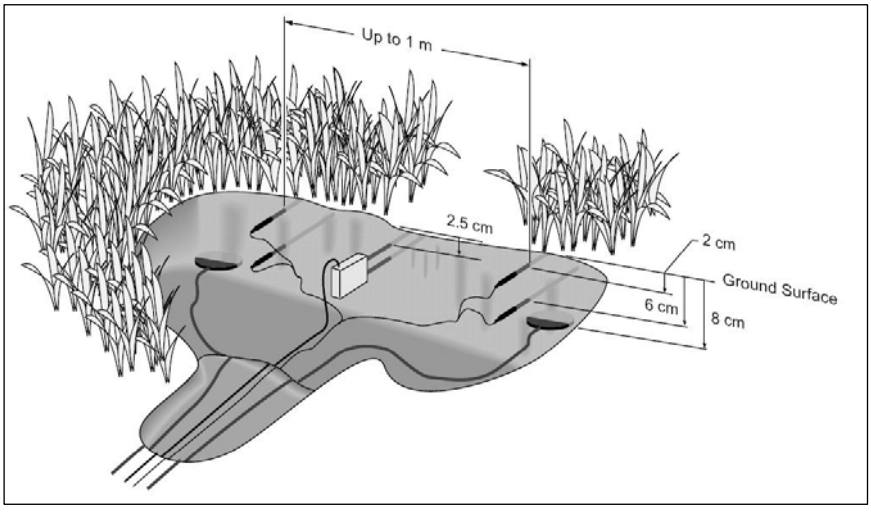

Fig. 5.8. Recommended layout of sensors used to estimate soil heat flux (Campbell, 2003).

5.3.4. Tree Growth

Tree heights as well as stem diameters were sampled along the path length of the scintillometer at monthly intervals. Measurements were taken with a tree height rod every month for the same trees at 30 different sampling points, equally spaced on the LAS transect.

A Li-Cor (Lincoln, Nebraska, USA) LAI-2000 Plant Canopy Analyser was used to measure leaf area index (LAI) to give an indication of tree canopy growth. LAI is the one sided surface area of leaf material per unit area of ground. Direct measurement of LAI is tedious and labour-intensive but Li-Cor have developed an optical sensor that connects to a control unit which is able to estimate LAI based on the canopy architecture. Light readings made below the canopy are divided by readings made above the canopy to compute transmittances at five angles. A control unit records these readings and calculates LAI from the transmittances. There are a number of operating principles and limitations to the use of the LAI-2000 that should be noted. Sky conditions, sky brightness non-uniformity, field of view, canopy conditions and foliage size can cause error and need to be within the specification of the instrument (LAI-2000 Plant Canopy Analyser, 1989). Most critical is that measurements are taken when there is no direct solar irradiance and only diffuse light is recorded. This occurs predawn or post dusk or when the sky is completely cloudy.

As the crop height increased, two plant canopy analysers were used. One was used for below canopy measurements and the other was set to measure above canopy light on scaffolding above the trees. The data files were downloaded to a computer and Li-Cor software was used to merge the two files and calculate a LAI value at each of the 30 sampling points used along the transect.

5.4. Reliability of the Instrumentation

All the datalogging instrumentation was installed carefully according to the supplier's recommendations. Suitable grounding (earthing) was connected to

avoid damage from electrical charges such as lightning but also for accuracy of sensor voltage readings.

A rigorous schedule of routine maintenance and changing of batteries was employed and 37 visits to the site are recorded between 19 August 2006 and 29 September 2007 contributing to the completeness of the data sets.

5.5. Data Analysis

The data analysis of the energy balance weather station as well as that of the ASCE-EWRI weather station required minimal processing and the only calculations required were that of soil heat flux from the data. This was calculated according to Eqs. 2.6, 2.7 and 2.8 from the soil heat flux plates, soil temperature averaging probes and volumetric soil water data. Values for soil bulk density, specific heat capacity of dry soil and specific heat capacity of water were estimated as 1000 kg m^{-3}, 837 J kg^{-1} K^{-1} and 4190 J kg^{-1} K^{-1}, respectively. The data was verified by plotting graphs in order to confirm that the results were reasonable. No further calculation or statistical analysis of the data was required.

The Winlas software is used to process LAS data which is stored on the logger at 10 min intervals. Winlas is able to process either: (1) the structure parameter of the refractive index of air (C_n^2), (2) the output signal from the receiver (U_{CN2}) together with the variance of U_{CN2}, or (3) scaled values of C_n^2 (PU_{CN2}) that have been multiplied by 10^{-15} on the logger as most loggers cannot store the values of C_n^2 because they are so small.

For the Two Streams study PU_{CN2} was used, together with the horizontal wind speed, air temperature, air pressure and Bowen ratio. The software offers the user a number of options regarding ancillary inputs. Constant values of air temperature, relative humidity, air pressure and Bowen ratio can be used if data is not available although some of these reduce the accuracy of the final results of F_h. If a constant value of windspeed is used then Winlas uses the free convection method to calculate the sensible heat flux (Eq. 4.9). For this

study windspeed and temperature data were collected as these have a significant impact on the calculation of sensible heat (Meijninger *et al*, 2000). The data were processed in two week intervals due to the importance of capturing the changes in effective height, roughness length (z_o) and displacement height (d) of the trees over time.

The processed file includes a summary of the input data as well as a stable and unstable solution of sensible heat flux, the free convection solution of sensible heat flux, the friction velocity and the Obukhov length. For the estimation of ET_{LAS}, while the net radiation was positive, the unstable solution of F_h was used and while it was negative, zero evaporation was assumed. In reality it is not this simple and the sensible heat flux data required careful verification and checking, particularly in the early morning and late afternoon when there was a change from stable to unstable conditions or *vice versa*. Typically the first and last few values of F_h for a day were out of range and incorrect and were excluded. In Fig. 5.9, typical values for the unstable solution of F_h have been plotted while the net irradiance is positive. The values indicated by the dashed circles would have been omitted. Data requiring exclusion are easily identified as typically the sensible heat values are in excess of the net radiation for the first few 10 min readings in the morning. They then decrease to a minimum (usually < 5) from where they then begin to climb and can be considered actual values of sensible heat flux. This transition period usually affected the data for about one hour in the morning and evening.

This verification process is performed using net radiation, air temperature and rainfall records. Problems with the ET_{LAS} data are usually associated with mist or rain which is captured in the solar and rainfall data, respectively. During the early morning transition period or when there is mist the values of sensible heat flux are unrealistically high but in actual fact are likely to be close to zero and therefore unrealistic values where reduced to zero. This can however impact on the ET_{LAS} results because then by virtue of using the simplified energy balance equation all the available energy goes into latent energy resulting in elevated ET_{LAS} results for the day. For this reason the process of data collection involved: (1) removing all sensible heat data while net

radiation was negative, (2) reducing all unrealistically high sensible heat values, on a day by day basis, during the early morning and late afternoon, caused by mist or near neutral flux conditions, to zero, (3) excluding all latent energy values while sensible heat flux is zero.

Much of the data in the results chapter are presented graphically, and where required, trend lines have been plotted and a coefficient of determination calculated. Further statistical analysis may reveal more information regarding relationships between different variables but are unnecessary and beyond the scope of this study.

For this study although values for sensible heat flux from the stable solution were excluded, it is also possible to use the stable solution for the determination of night-time values of F_h and hence ET_{LAS}, and this would make a good study in the future.

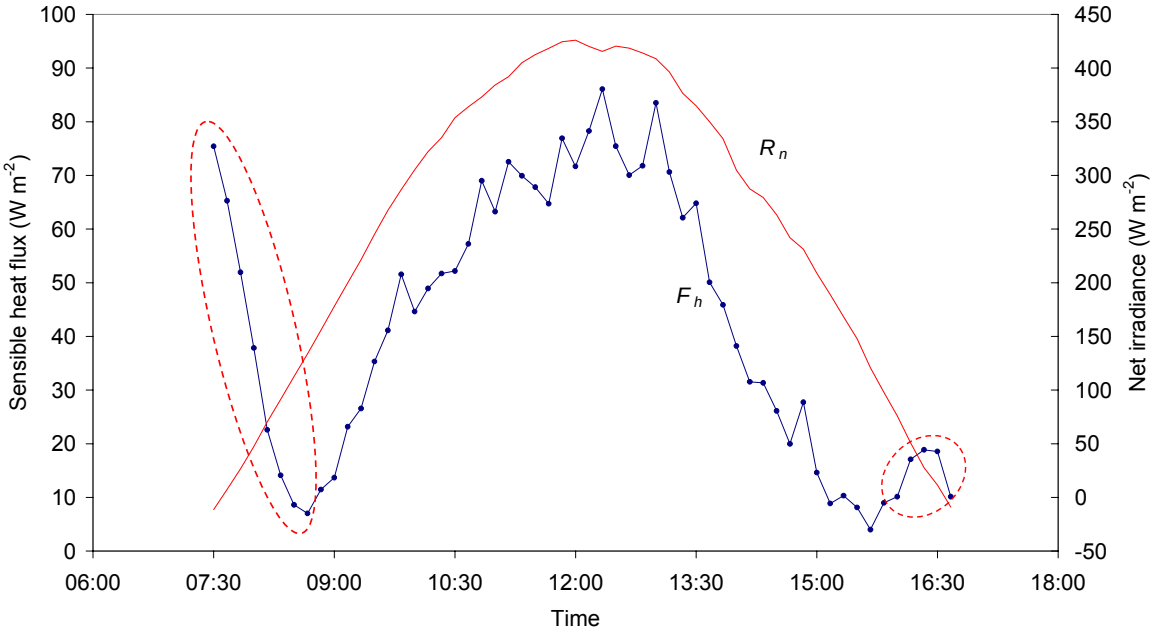

Fig. 5.9. The diurnal variation in net irradiance (R_n) and sensible heat flux (F_h) for 20 July 2007 at Two Streams, showing that the early morning and late afternoon values of sensible heat flux (using the unstable solution) require correction.

6. Results and Discussion

6.1. Plant Growth

Fig. 6.1 shows the tree growth in terms of height and stem diameter over time. Measurements started on the 15 August 2006 with a tree height of 0.28 m. The most recent measurement on 11 October 2007 showed an average tree height of 5.5 m. The growth was fairly consistent over this period and there was no significant seasonal impact visible from the data. This indicated that climatic variables such as rainfall, air temperature and solar irradiance did not limit tree growth significantly at Two Streams. During the early stages in crop growth up to 14 months, the average tree height growth rate was 0.37 m per month or 4.5 m per year.

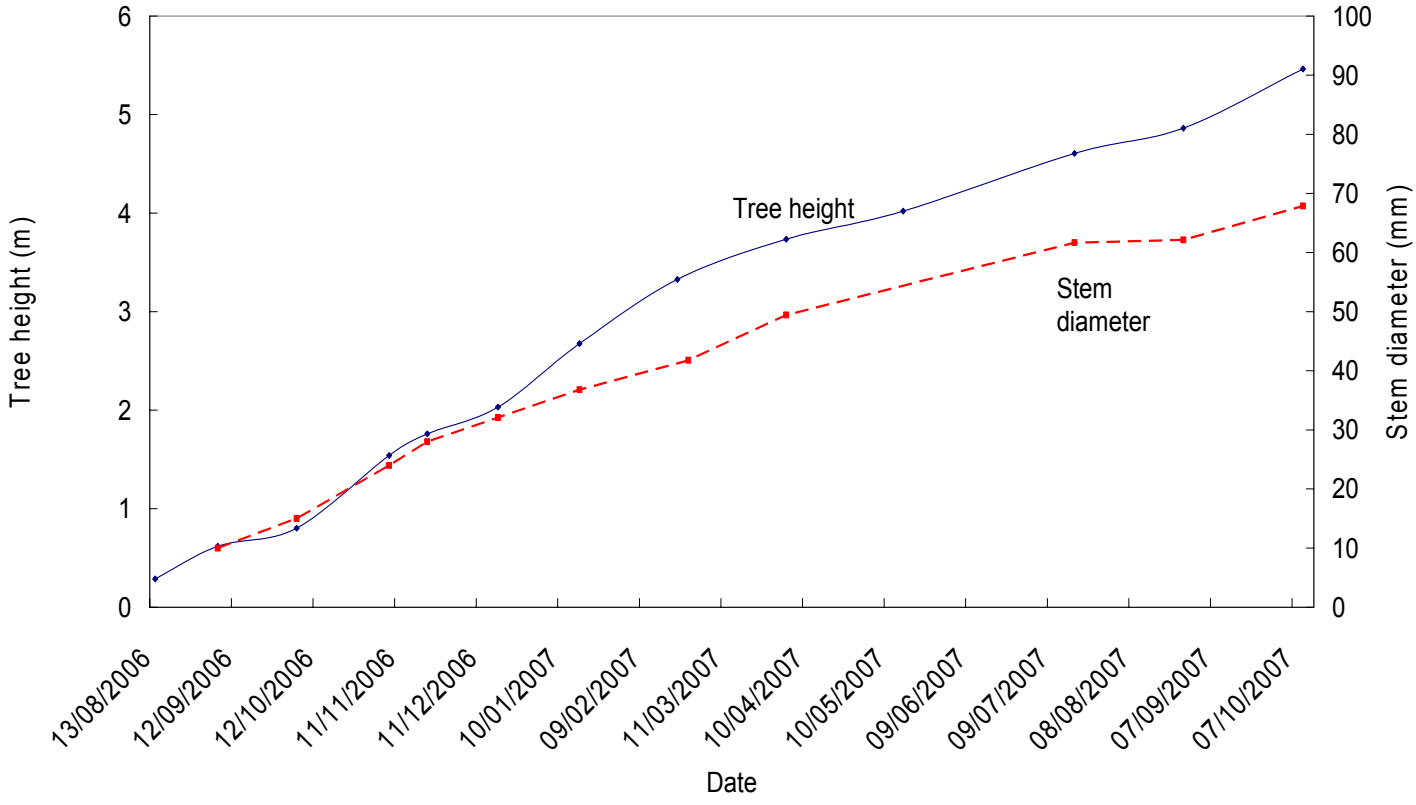

Fig. 6.1. Tree height (m) and stem diameter (mm) growth data.

6.2. Energy Balance Weather Station

Daily net irradiance values on cloudless days reached 21 MJ m^{-2} in summer and 8 MJ m^{-2} in winter indicating a significant reduction in available energy flux in winter (Fig. 6.2). Instantaneous night-time values (data not shown) show a larger surface energy flux away from the surface during winter than in summer, despite the lower solar irradiance in winter. This occurs for a number of reasons including reduced weed cover, clearer skies and cooler air temperatures in winter.

The soil heat flux in Fig. 6.3 showed a noticeable decreasing trend with time. This was due to plant growth and leaf cover shielding the soil surface. Initially, daily day-time values of soil heat flux increased to 3.0 MJ m^{-2} as the summer of 2006/2007 approached and then decreased to approximately 1 MJ m^{-2} as net irradiance decreased in winter and the plant cover became denser.

Of interest in Figs 6.2 and 6.3 is the ratio of the soil heat flux to net irradiance which is calculated in Fig. 6.4 and is assumed to be 0.1 in the daily grass reference evaporation (Penman-Monteith) calculation. When daily net irradiance peaks or troughs, about the end of December and early June respectively, the ratio is about 0.08 to 0.16 indicating that F_s fluctuates significantly during the initial growth cycle of trees. Initially at planting, the ratio of F_s to R_n was at its peak of 0.16 due to soil surface exposure. The ratio dropped until December 2006 to 0.08 due to rapid weed growth. Spraying of the weeds was recorded in December 2006. From this point on the ratio begins to increase again as the leaves of the weeds die off. Again a drop in the ratio is experienced in July 2007 as canopy closure becomes a factor in preventing the solar irradiance from reaching the soil surface.

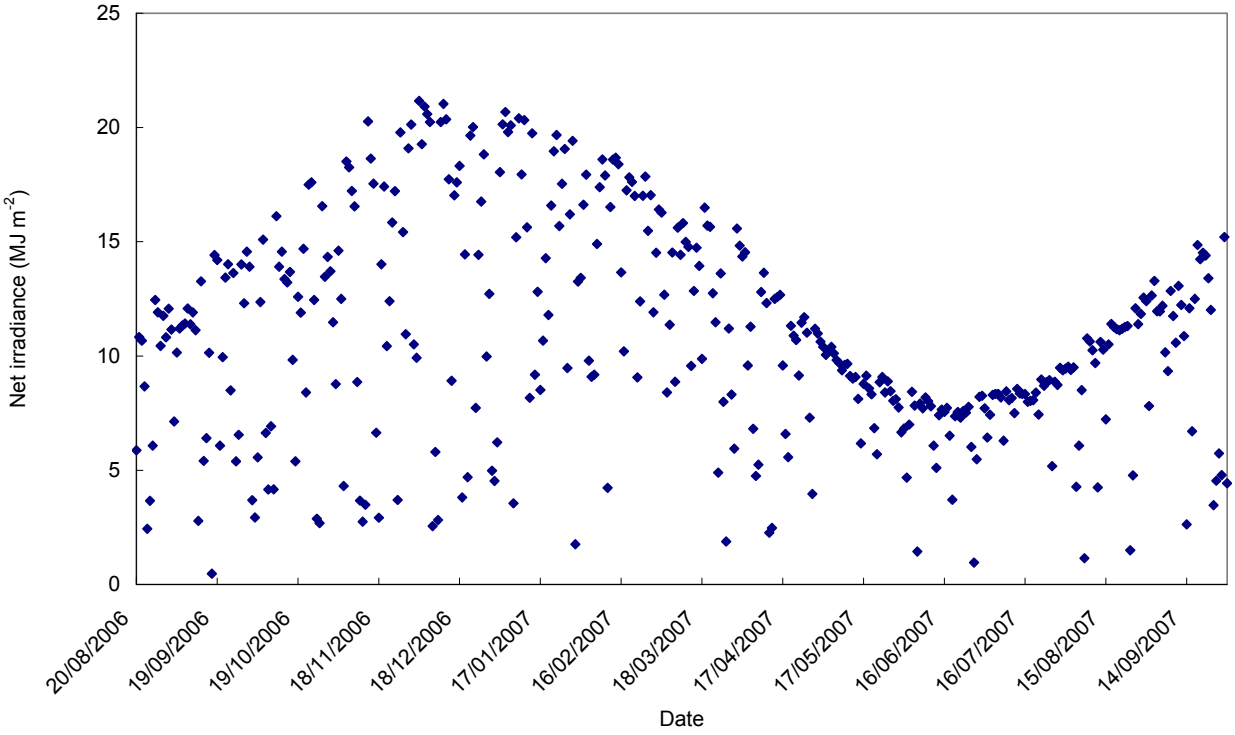

Fig. 6.2. Temporal variation in daily net irradiance for the duration of the experiment.

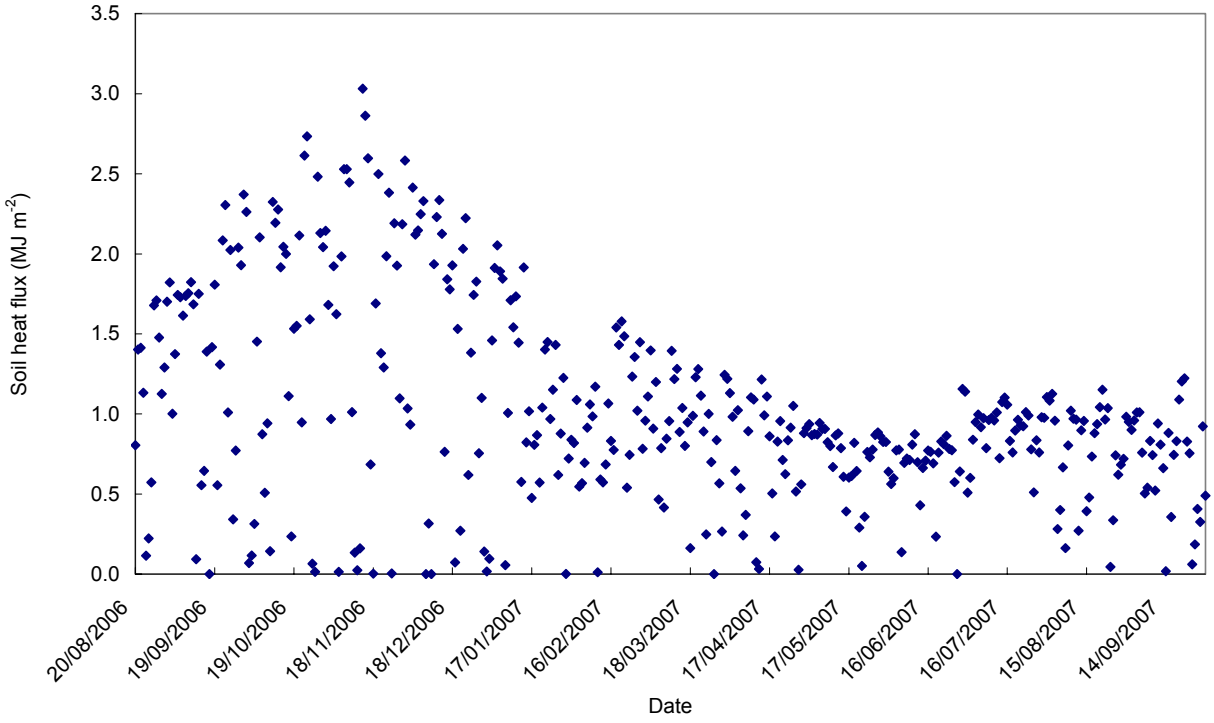

Fig. 6.3. Temporal variation in daily soil heat flux (Eq. 2.6).

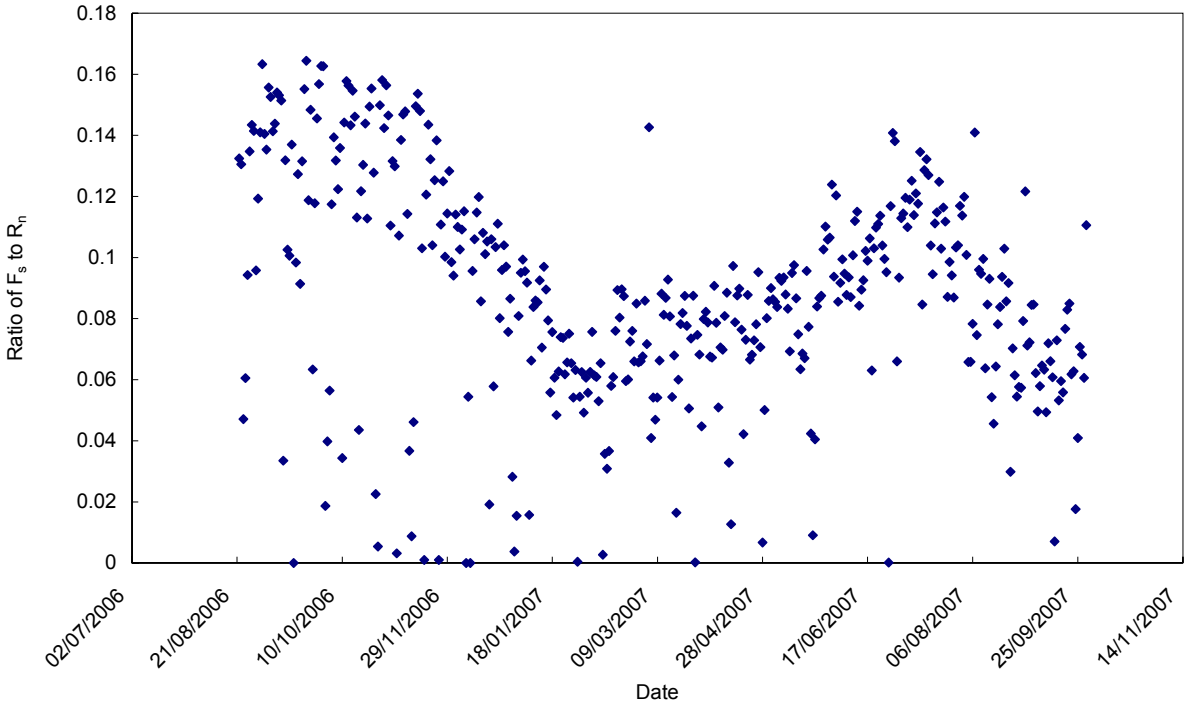

Fig. 6.4. Temporal change in the ratio of soil heat flux (F_s) to net irradiance (R_n) showing the impact of weeds and canopy closure.

Fig. 6.5 shows the four components of the energy balance equation for a cloudless day. The shape of the net irradiance curve indicates that cloudless conditions prevailed. Soil heat flux and net irradiance are both negative at night while the earth's surface emits infrared radiation. The soil heat flux indicates that the initial cooling of the earth's surface when the sun sets, takes place rapidly and then stabilises towards the early morning. This again indicates cloudless conditions and minimal vegetation cover.

Fig. 6.6 shows the four components of the energy balance at the site a year later when the air temperature, water vapour pressure and wind speed were similar. The main differences are as a result of the vegetation cover. In 2006, the response in soil heat flux in the morning and evening to changes in available energy is rapid whereas in 2007 the response is gradual due to shading of the soil surface by vegetation. On both days, the Bowen ratio at midday, when evaporation peaks, is approximately 0.5 indicating that evaporation dominates at the site.

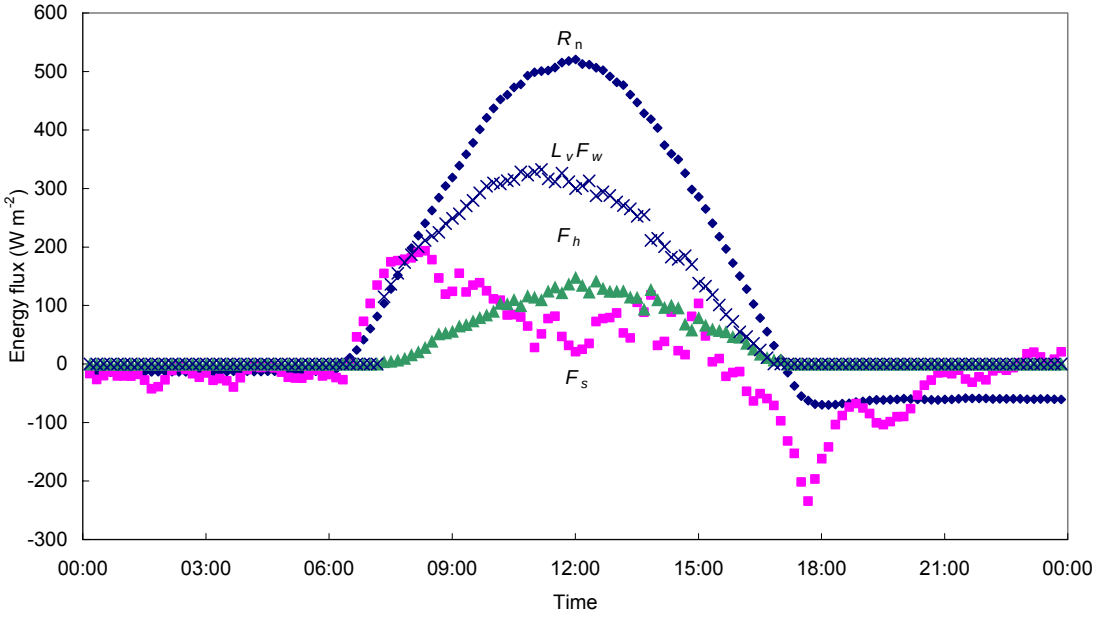

Fig. 6.5. Net irradiance (R_n), latent heat flux (L_vF_w), sensible heat flux (F_h) and soil heat flux (F_s), every 10 minutes, for 8 September 2006 with L_vF_w estimated as a residual.

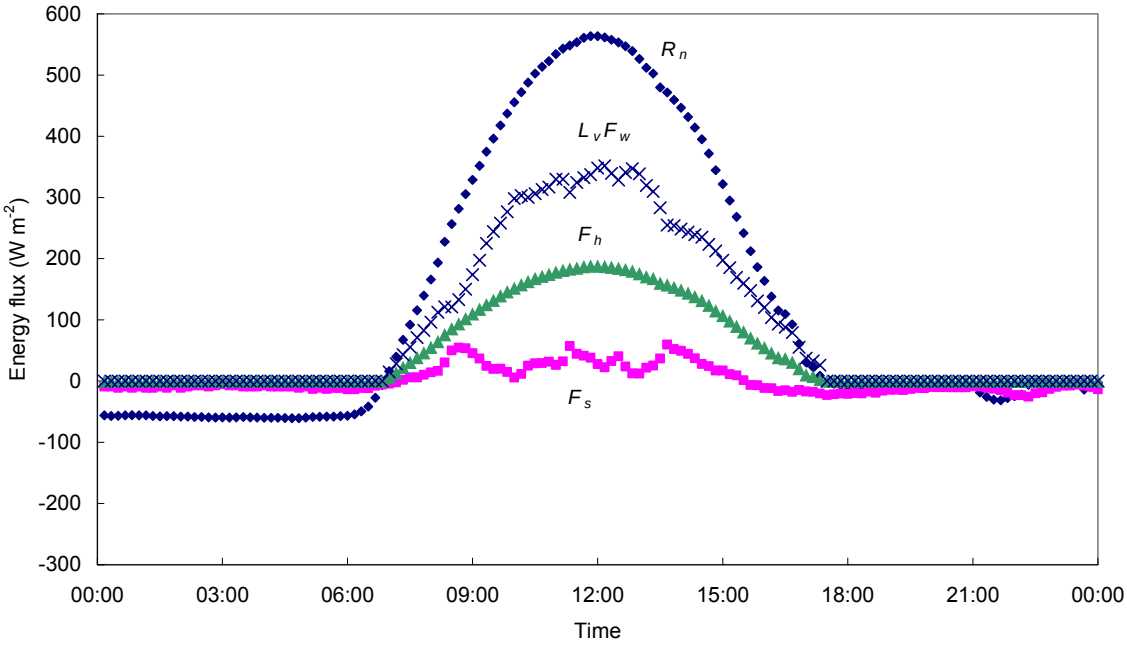

Fig. 6.6. Net irradiance (R_n), latent heat flux (L_vF_w), sensible heat flux (F_h) and soil heat flux (F_s), every 10 minutes, for 8 September 2007 with L_vF_w estimated as a residual.

Wind speed is an auxiliary measurement required for the calculation of sensible heat from the LAS data. It was measured throughout the year above the canopy. The wind speed was not particularly high at the site, although for short periods of time wind speeds in excess of 10 m s^{-1} were recorded (Fig. 6.7). The resolution of the wind speed data is every 10 min to coincide with the LAS data measurements.

Fig. 6.8 shows the daily rainfall measured above the canopy. The highest daily rainfall was 54 mm in summer and there was an event of 45 mm in winter as a result of a cold front. The total annual rainfall for the 2006/2007 hydrological year was 685.6 mm. The lowest rainfall measured at Two Streams between 2000 and 2006 was 605 mm in 2003 and the highest rainfall was 1151 mm in 2006. The annual rainfall is thus variable at the site.

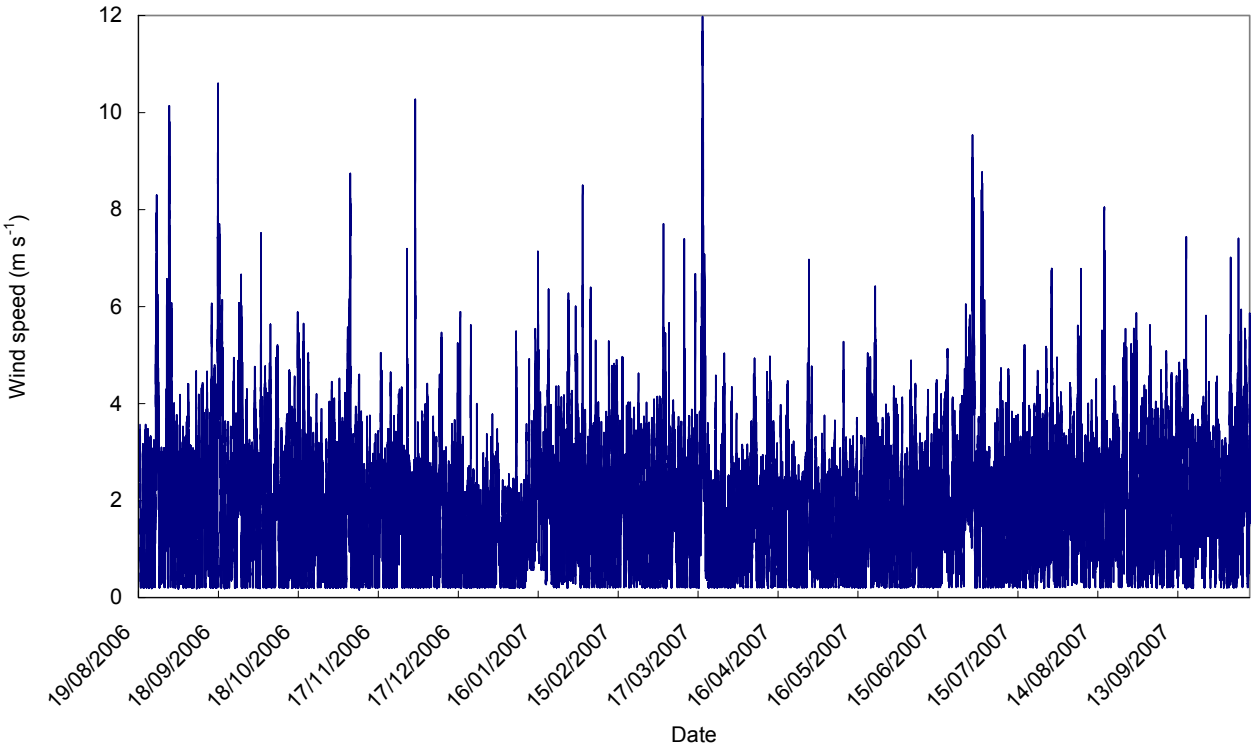

Fig. 6.7. Vector averaged wind speed readings above the tree canopy averaged every 10 min.

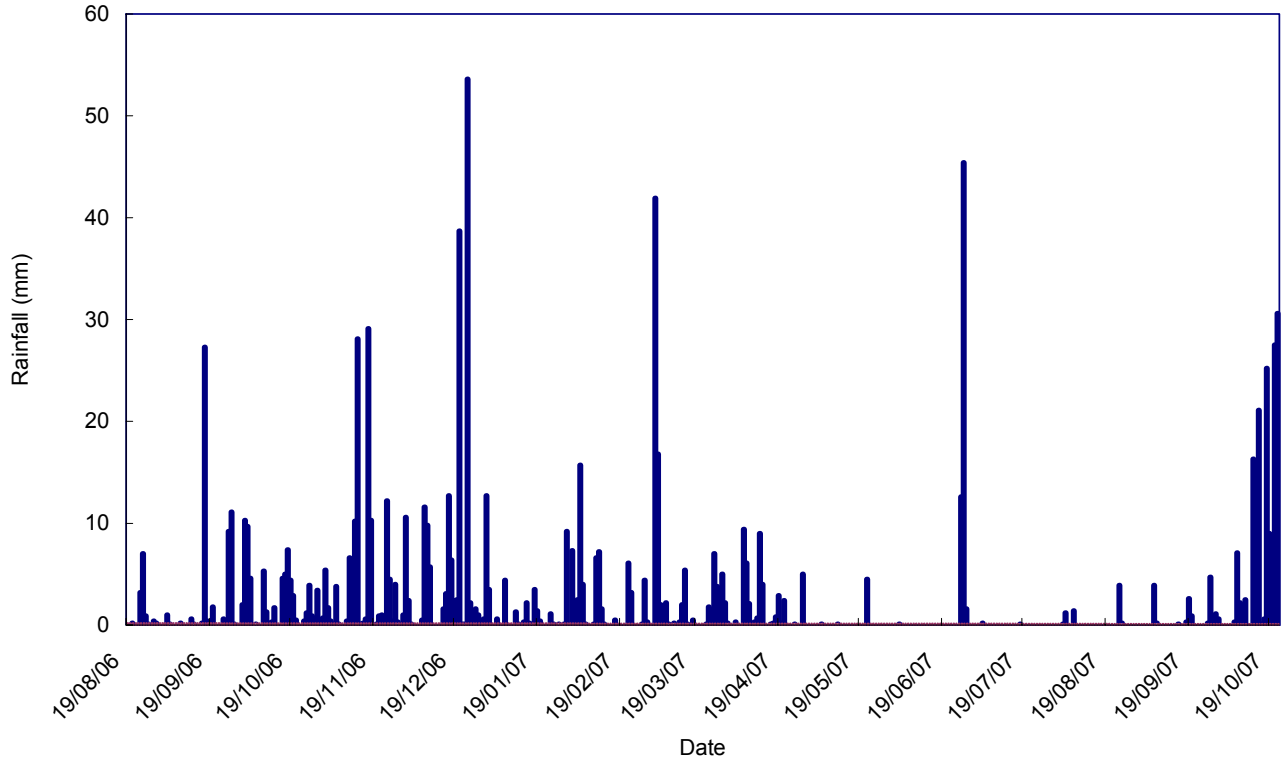

Fig. 6.8. The daily total rainfall at Two Streams.

6.3. ASCE-EWRI Automatic Weather Station

The data record for the AWS begins on 14 February 2007. The maximum and minimum air temperatures measured at the site are 38 ºC and -0.8 ºC, respectively. Fig. 6.9 shows the total daily solar irradiance data. Solar irradiance is a significant driver of evaporation. The maximum daily solar irradiance fluctuated between 29 MJ m^{-2} in summer and 13 MJ m^{-2} in winter.

Water vapour pressure deficit (VPD) is the difference between the saturated water vapour pressure at the air temperature and the atmospheric water vapour pressure. VPD was calculated from RH and air temperature at the site every 10 s. The hourly VPD values fluctuated diurnally. Fig. 6.10 shows the VPD ranges at the site to be high, peaking at 4.9 kPa. This correlates to days when berg wind conditions with hot dry air dominated at the site.

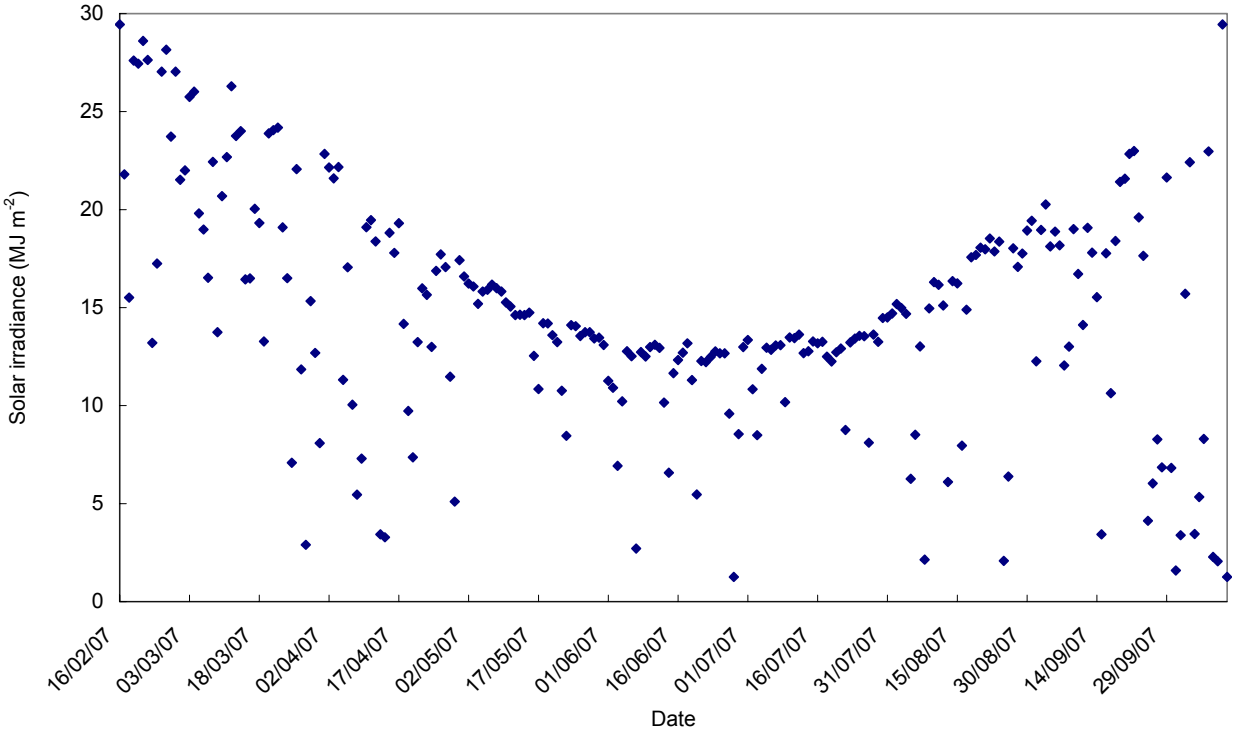

Fig. 6.9. Temporal variation in the daily total solar irradiance at Two Streams.

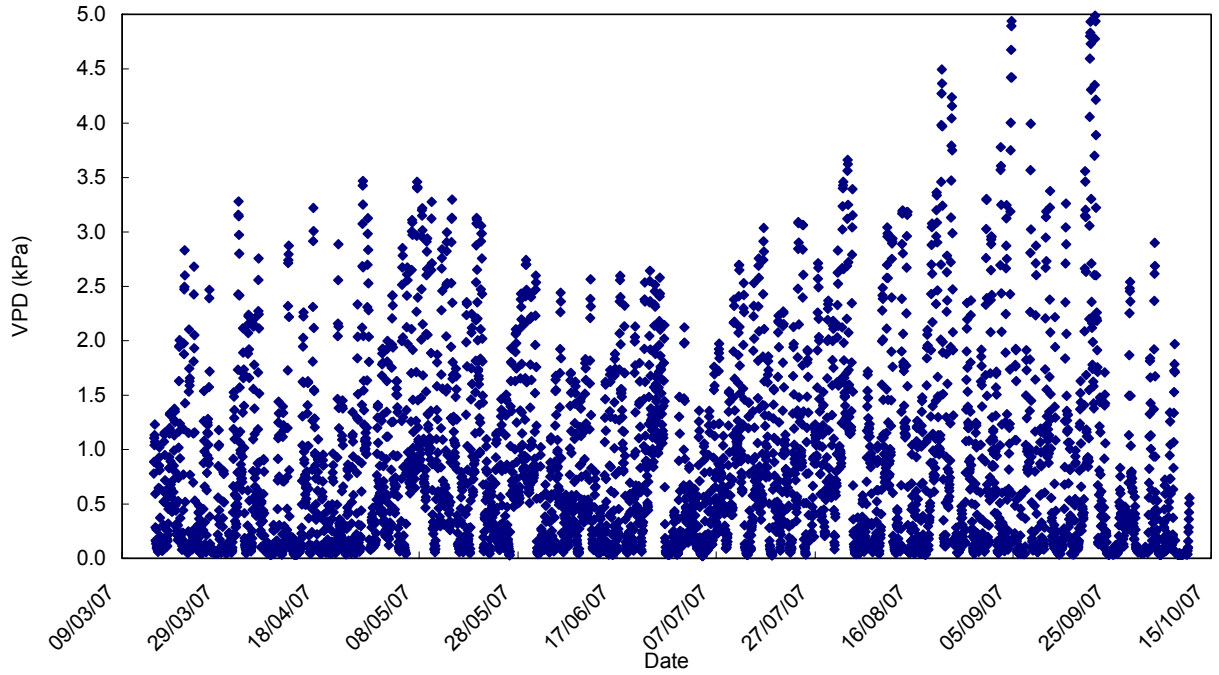

Fig. 6.10. Hourly water vapour pressure deficit (*VPD*) at Two Streams.

The output interval of ET_{sz}, the standardised grass reference evaporation (Eq. 3.7), is hourly and daily. The hourly and daily outputs are calculated from different algorithms. Fig. 6.11 shows that the hourly values summed for a day, do not equal the daily values of ET_{sz}. Fig. 6.12 shows that the hourly data totalled for a day was approximately 17 % higher than the daily data. This shows that where hourly data is available it should be used rather than the daily data and where calculations with only daily data are performed a possible error (in the case of Two Streams) of 17 % in the data is possible.

The ASCE-EWRI method of calculating ET_{sz} gives results for day-time and night-time (usually very small) conditions separately. The day-time values are usually positive and the night-time are positive or negative indicating evaporation or condensation, respectively. The handbook to the ASCE-EWRI equations (Allen *et al.*, 2000) recommends that the night-time values be included in the calculation of daily ET_{sz} from hourly values. Fig. 6.13 shows that the inclusion of night-time values generally increases the daily ET_{sz} slightly. This may not be significant at a daily level (5.7 %) but over a longer period of time could accumulate to affect results (Fig. 6.14).

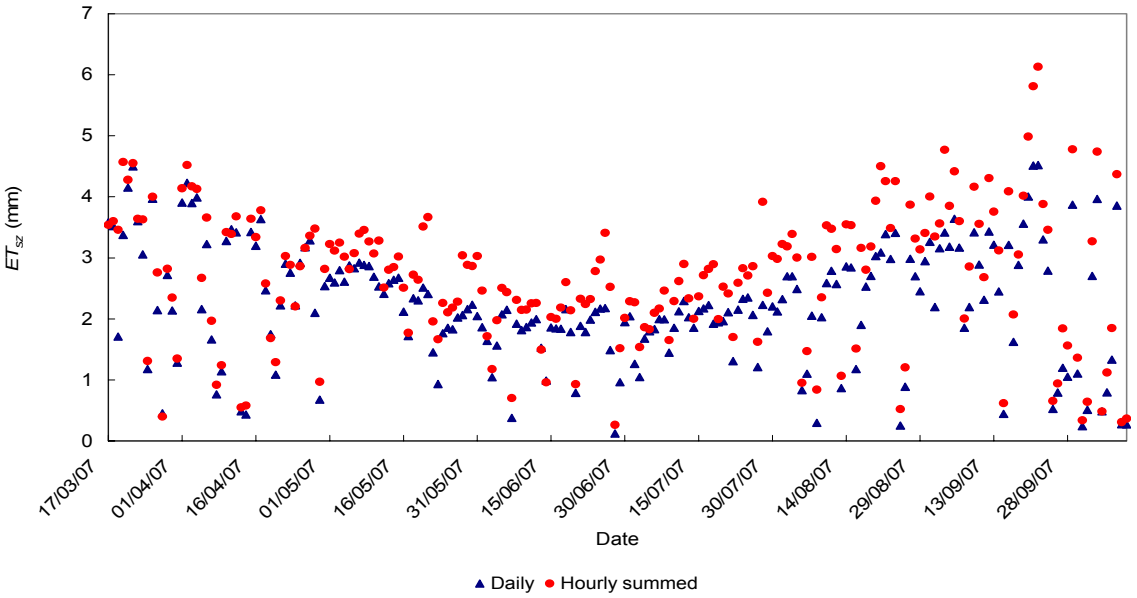

Fig. 6.11. The daily values of ASCE-EWRI short grass reference evaporation (ET_{sz}) calculated using the daily formula vs hourly values summed to a day.

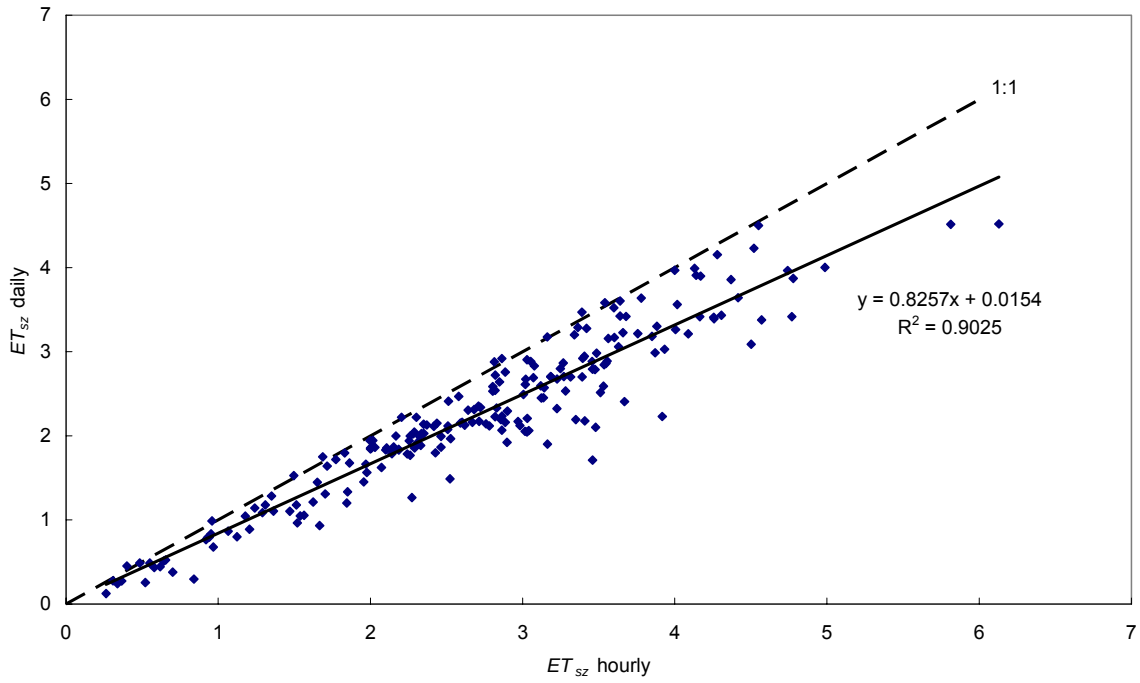

Fig. 6.12. The relationship between the daily values of ASCE-EWRI short grass reference evaporation (ET_{sz}) and hourly values of ET_{sz} summed to a day but including night-time values.

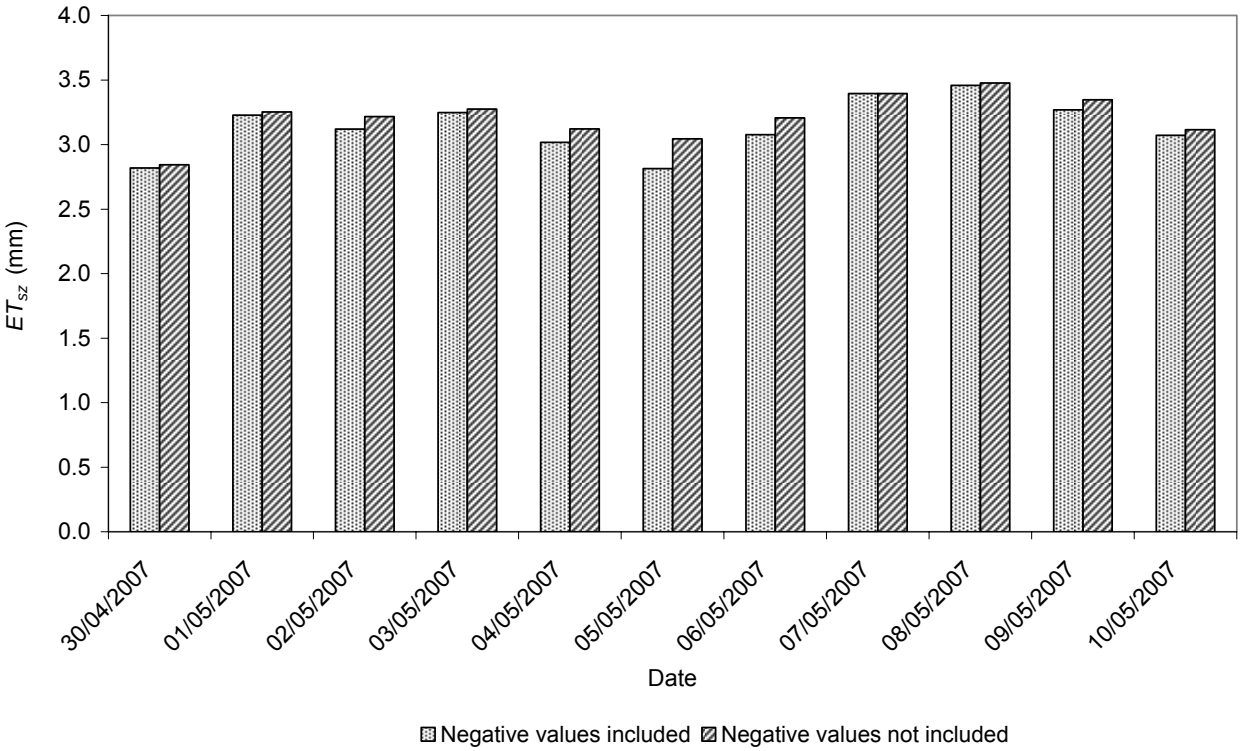

Fig. 6.13. The impact of including negative hourly night-time values of ASCE-EWRI short grass reference evaporation (ET_{sz}) in a daily summation of ET_{sz} values.

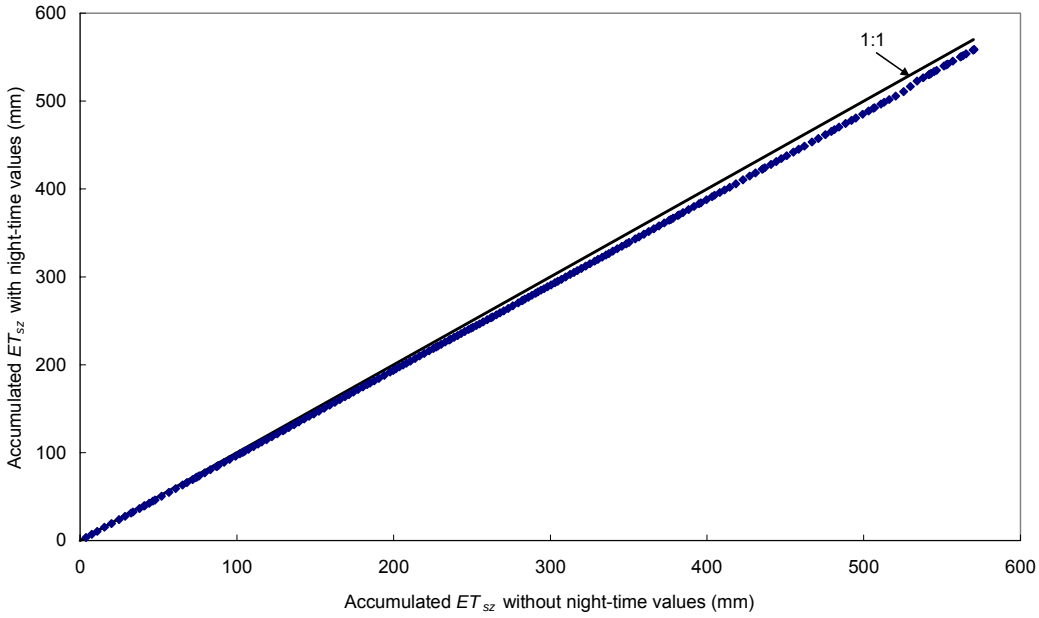

Fig. 6.14. The impact of including night-time values of ASCE-EWRI short grass reference evaporation (ET_{sz}) over a period of 7 months from March to October is 15 mm with an average daily error of 5.7 %.

6.4. LAS Estimates of Sensible Heat

The LAS operated continuously from 19 August 2006 to 10 October 2007 after which the instrument was removed for 3 weeks for servicing and use at another site. Data up to 29 September 2007 has been processed and presented in this document. Twenty four hours of data were not collected by the logger during the period of measurement due to battery or logger failure. This continuous data set indicates the reliability of the LAS.

Fig. 6.15 shows a typical diurnal pattern of the structure parameter of the refractive index of air (C_n^2) taken from the Two Streams Catchment on the 22 August 2006, a cloudless day. The C_n^2 values typically decrease at sunrise and sunset where there is a change from stable to unstable atmospheric conditions.

Fig. 6.16 shows daily F_h, and L_vF_w,, estimated as a residual at the site since 19 August 2007. The daily total available energy flux (R_n-F_s) has been included as the main driver of evaporation and is useful in assessing whether the calculated F_h and L_vF_w values are realistic. The available energy is calculated by re-arranging the shortened energy balance equation (Eq. 2.1),

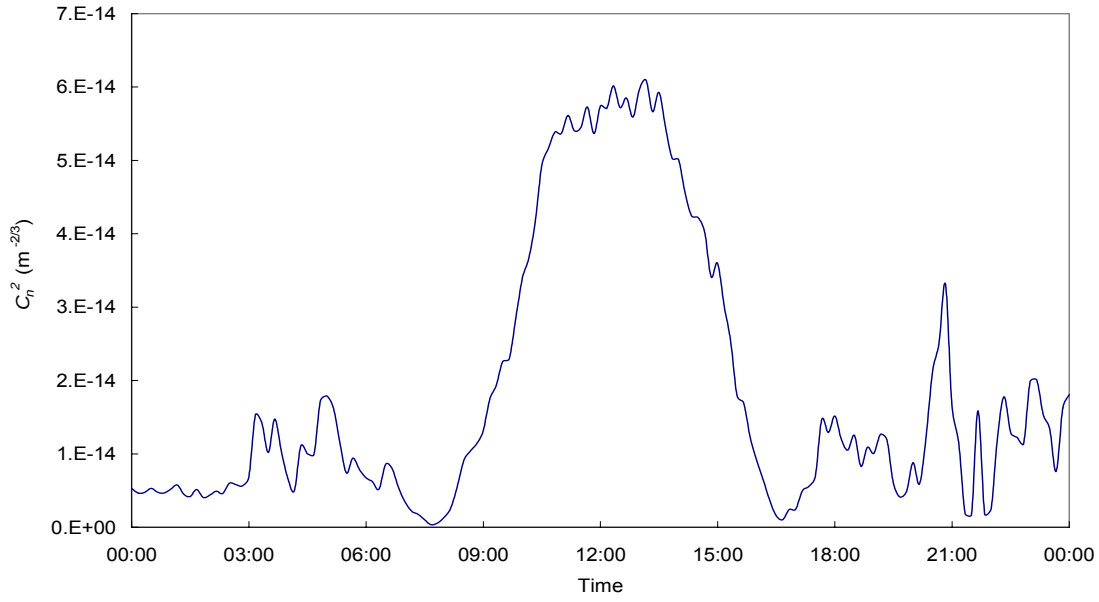

Fig. 6.15. LAS results from the unstable solution for the structure parameter of the refractive index of air (C_n^2) measured at Two Streams on 22 August 2006.

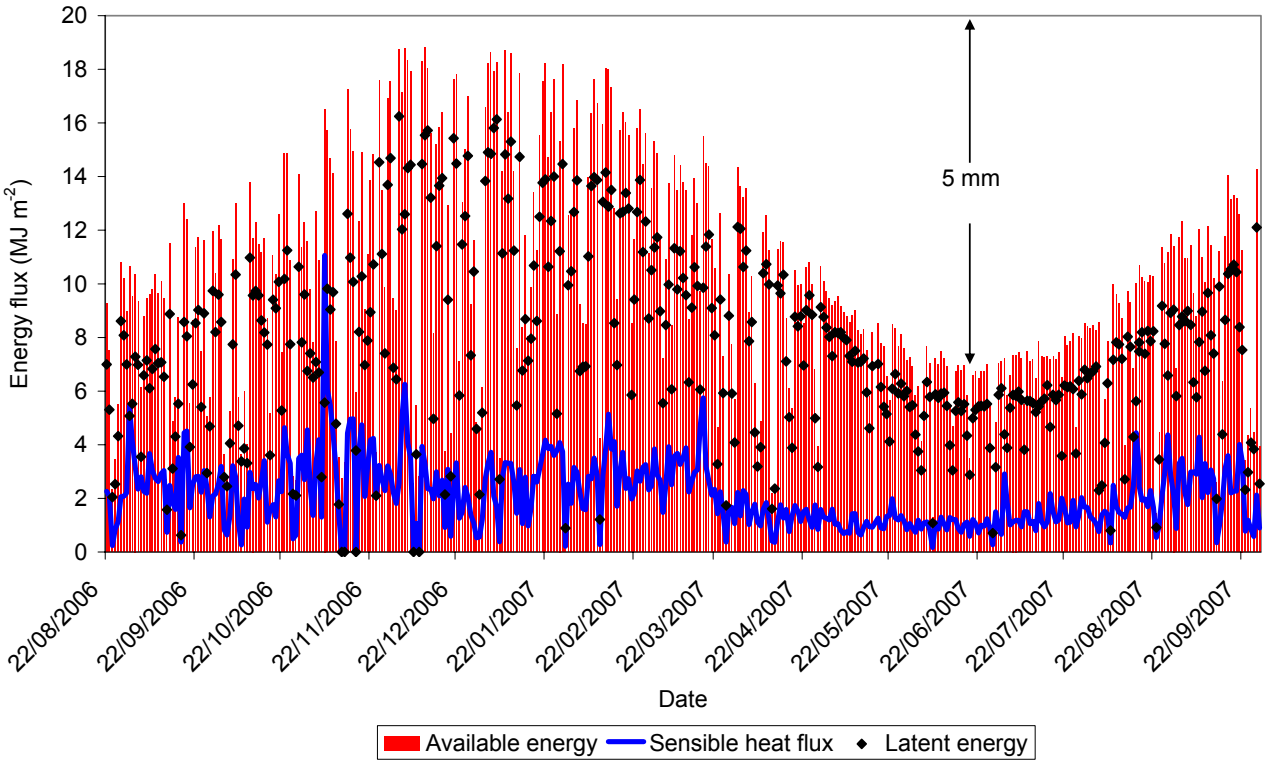

Fig. 6.16. Temporal variation in the daily available energy (R_n-F_s) flux, sensible heat flux (F_h) and latent energy (L_vF_w) from 20 August 2006 to 29 September 2007 at Two Streams. The latent energy flux is the difference between R_n-F_s and F_h and an energy flux of 12.2 MJ m^{-2} translates into approximately 5 mm of evaporation.

to $(R_n - F_s) = L_v F_w + F_h$ where $R_n - F_s$ is the available energy flux. For any day, the magnitude of $L_v F_w$ is then equal to the difference between the available energy and F_h.

The sensible heat flux was greater but more variable in summer and lower and more consistent in winter. Variability in summer was due to an increased number of cloudy or rain days. Summer values of total daily F_h on clear days was in the region of 4 MJ m^{-2} when the available energy was approximately 19 MJ m^{-2}. Winter values of total daily F_h were in the region of 1.5 MJ m^{-2} when the daily available energy flux was 7 MJ m^{-2}.

A number of cloudless days where analysed, showing that F_h varied during the course of a day. At midday when the available energy flux was at its peak, the instantaneous values of F_h were usually 20 to 30 % of the available energy flux. If however, a distribution of the daily total fluxes is plotted (Fig. 6.17) it can be seen that the daily total sensible heat flux (MJ m^{-2}) is between 5 and 15 % of the total daily energy distribution. This simply indicates that the proportion of instantaneous values of F_h to available energy is not constant during a day. The proportion is low at the beginning and end of the day and higher at midday.

As would be expected, using the simplified energy balance method to determine the latent energy, the available energy is 50 % of the distribution of total daily fluxes and the rest is split between sensible heat flux and latent energy (Fig. 6.17). This is intuitively what would be expected as by the law of conservation of energy, the available energy must equal the sum of the sensible heat flux and the latent energy.

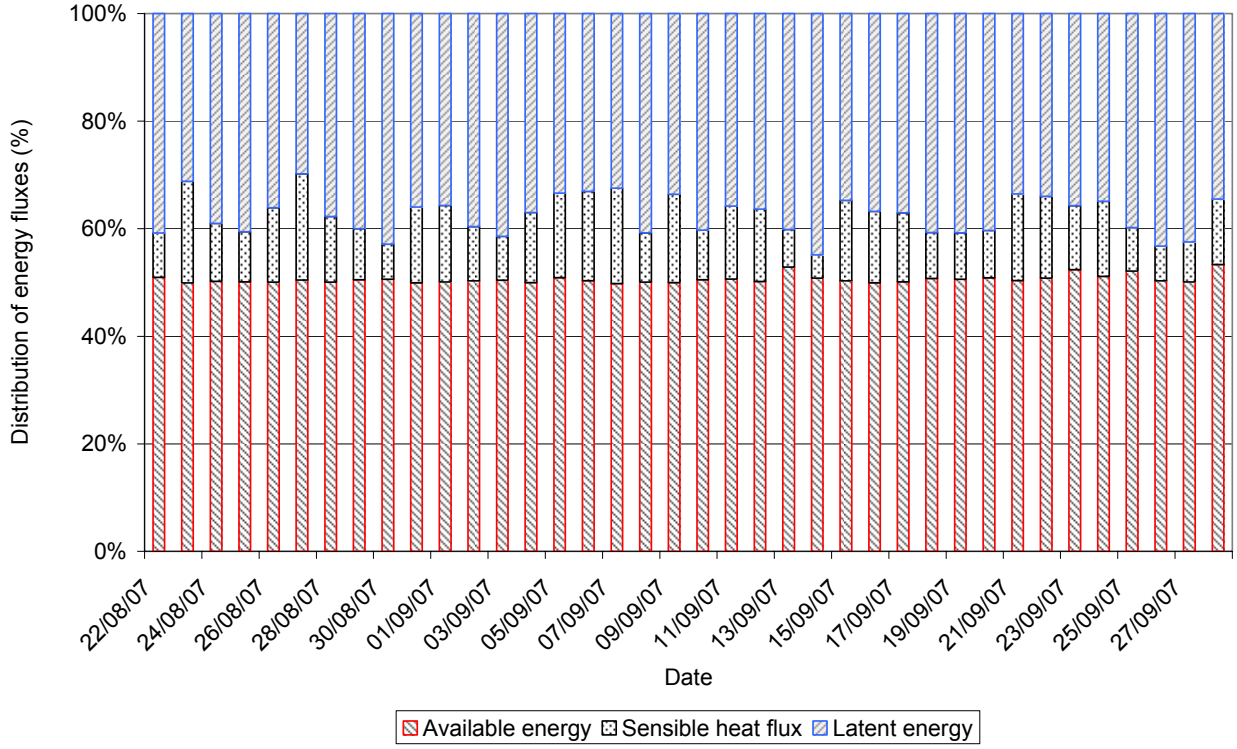

Fig. 6.17. A relative allocation chart showing the daily total distribution of the available energy, the sensible heat flux and the latent energy at Two Streams from the 23 September 2007 to 28 October 2007.

In a few cases such as 6 November 2007, the sensible heat flux was unrealistically high in comparison to the net irradiance (Fig. 6.18). On these days high wind speeds in excess of 6 m s^{-1} were measured. Wind, or advection, results in an addition or subtraction of energy from the system which is not accounted for. The wind at Two Streams is typically a warm and dry berg wind or a cold frontal wind. Both appear to affect the sensible heat flux measurement due to the exclusion of advection flux in the shortened energy balance equation (Eq. 2.1). Fig. 6.18 shows that an increase in wind speed between 12 pm and 3 pm corresponds with an increase in F_h estimates.

In Fig. 6.19 the LAS-based total evaporation (ET_{LAS}) clearly reflects the seasonal change between summer and winter. Daily summer values, when not affected by rain, were up to 6 mm whereas winter evaporation was 2 mm. This can be attributed to reduced net irradiance in winter.

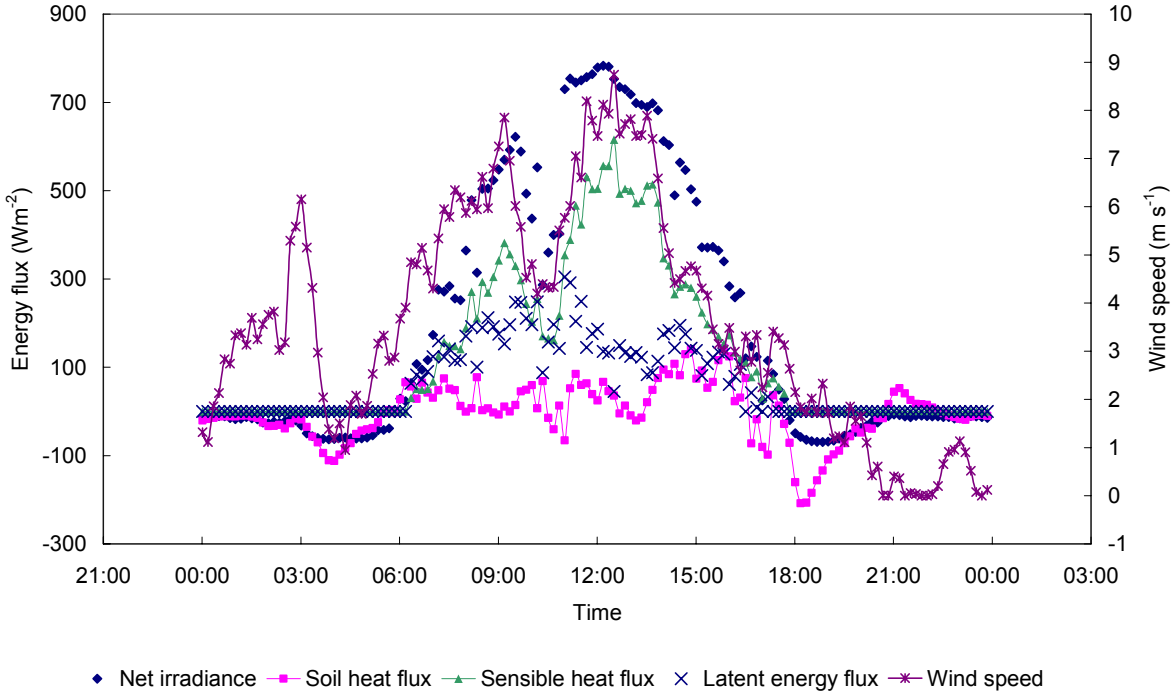

Fig. 6.18. Energy balance components of the shortened energy balance equation including the wind speed for a day when advection influenced the results of sensible heat flux. Sensible heat flux and latent energy flux are assumed to be zero when net irradiance is negative.

Fig. 6.20 shows that the Bowen ratio from December 2006 to June 2007 was generally between 0.1 and 0.5 with a few exceptions due to the effect of advection on the sensible heat flux measurements. This indicates that the latent energy flux was the dominant flux at the site during the wetter months. This translates into evaporation being the dominant process. From August to November 2006 and July to September 2007, the Bowen ratio was generally slightly higher with values between 0.2 and 0.8. This indicates that although the Bowen ratio was marginally higher during the drier months, the latent energy flux and hence evaporation was still the dominant processes.

Validation of the L_vF_w estimate from the sensible heat flux measurements using the LAS is possible by comparing the results with the Priestley and Taylor (1972) estimate of latent energy flux:

$$L_v F_{w\ (P\text{-}T)} = \frac{1.26\Delta}{\Delta + \gamma}(R_n - F_s)$$

where

$$\frac{\Delta}{\Delta + \gamma} = 0.4132 + 0.0158T_z - 0.000115T_z^2$$

and

$$T_z = \frac{T_{\max} + T_{\min}}{2}$$

(Savage *et al.*, 1997)

where $L_vF_{w\ (P\text{-}T)}$ is the Priestley and Taylor total daily latent energy flux (W m^{-2}), T_{max} is the maximum daily air temperature (ºC) and T_{min} is the minimum daily air temperature (ºC).

The Priestley and Taylor daily total latent energy flux estimate is based on the equilibrium evaporation under conditions of a weak flow of humid air over a well-watered crop. The temporal variation in $L_vF_{w\ (LAS)}$ and $L_vF_{w\ (P\text{-}T)}$ is shown in Fig. 6.21 and Fig. 6.22, respectively. Results from the two methods are very similar on a daily basis with L_vF_w peaking in summer at approximately 16 MJ m^{-2} and dropping in winter to 6 MJ m^{-2} for both methods. Fig. 6.23 shows good agreement between $L_vF_{w\ (LAS)}$ and $L_vF_{w\ (P\text{-}T)}$ with a coefficient of determination of 0.94 and an average difference (slope of the trend-line) of 9 % between the daily values of L_vF_w.

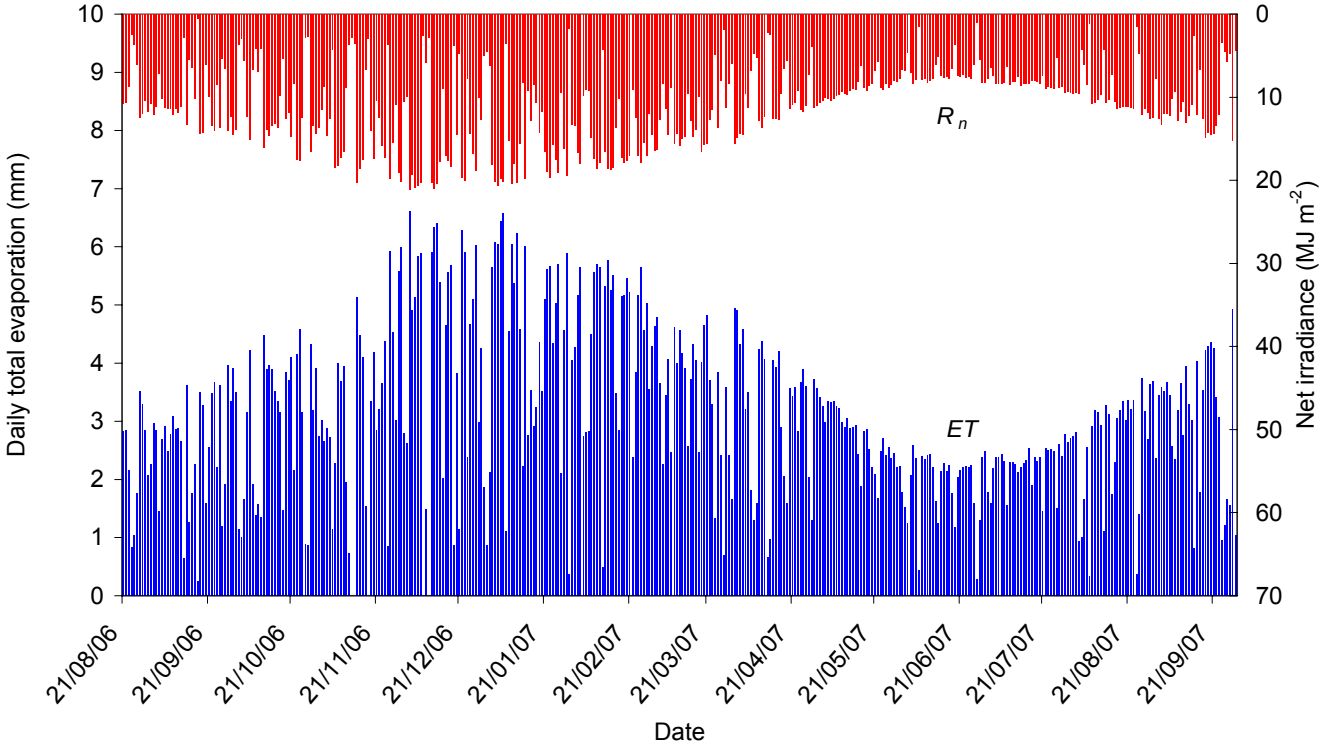

Fig. 6.19. Daily net irradiance and daily *ET* estimated from a LAS using the shortened energy balance equation (Eq. 2.1).

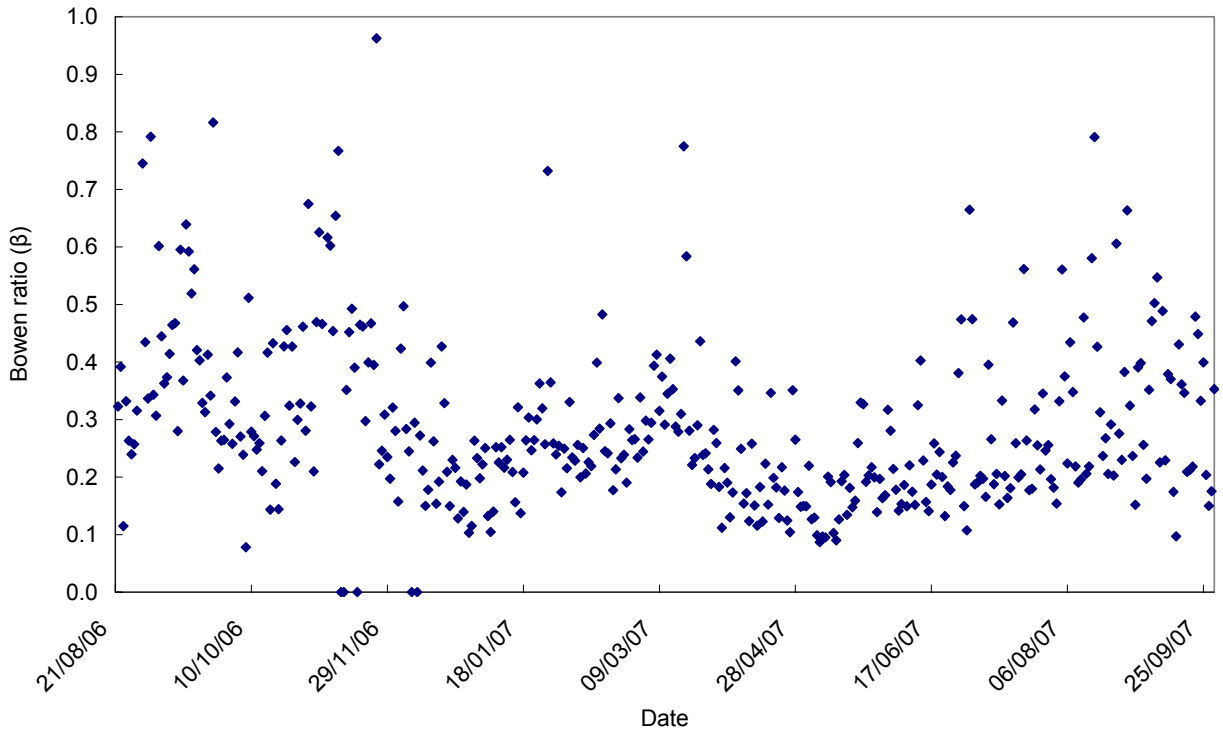

Fig. 6.20. The daily Bowen ratio from 21 August 2006 to 29 September 2007.

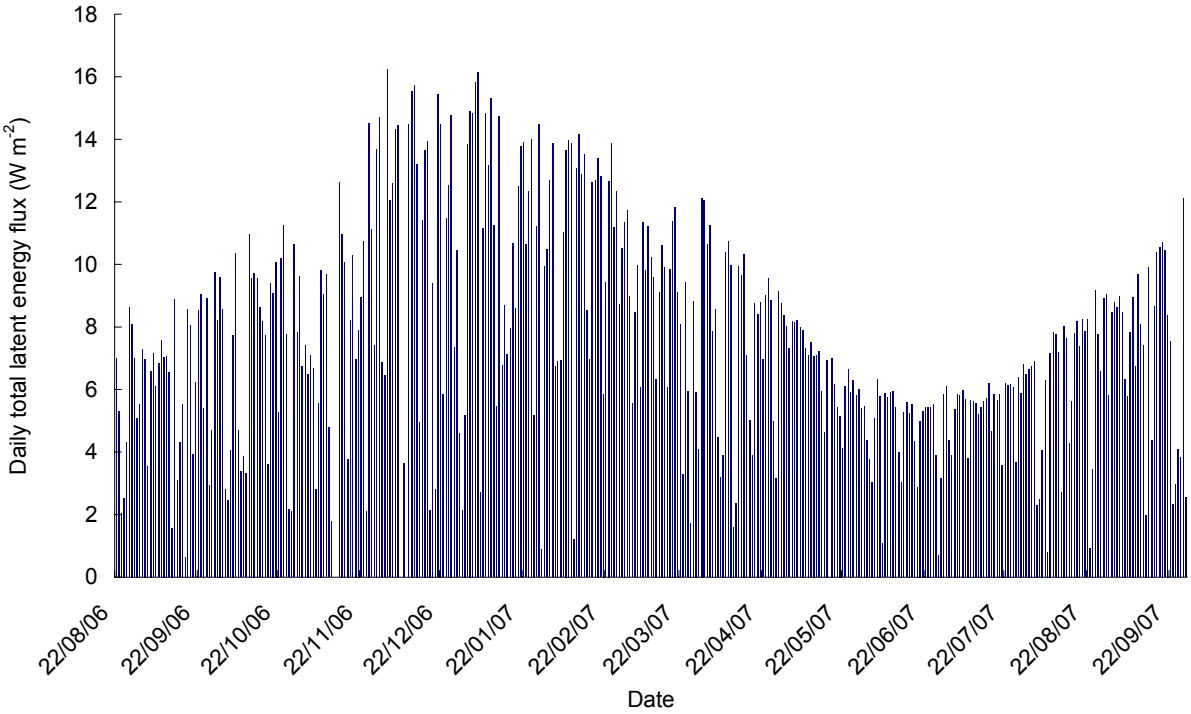

Fig. 6.21. Temporal variation in daily total latent energy flux using the LAS-based method from 22 August 2006 to 29 September 2007.

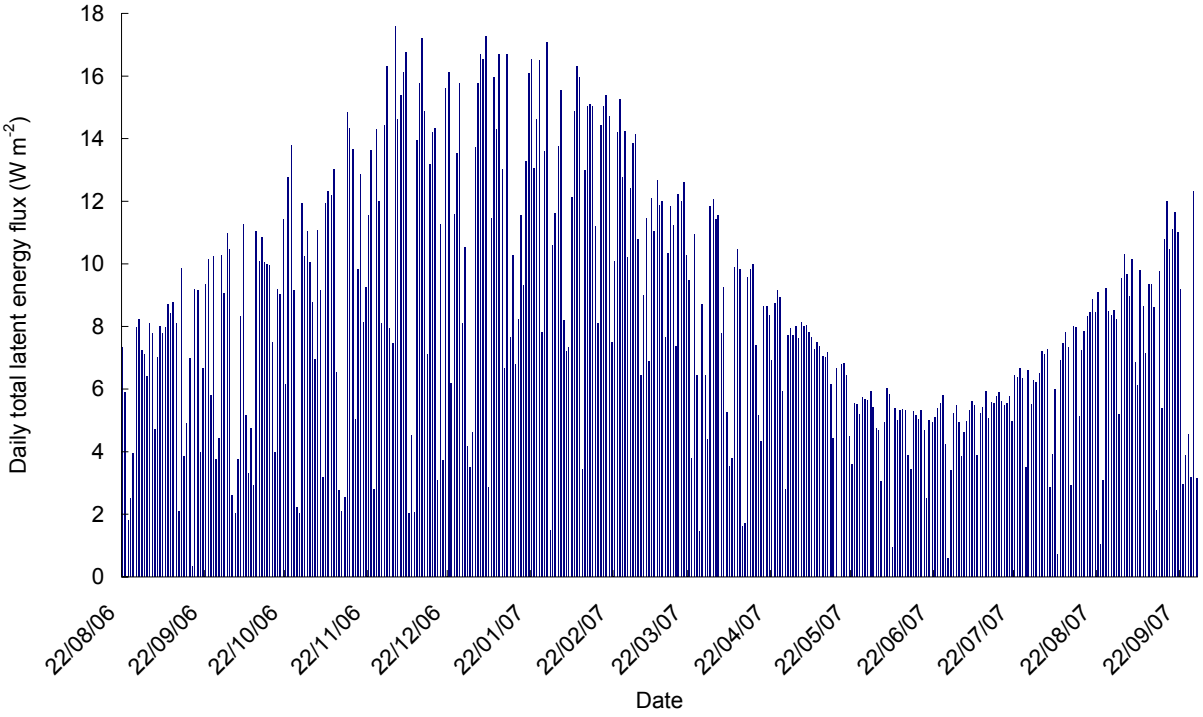

Fig. 6.22. Temporal variation in daily total latent energy flux using the Priestley and Taylor (1972) method from 22 August 2006 to 29 September 2007.

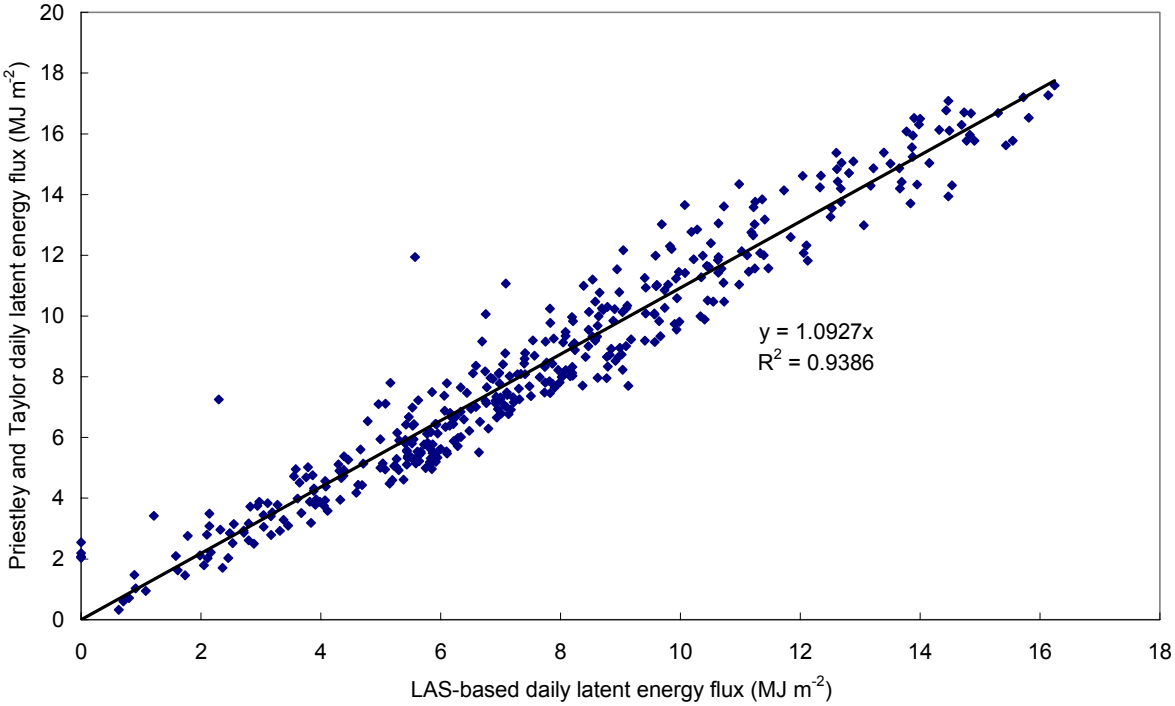

Fig. 6.23. Relationship between the LAS and the Priestley and Taylor estimates of daily total latent energy from 22 August 2006 to 29 September 2007.

6.5. A Comparison between the Automatic Weather Station Reference Evaporation (ET_{sz}) and the LAS Total Evaporation (ET_{LAS})

Fig. 6.24 shows the relationship between ET_{sz} and ET_{LAS}. The coefficient of determination shows that relatively close agreement was found between the two data sets (R^2 = 0.78). In most cases, poor agreement was attributed to advection or rainfall. At the Two Streams site, hot and dry berg wind conditions frequently prevail. Under these conditions, the LAS estimated an unrealistically high F_h. The energy balance equation, translates this into a low ET creating a mismatch between ET_{sz} and ET_{LAS} estimates. Advection is problematic in evaporation studies based on MOST (Hoedjes *et al.*, 2002). Further research is required in order to adequately take the affects of advection into account.

Fig. 6.25 shows the daily crop factor calculated from ET_{LAS} and ET_{sz} hourly data excluding night-time values. The crop factor was calculated from March

to September 2007. In March the average tree height was 3.5 m and in September approximately 5.2 m. With the increase in tree height and leaf area, the crop factor would be expected to increase, but the trend of the data shows a decrease in winter. This could be a seasonal influence and the crop factor may show an increasing trend in the approaching summer. Many of the outliers below the regression line are as a result of days when rain or wind affected measurements. The variability of the crop factor data is not as large as it may appear from the graph. For example, the outlier in March 2007, circled in Fig. 6.25, of 1.66 is as a result of an ET_{LAS} of 1.0 mm and an ET_{sz} of 0.58 mm. In August 2007 a crop factor of 0.39 results from at ET_{LAS} of 0.3 mm and an ET_{sz} of 0.84 mm. In both these cases the absolute differences in the evaporation is small but the ratio between the values is large resulting in variability in the crop factor results. Further investigation shows that on these days, rain and/or high wind speeds were recorded. Further research is required to establish criteria to exclude days that would not be representative for calculation of crop factors.

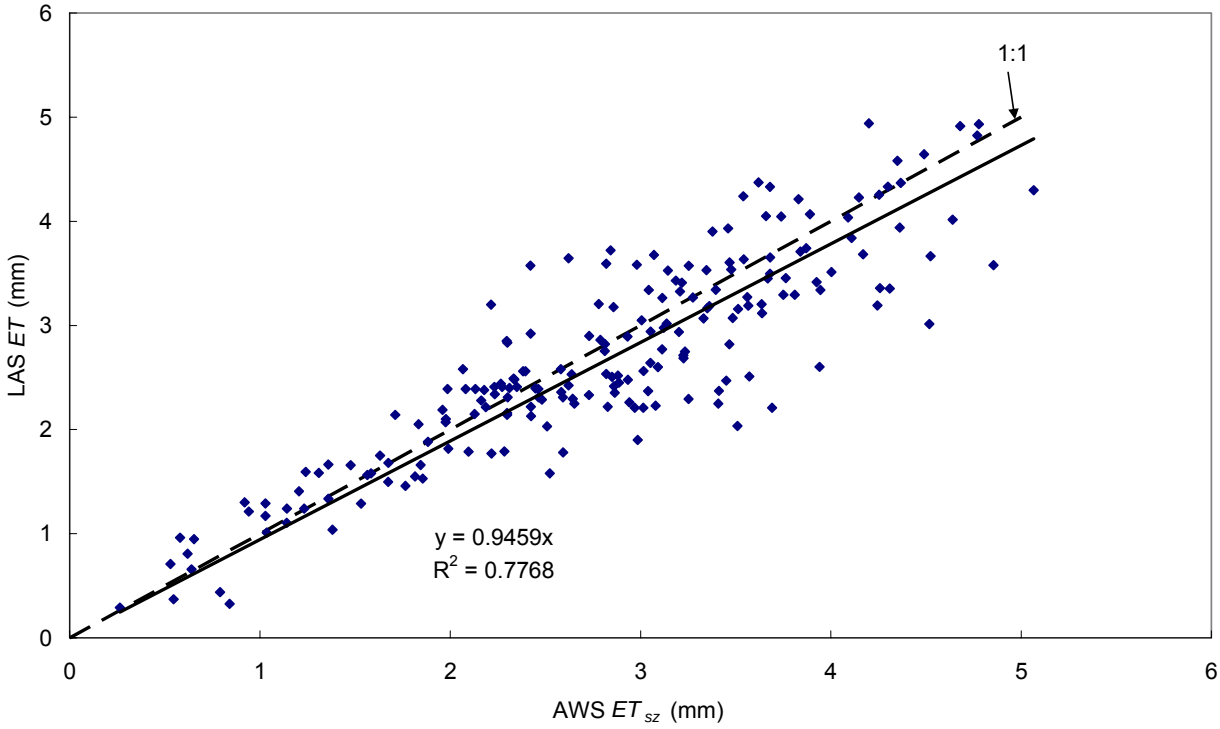

Fig. 6.24. The relationship between the daily AWS short grass reference evaporation (ET_{sz}) and the LAS total evaporation (ET_{LAS}).

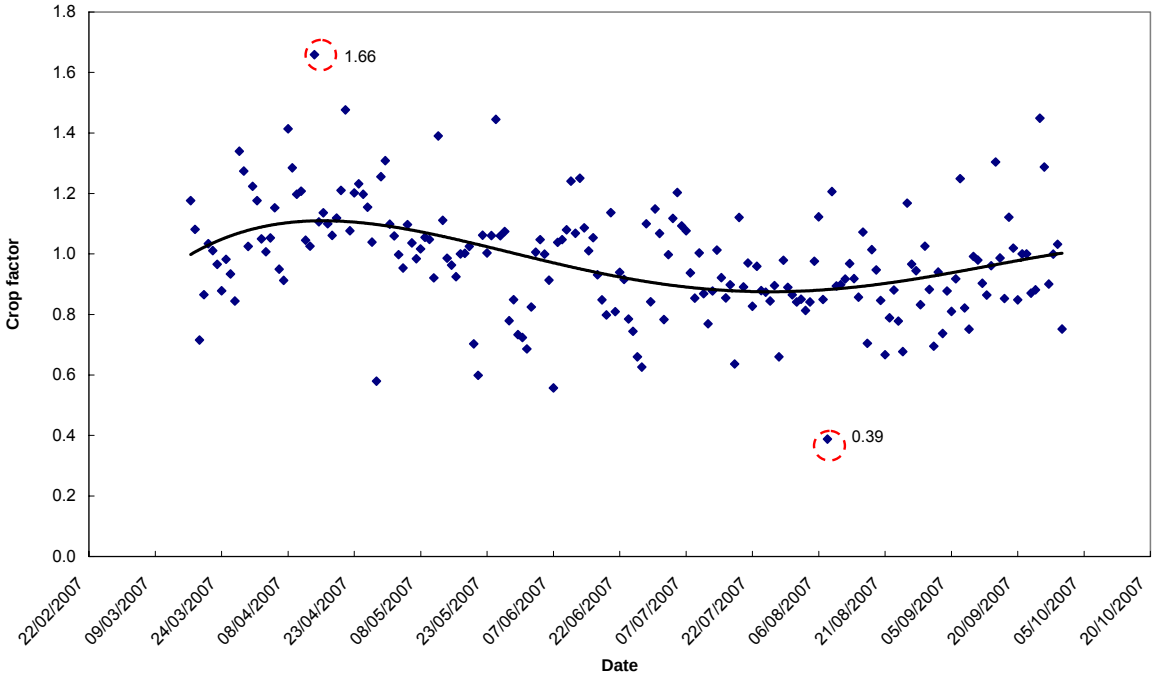

Fig. 6.25. The daily crop factor calculated from ET_{sz} and ET_{LAS}. A second order polynomial trend line has been fitted to the data.

6.6. Total Evaporation, Reference Evaporation (ET_{sz}) and Rainfall

Fig. 6.26 shows the accumulated total evaporation from the LAS (ET_{LAS}) and Priestley and Taylor ($ET_{P\text{-}T}$) vs the total rainfall. The ET_{LAS} and $ET_{P\text{-}T}$ over a period of 13 months was 1250 mm and 1322 mm, respectively, and the total rainfall was 750 mm. The ET_{LAS} therefore exceeds the rainfall by 500 mm or 67 % and the $ET_{P\text{-}T}$ exceeds the ET_{LAS} by 72 mm or 6 %.

Significant deviation from the 1:1 line of ET_{LAS} in Fig. 6.26 occurred on approximately 17 January 2007. On this date, the average height of the crop was 2.6 m and the LAI was 1.21. Up until this point total evaporation had not significantly exceeded total rainfall. These data indicate the point at which the trees begin to use more water than was supplied by rainfall. This occurred in part, due to a dry period in January 2007 as well as increased tree growth and the ability to use more water.

Both the ET_{LAS} and $ET_{P\text{-}T}$ estimates of peak summer values and winter values were 6 mm and 2 mm respectively (data not shown). The Priestley and Taylor method, although relatively coarse in comparison with the LAS measurements, verifies that the LAS measurements are within range of what could be expected at the site and gives confidence to the results obtained thus far.

Fig. 6.27 shows the monthly values of ET_{LAS}, $ET_{P\text{-}T}$, ET_{sz} and rainfall. The low rainfall of January and February indicates the rainfall variability at the site and the importance of using long-term measurements to evaluate evaporation and rainfall. The low rainfall of January and February will influence the comparison of evaporation and rainfall but with time as the individual values of accumulated ET and rainfall become greater, the impact of unusual weather conditions will be reduced.

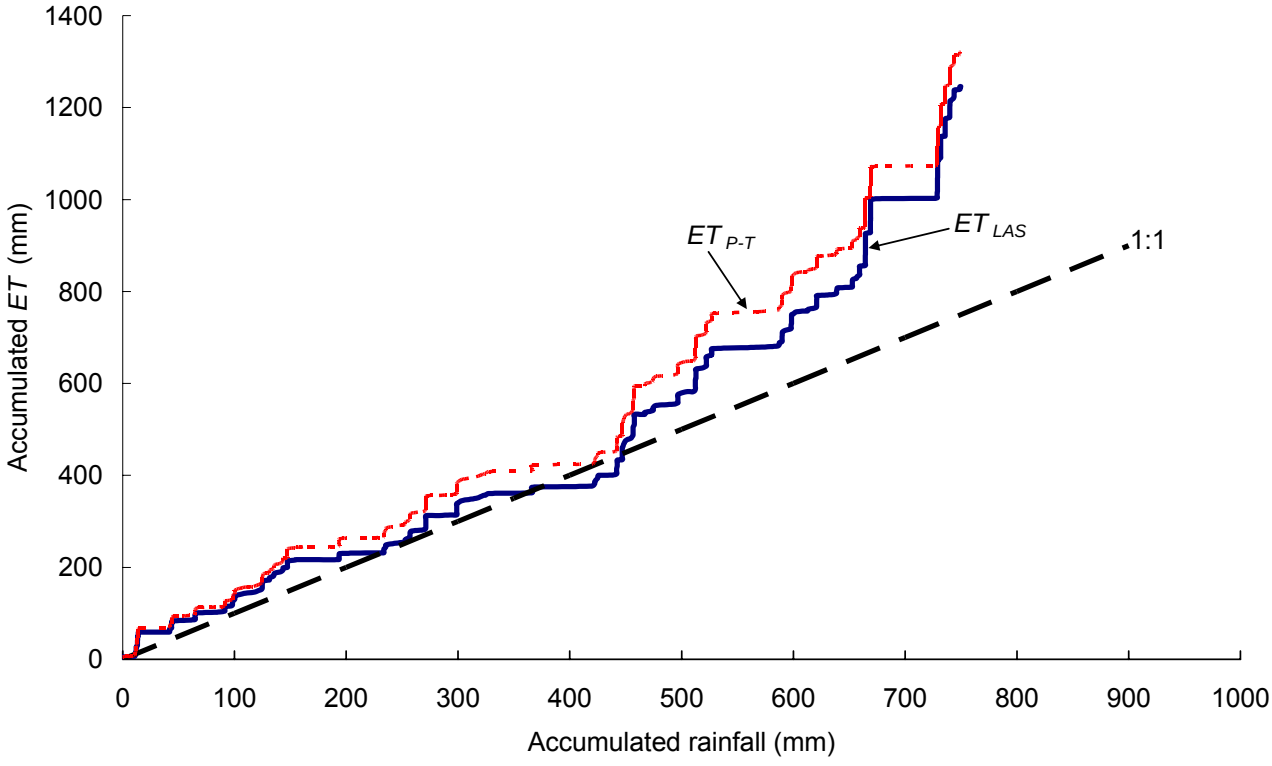

Fig. 6.26. A comparison between ET_{LAS}, $ET_{P\text{-}T}$ and rainfall from 22 August 2006 to 29 September 2007.

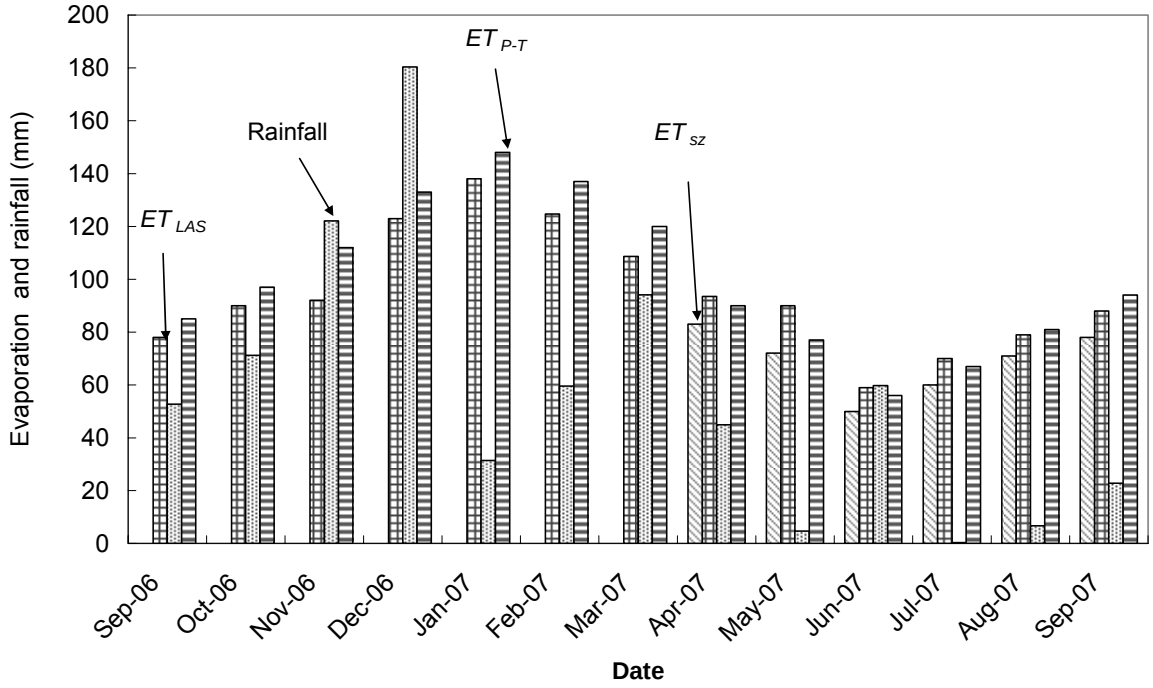

Fig. 6.27. Monthly totals showing a comparison between ET_{LAS}, ET_{P-T}, ET_{sz} and rainfall.

7. Conclusion and Recommendations for Future Research

Six hectares of Black Wattle (*A. mearnsii)* was planted in July 2006 in the Two Streams catchment. The trees have grown to an average height of 5.5 m in 13 months with a growth rate of 0.37 m month^{-1} or 4.5 m year^{-1}. At this stage, growth has not been significantly affected by seasonality. The main component of the energy balance altered during the course of the year due to the influence of the tree growth was the soil heat flux.

A large aperture scintillometer (LAS) was used successfully to measure at sub-hourly intervals the sensible heat flux and estimate total evaporation (*ET*) over the trees as a residual term of the shortened energy balance. Daily summer *ET* values are in the region of 6 mm on cloudless days and 2 mm in winter. The LAS functioned continuously with minimal loss of data for a period of 13 months showing the reliability of the instrument. The sensible heat flux data required filtering particularly in the early morning and late afternoon when there is a change in the condition of the atmosphere from stable to unstable in the morning and unstable to stable in the late afternoon. This filtering of the data was required throughout the period of measurement from 21 August 2006 to 29 September 2007.

Zero plane displacement and wind speed, required for the calculation of the sensible heat flux, have a significant impact on the sensible heat flux magnitude and should be determined as accurately as possible. Zero plane displacement may be estimated but can be subjective. It should be well understood before being applied. Accurate wind speed measurements are also required to calculate sensible heat flux. Wind speed sensors should be mounted at a suitable height above the canopy close to the LAS beam.

The LAS does not provide a sensible heat flux direction. This should be monitored at a site by using eddy covariance methodology or by measuring the air temperature gradient at two significantly different heights above the ground.

The LAS *ET* was compared with the grass reference evaporation (ET_{sz}) calculated from an automatic weather station using the daily and sub-daily ASCE-EWRI methods. The relationship was reasonably good with $R^2 = 0.78$. Outliers are mainly as a result of wind advection affecting the LAS sensible heat flux measurements or rain. This proves the reliability of the ASCE-EWRI method in determining a reference evaporation. Results showed that night-time and negative values of ET_{sz} should be included in long-term calculations and that hourly data summed for a day gives marginally different results to the daily solution. When available, the hourly values of ET_{sz} should be summed and used instead of the daily calculated reference evaporation. A crop factor was calculated from the data which shows a decreasing trend into winter starting at 1.1 when the trees were planted and decreasing to 0.9 when the trees were at a height of 5.5 m. This is thought to be as a result of the dry winter season over which the data was collected and would be expected to increase in summer again.

The LAS *ET* measurements were validated against the Priestley and Taylor evaporation estimate. The two estimates were in agreement with a coefficient of determination of 0.94. The Priestley and Taylor estimates were on average 9 % higher than the LAS *ET* estimates. Although less accurate, the Priestley and Taylor method provides a good validation the LAS *ET* results.

The total rainfall for the period of measurement was 750 mm and the *ET* estimated from the LAS was 1250 mm. The *ET* thus exceeded the rainfall for this period by 67 %. Burger (1999) found that the total evaporation, using the Bowen ratio method, over *A. mearnsii* at Two Streams, exceeded the rainfall by 45%. The results from the LAS measurements confirm that the total evaporation can be higher than the total rainfall and for this period of measurement, the total evaporation exceeded the rainfall by 67%. This shows that the trees are relying on water over and above the direct rainfall at the site. This finding justifies the need for a further investigation on the deep soil water movement to determine whether the trees are in fact using ground water. Variability in rainfall for the area however indicates that long-term studies are critical in a comparison between rainfall and evaporation.

The daily averaged Bowen ratio was found to be between 0.1 and 0.5 from December 2006 to June 2007 and between 0.2 and 0.8 for the rest of the period. This indicates that although slightly higher in late summer, the latent energy flux dominates over the sensible heat flux for the entire year. Metelerkamp (1993) shows values for the Bowen ratio during winter in a high rainfall area over natural grassland to be consistently as high as 4 indicating that the sensible heat flux dominates. This shows the significantly different response between trees and grassland during the winter months indicating that trees continue to use water during winter whereas grassland water use decreases. Commercial forestry potentially impacts on catchment hydrology in the winter months when water is not readily available. Tree roots have access to water deep within the profile and long-term forestry could thus have a detrimental effect on the water resources in a catchment.

Baldocchi and Xu (2006) find similar results when investigating the Mediterranean Oak (*Quercus douglasii*). They attribute the ability of the trees to endure extended periods when total evaporation exceeds rainfall to physiological adjustment of the trees such as down-regulation of stomatal conductance and the tapping of deep sources of water. The water holding capacity of the soils also plays an important, long-term role allowing the trees to survive. These findings confirm that the results and conclusions reached in the study at Two Streams have been found elsewhere in the world and highlight the need to investigate root, soil water and ground water dynamics further.

In summary the following recommendations can be made from the work at Two Streams: (1) it would be beneficial in the future, in terms of energy balance closure, to run an eddy covariance system at the site in conjunction with the LAS in order to confirm the results obtained thus far and confirm to what extent the assumption that sensible heat flux is positive during unstable conditions is true, (2) this would also provide some indication of the magnitude of the errors introduced during neutral or near-neutral conditions in the early morning and late afternoon that the LAS was unable to measure, (3)

the LAS is a very reliable instrument and can be used to accurately measure the long-term total evaporation over trees, (4) where possible hourly data should be used in the calculation of short grass reference evaporation rather than daily, (5) night-time values of short grass reference evaporation should be included in daily summations, (6) there appears to be a variability in crop factors associated with seasonality, (7) the Priestly and Taylor method performed very well against the LAS and can be used to estimate total evaporation in the Two Streams area over *A. mearnsii* with confidence.

Further work in this catchment should include using the evaporation data in modelling the water balance of the catchment with a processed based model. The model would have to be able to cope with deep soils and interactions between the ground water and tree roots and an addition or subtraction of water from the water balance. This would enable the modelling of commercial forestry applications to closer reflect the true picture in catchments with deep soils and shallow ground water levels.

8. References

Alados I, Foyo-Moreno I, Olmo FJ, Alados-Arboledas L, 2003. Relationship between net radiation and solar radiation for semi-arid shrub-land, *Agricultural and Forest Meteorology*, 116, 221–227.

Allen R G, Pereira L S, Raes D, Smith M, 1998. Crop evapotranspiration: Guidelines for computing crop water requirements, *FAO Irrigation and Drainage Paper 56*, Food and Agriculture Organization of the United Nations, Rome, Italy, 315pp.

Allen R G, Walter I A, Elliott R, Mecham B, Jensen M E, Itenfisu D, Howell T A, Snyder R, Brown P, Echings S, Spofford T, Hattendorf M, Cuenca R H, Wright J L, Martin D, 2000. Issues, requirements and challenges in selecting and specifying a standardized ET equation, *Proc., 4th National Irrig. Symp.*, American Society of Agricultural Engineers, Phoenix, AZ, USA.

Allen R G, Pruitt W O, Wright J L, Howell T A, Ventura F, Snyder R, Itenfisu D, Steduto P, Berengena J, Yrisarry J B, Smith M, Pereira L S, Raes D, Perrier A, Alves I, Walter I, Elliott R, 2006. A recommendation on standardized surface resistance for hourly calculation of reference ET_o by the FAO56 Penman-Monteith method, *Agricultural. Water Management*, 81, 1–22.

Andreas E L (ed.), 1990. Selected papers on turbulence in refractive medium, *SPIE Milestones Series*, 25, 693pp.

Ayra S P, 2001. *Introduction to Micrometeorology*, 2nd ed., Academic Press, London, UK, 420pp.

Baldocchi D D, Xu L, 2006. What limits evaporation from mediterranean oak woodlands - the supply of moisture in the soil, physiological control by plants or the demand by the atmosphere? *Advances in Water Resources*, 30:10, 2113-2122.

Beyrich F, de Bruin H A R, Meijninger W M L, Schipper J W, Lohse H, 2002. Results from a one-year continuous operation of a large aperture scintillometer over a heterogeneous land surface, *Boundary-Layer Meteorology*, 105, 85-97.

Blaney, H F, Criddle W D, 1950. *Determining water requirements in irrigated areas from climatological and irrigation data*, ASDA Soil Conservation Services, SCS-TP96,44pp

Brutsaert W H, 1982. Evaporation into the Atmosphere, Theory, History, and Applications, D. Reidel Publishing Co, Dordrecht, Holland, 299pp.

Burger C, 1999. *Comparative evaporation measurements above commercial forestry and sugarcane canopies in the KwaZulu-Natal midlands*, M.Sc. Agric. thesis, University of Natal, Pietermaritzburg, KwaZulu-Natal, South Africa.

Campbell G S, Norman J M, 1998. *Environmental Biophysics*, 2nd ed. Springer-Verlag New York, NY, USA, 286pp.

Campbell Scientific, 1999. Application note: *On-line estimation of grass reference evapotranspiration with the campbell scientific automatic weather station*, Logan, Utah, USA.

Campbell Scientific, 2003. Instruction manual: *HPT3 soil heat flux plate*. Campbell Scientific Inc., Logan, Utah, USA, 12pp.

Cava D, Contini D, Donateo A, Martano P, 2007. Analysis of short-term closure of the surface energy balance above short vegetation, *Agricultural and Forest Meteorology*, In Press.

Cellier P, Richard G, Robin P, 1996. Partition of sensible heat fluxes into bare soil and the atmosphere. *Agriculture and Forest Meteorology*, 82, 245–265.

Chehbouni A, Hartogensis O, Kerr Y H, Hipps L, Brunel J-P, Watts C, Rodriguez J, Boulet G, Dedieu G, de Bruin H, 1998. Sensible heat flux measurements using a large aperture scintillometer over a heterogeneous surface, *American Meteorological Society*, Special Symposium on Hydrology, Phoenix, Arizona, 11-16 Jan.

de Bruin H A R, 2002. Renaissance of scintillometry, *Boundary-Layer Meteorology*, 105, 1-4.

de Vries D A, Philip J R, 1986. Soil Heat Flux, Thermal Conductivity, and the Null-alignment Method, *Soil Science Society of America Journal*, 50, 12-18.

Doorenbos J, Pruitt W O, 1975. Guidelines for predicting crop water requirements, *Irrigation and Drainage paper 24*, Food and Agriculture Organisation of United Nations, Rome, Italy.

Everson C E, Gush M B, Moodley M, Jarmain C, Govender M, Dye P, 2007. *Effective management of the riparian zone vegetation to significantly reduce the cost of catchment management and enable greater productivity of land resources*, WRC Report No. 1284/1/07. ISBN 978-1-77005-613-8, Pretoria, South Africa.

Ezzahar J, Chehbaouni A, Hoedjes J C B, Chehbouni A H, 2006. On the application of scintillometry over heterogeneous grids, *Journal of Hydrology*, 334, 493-501.

Foken T, 2006. 50 years of the Monin-Obukhov similarity theory. *Boundary-Layer Meteorology*, 119, 431-447.

Foken T, Mauder M, Liebethal C, Wimmer F, Beyrich F, Siegfried R, de Bruin H A R, Meijninger W M L, Bange J, 2006a. *Attempt to close the energy balance for the Litfass-2003 experiment*, Dept. of Micrometeorology, University of Bayreuth, Bayreauth, Germany.

Foken T, Wimmer F, Mauder M, Thomas C, Liebethal C, 2006b. Some aspects of the energy balance closure problem, *Atmospheric Chemistry and Physics Discussions*, 6, 3381-3402.

Gavilan P, Lorite I J, Tornero S, Berengena J, 2006. Regional calibration of the Hargreaves equation for estimating reference ET in a semi-arid environment, *Agricultural Water Management*, 81, 257–281.

Hartogensis O K, Watts C J, Rodriguez J-C, de Bruin H A R, 2003. Derivation of an effective height for scintillometers: La Poza experiment in Northwest Mexico, *American Meteorological Society*, 4, 915-928.

Hill R J, 1992. Review of optical scintillation methods of measuring the refractive-index spectrum, inner scale and surface fluxes, *Waves in Random and Complex Media*, 2, 179-201.

Hill R J, Clifford S F, 1981. Theory of saturation of optical scintillation by strong turbulence for arbitrary refractive-index spectra, *Journal of Optical Society of America,* 71, 675–686.

Hoedjes J C B, Zuurbier R M, Watts C J, 2002. Large aperture scintillometer used over a homogeneous irrigated area, partly affected by regional advection, *Boundary-Layer Meteorology*, 105, 99-117.

Horst T W, Weil J C, 1992. Footprint estimation for scalar flux measurements in the atmospheric surface layer, *Boundary-Layer Meteorology,* 59,279-296.

Howell T A, Evett S R, 2004. The *Penman-Monteith method*. Section 3 in Evapotranspiration: Determination of consumptive use in water rights proceedings. Continuing Legal Education in Colorado, Denver, USA, 16pp.

Kanda M, Moriwaki R, Roth M, Oke T, 2002. Area-averaged sensible heat flux and a new method to determine zero-plane displacement length over an urban surface using scintillometry, *Boundary-Layer Meteorology*, 105, 177-193.

Kimball B A, Jackson R D, Nakayama F S, Idso S B, Reginato R J, 1976. Soil-heat Flux Determination: Temperature Gradient Method with Computed Thermal Conductivities*, Soil Science Society of America Journal*, 40, 25-28.

Kipp and Zonen, 2007. *Instruction Manual to the Large Aperture Scintillometer*, Delft, Holland, 74pp

Kohsiek W, Meijninger W M L, de Bruin H A R, Beyrick F, 2005. Saturation of the large aperture scintillometer, *Boundary-Layer Meteorology*, 121, 111-126.

LAI-2000 Plant Canopy Analyser, 1989. LAI-*2000 Technical Information*, LI-COR Inc., Lincoln, Nebraska, USA.

Mayocchi C L, Bristow K L, 1995. Soil surface heat flux: some general questions and comments on measurements, *Agricultural and Forest Meteorology*, 75, 43-50.

Meijninger W M L, de Bruin H A R, 2000. The sensible heat flux of irrigated areas in western Turkey determined with a large aperture scintillometer, *Journal of Hydrology*, 229, 42-49.

Meijninger W M L, Hartogensis O K, Kohsiek W, Hoedjes J C B, Zuurbier R M, de Bruin H A R, 2002. Determination of area-averaged sensible heat fluxes with a large aperture scintillometer over a heterogeneous surface – Flevoland field experiment, *Boundary-Layer Meteorology*, 10, 63-83.

Meijninger W M L, Beyrich F, Ludi A, Kohsiek W, de Bruin H A R, 2006. Scintillometer-based turbulent fluxes of sensible and latent heat over a

heterogeneous land surface – a contribution to LITFASS-2003, *Boundary-Layer Meteorology,* 121, 89-110.

Meijninger W M L *pers. comm*., 2007. *Waterwatch*, Wageningen, The Netherlands.

Metelerkamp B R, 1993. *The use of the Bowen ratio energy balance method for the determination of total evaporation over a grassed surface*. M.Sc. Agric. thesis, University of Natal, Pietermaritzburg, South Africa.

Monin A S, Obukhov A M, 1954. Basic laws of turbulent mixing in the ground layer of the atmosphere, *Tr. Goefiz. Institute Akad*. Nauk. SSSR. 24 (151), 163-187.

Monteith J L, Unsworth M, 1990. *Principles of Environmental Physics*. 2nd ed., Edward Arnold, London, UK, 291pp.

Mucina L, Rutherford M C (eds), 2006. The Vegetation of South Africa, Lesotho and Swaziland. *Strelitzia 19*, South African National Biodiversity Institute, Pretoria, South Africa.

Nicholls S, Smith F B, 1982. On the definition of the flux of sensible heat, *Boundary-Layer Meteorology*, 24, 121-127.

Ochs G, Clifford S, Wang T, 1976. Laser wind sensing: The effects of saturation of scintillation. *Applied Optics*, 15, 403-408.

Odhiambo G O, 2007. Long-term measurements of spatially averaged sensible heat flux for a mixed grassland community, using surface layer scintillometry. PhD thesis, University of KwaZulu-Natal, Pietermaritzburg, South Africa.

Oncley S P, Foken T, Vogt R, Kohsiek W, de Bruin H A R, Bernhofer C, Christen A, van Gorsel E, Grantz D, Feigenwinter, C, Lehner I, Liebethal C, Liu H, Mauder M, Pitacco A, Ribeiro L, Weidinger T, 2007. The energy

balance experiment EBEX-2000. Part I: overview and energy balance. *Boundary-Layer Meteorol*. 123, 1-28.

Ortega-Farias S, Antonioletti R, Olioso A, 2000. Net radiation model evaluation at an hourly time step for mediterranean conditions, Agronomie, 20, 157-164.

Penman H L, 1948. Natural evaporation from open water, bare soil and grass. *Proc. Royal Society of London*, A193, 120-146.

Priestley C H B, Taylor R J, 1972. On the assessment of surface heat flux and evaporation using large scale parameters, *Monthly Weather Rev*., 100, 81-92.

Riou C, 1984. Simplified calculation of zero-plane displacement from windspeed profiles, *Journal of Hydrology*, 69, 351-357.

Rosenberg N J, Blad B L, Verma S B, 1983. *Microclimate: The Biological Environment*, 2nd ed., John Wiley and Sons Inc., New York, 495pp.

Savage M J, Everson C S, Metelerkamp B R, 1997. *Evaporation measurement above vegetated surfaces using micrometeorological techniques*, Water Research Commission Report No. 349/1/97. ISBN 1-86845-363-4, Pretoria, South Africa, 227pp.

Savage M J, Everson C S, Odhiambo G O, Mengistu M G, Jarmain C, 2004. Theory and practice of evaporation measurement, with a special focus on SLS as an operational tool for the estimation of spatially-averaged evaporation, Water Research Commission Report No. 1335/1/04. ISBN 1-77005-247-X, Pretoria, South Africa, 204pp.

Stannard D I, Rosenberry D O, 1991. A comparison of short-term measurements of lake evaporation using eddy correlation and energy budget methods, *Journal of Hydrology*, 122, 15-22.

Takagi K, Miyata A, Harazono Y, Ota N, Komine M, Yoshimoto M, 2003. An alternative approach to determining zero-plane displacement, and its application to a lotus paddy field, *Agricultural and Forest Meteorology*, 115, 173-181.

Tatarskii V I, 1961. *Wave Propagation in a Turbulent Medium*, Dover Publications, New York, USA, 285pp.

Thornthwaite C W, 1948. *An approach toward a rational classification of climate*, Geographical Review, 38, 50.

Twine T E, Kustas W P, Norman J M, Cook D R, Houser P R, Meyers T P, Prueger J H, Starks P J, Wesely M L, 2000. Correcting eddy-covariance flux underestimates over a grassland, *Agricultural and Forest Meteorology*, 103, 279-300.

Verhoef A, McNaughton K G, Jacobs J F G, 1997. A parameterization of momentum roughness length and displacement height for a wide range of canopy densities, *Hydrology and Earth Sciences*, 1, 81-91.

Wang T I, Ochs G R, Clifford S F, 1978. A saturation resistant optical scintillometer to measure C_n^2, *Journal of Optical Society of America*, 69, 334-338.

Wieringa J,1998. *How far can agrometeorological station observations be considered representative?* Prepr. 23rd American Meteorological Society Conference on Agricultural and Forest Meteorology (Albuquerque, N.M.),9-12.

Wesley M L, 1976. The combined effect of temperature and humidity on the refractive index, *Journal of Applied Meteorology*, 15, 43-49.

Wilson K, Goldstein A, Falge E, Aubinet M, Baldocchi D D, Berbigier P, Bernhofer C, Ceulemans R, Dolman H, Field C, Grelle A, Ibrom A, Law B E, Wyngaard J C, Izumi Y, Collins S A, 1971. Behaviour of the refractive index structure parameter near the ground, *Journal of Optical Society of America*, 61, 1646-1650.

Zhang H, Park S, 1999. Comments on 'a new method to determine the zero-plane displacement', *Boundary-Layer Meteorology*, 91, 135-139.

Zoumakis N M, 1992. Estimating the zero-plane displacement and roughness length for tall vegetation and forest canopies using semi-empirical wind profiles, *Journal of Applied Meteorology*, 32, 574-579.

Appendix A. Program used on a Campbell Scientific CR23X logger to collect data from the LAS

```
;{CR23X}
*Table 1 Program
  01: 1.0000    Execution Interval
(seconds)

1:  If time is (P92)
 1: 0        Minutes (Seconds --) into a
 2: 10       Interval (same units as above)
 3: 12       Set Flag 2 High

2:  If Flag/Port (P91)
 1: 22       Do if Flag 2 is Low
 2: 30       Then Do

3:  Beginning of Loop (P87)
 1: 0        Delay
 2: 12       Loop Count

4:  Z=F x 10^n (P30)
 1: 0        F
 2: 0        n, Exponent of 10
 3: 1     -- Z Loc [ UCN2      ]

5:  Z=F x 10^n (P30)
 1: 0        F
 2: 0        n, Exponent of 10
 3: 6        Z Loc [ N         ]

6:  End (P95)

7:  End (P95)

8:  If Flag/Port (P91)
 1: 22       Do if Flag 2 is Low
 2: 0        Go to end of Program Table

9:  Volt (Diff) (P2)
 1: 1        Reps
 2: 35       5000 mV, 50 Hz Reject, Fast
Range (same as code 55)
 3: 1        DIFF Channel
 4: 1        Loc [ UCN2      ]
 5: .001     Mult
 6: 0        Offset

10:  Volt (Diff) (P2)
 1: 1        Reps
 2: 35       5000 mV, 50 Hz Reject, Fast
Range (same as code 55)
 3: 2        DIFF Channel
 4: 2        Loc [ demod     ]
 5: 1        Mult
 6: 0        Offset

11:  If Flag/Port (P91)
 1: 23       Do if Flag 3 is Low
 2: 1        Call Subroutine 1

12:  Z=F x 10^n (P30)
 1: 10       F
 2: 0        n, Exponent of 10
 3: 3        Z Loc [ Ten       ]

13:  Z=X^Y (P47)
 1: 3        X Loc [ Ten       ]
 2: 1        Y Loc [ UCN2      ]
 3: 4        Z Loc [ PowerUCN2 ]

14:  Z=X*F (P37)
 1: 4        X Loc [ PowerUCN2 ]
 2: 1000     F
 3: 5        Z Loc [ PUCN21000 ]

15:  Z=X+F (P34)
```

```
 1: 6       X Loc [ N        ]
 2: 1       F
 3: 6       Z Loc [ N        ]

16:  Z=X-Y (P35)
 1: 1       X Loc [ UCN2     ]
 2: 7       Y Loc [ UCN2_c   ]
 3: 9       Z Loc [ UCN2_P62  ]

17:  Z=X-Y (P35)
 1: 2       X Loc [ demod    ]
 2: 8       Y Loc [ demod_c  ]
 3: 10      Z Loc [ demod_P62 ]

18:  If time is (P92)
 1: 0       Minutes (Seconds --) into a
 2: 10      Interval (same units as above)
 3: 10      Set Output Flag High (Flag 0)

19:  Covariance/Correlation (P62)
 1: 2       No. of Input Locations
 2: 0       No. of Means
 3: 2       No. of Variances
 4: 0       No. of Std. Dev.
 5: 0       No. of Covariance
 6: 0       No. of Correlations
 7: 600     Samples per Average
 8: 9       First Source Loc [ UCN2_P62  ]
 9: 11      First Destination Loc [
Var_UCN2  ]

20:  Real Time (P77)
 1: 110     Day,Hour/Minute (midnight =
0000)

21:  Average (P71)
 1: 2       Reps
 2: 1       Loc [ UCN2     ]

22:  Sample (P70)
 1: 2       Reps
 2: 11      Loc [ Var_UCN2  ]

23:  Resolution (P78)
 1: 1       High Resolution

24:  Average (P71)
 1: 1       Reps
 2: 5       Loc [ PUCN21000 ]

25:  Resolution (P78)
 1: 0       Low Resolution

26:  Sample (P70)
 1: 1       Reps
 2: 6       Loc [ N        ]

27:  If time is (P92)
 1: 0       Minutes (Seconds --) into a
 2: 10      Interval (same units as above)
 3: 30      Then Do

28:  Do (P86)
 1: 23      Set Flag 3 Low

29:  Z=F x 10^n (P30)
 1: 0       F
 2: 0       n, Exponent of 10
 3: 6       Z Loc [ N        ]

30:  End (P95)

*Table 2 Program
  01: 10.0000   Execution Interval
(seconds)

1:  Batt Voltage (P10)
 1: 13      Loc [ Batt_V    ]

2:  Panel Temperature (P17)
```

```
 1: 14      Loc [ _________ ]

3:  If time is (P92)
 1: 0       Minutes (Seconds --) into a
 2: 60      Interval (same units as above)
 3: 10      Set Output Flag High (Flag 0)

4:  Real Time (P77)
 1: 110     Day,Hour/Minute (midnight =
0000)

5:  Sample (P70)
 1: 1       Reps
 2: 13      Loc [ Batt_V    ]

*Table 3 Subroutines

1:  Beginning of Subroutine (P85)
 1: 1       Subroutine 1

2:  Do (P86)
 1: 13      Set Flag 3 High

3:  Block Move (P54)
 1: 2       No. of Values
 2: 1       First Source Loc [ UCN2      ]
 3: 1       Source Step
 4: 7       First Destination Loc [ UCN2_c
]
 5: 1       Destination Step

4:  End (P95)

End Program


1     [ UCN2      ] RW--  4      2      ----- -
----- ---
2     [ demod     ] RW--  3      1      ----- -
----- ---
3     [ Ten       ] RW--  1      1      ----- ---
--- ---
4     [ PowerUCN2 ] RW--  1      1      ---
-- ------ ---
5     [ PUCN21000 ] RW--  1      1      ---
-- ------ ---
6     [ N         ] RW--  2      3      ----- ----
-- ---
7     [ UCN2_c    ] RW--  1      1      Start
------ ---
8     [ demod_c   ] RW--  1      1      -----
------ End
9     [ UCN2_P62  ] RW--  1      1      ----
- ------ ---
10    [ demod_P62 ] RW--  1      1      ---
-- ------ ---
11    [ Var_UCN2  ] RW--  1      1
Start ------ ---
12    [ Var_Demod ] RW--  1      1      ---
-- ------ End
13    [ Batt_V    ] RW--  1      1      ----- -
----- ---
```